NTNU
Norwegian University of
Science and Technology

Glycerol-3-phosphate and cell wall integrity maintenance mechanism - two sides to the same story?

Kristine Marie Svanø

Master of Science
Submission date: June 2018
Supervisor: Thorsten Hamann, IBI
Co-supervisor: Timo Engelsdorf, IBI

Norwegian University of Science and Technology
Department of Biology

Acknowledgment

First of all, I would like to express my gratitude to my supervisor: Associate Professor Thorsten Hamann of the Department of biology at Norwegian University of Science and Technology (NTNU). His office was always open whenever I had any questions. Associate Professor Hamann provided excellent help and support throughout the research process and writing this master's thesis. His comments and thoughts have been very valuable.

Furthermore, I would like to acknowledge my co-supervisor: Doctor rerum naturalium (Dr. rer. nat.) Timo Engelsdorf of Plant Physiology at Philipps University of Marburg (PU) for his support and patient guidance throughout this thesis. Dr. rer. nat. Engelsdorf provided tremendous help and guidance regarding experimental design, analysis of results and as a second reader of the master´s thesis.

My sincere thanks also go to Staff Engineer Trude Johansen, Senior Engineer Torfinn Sparstad, as well as additional researches at the Hamann lab: Nora Gigli Bisceglia and Lauri Vaathera, all of Department of Biology at NTNU, for their kind help and guidance in my co-supervisor's absence.

I addition, I would like to thank my fellow MSc students at the Hamann lab: Camilla Øvstebø and Eskil Nodeland Indregård, for their support and nice discussions.

Finally, I would like to thank my friends and family for their patience and amazing support throughout my years of study. I would especially like to thank my boyfriend, Thomas Norum Ur, for his willingness to proof read this thesis.

Kristine Marie Svanø

Abstract

Plants and pathogens are in a constant ”arms-race”, with the plant cell wall as one of the main battlefields. This arms-race have evolved to complex defense responses in plants against primary infections in local infected tissue. Moreover, local resistance induce systemic acquired resistance (SAR), a broad-spectrum and long lasting resistance in systemic tissue, with glycerol-3-phosphate (G3P) as a central signal metabolite. A well-known response to pathogen infections is reinforcement of the cell wall. The cell wall´s functional integrity is also maintained by the cell wall integrity (CWI) maintenance mechanism. Pathogen resistance and the CWI maintenance mechanism show overlapping responses to cell wall damage (CWD), but limited knowledge of their connections is available. However, pattern-triggered immunity (PTI), involved in local resistance, was recently shown to inhibit the CWI maintenance mechanism by e.g. downregulation of phytohormone synthesis. In this project, various CWD-induced responses (by Isoxaben) were studied in KO-mutants impaired in G3P-metabolism to investigate G3P-signalling´s association with CWI maintenance in *Arabidposis thaliana*. Moreover, sorbitol cotreatment was performed to examine how hyperosmotic conditions affected the responses. It was shown that genes involved in G3P-metabolism, or the resulting impairment of G3P-metabolism does not seem to be involved in ISX-induced CWD responses such as lignin biosynthesis and growth inhibition. However, the genes seem to act as negative regulators of ISX-induced phytohormone accumulation. Since G3P is a central signal metabolite in SAR, and there is a known interconnection between SAR and PTI, this raises the questions of a possible CWI maintenance-suppressing role of SAR, either directly, through G3P-metabolism gene activity or G3P-flux modulations, or indirectly, through activation of PTI.

Sammendrag

Planter og patogener er i en konstant kamp om overlevelse, der hovedslagmarken finner sted i plantens cellevegg. Dette har ført til en utvikling av komplekse forsvarsmekanismer i planten, både for å bekjempe primærinfeksjoner på lokalt nivå, og i form av en langvarig resistens mot sekundærinfeksjoner med glyserol-3-fosfat (G3P) som en sentral signaliseringsmetabolitt, bedre kjent som SAR (Systemic Acquired Resistance). Celleveggs-forsterkning "*lignin*" er en velkjent respons mot patogeninfeksjoner. Celleveggens funksjonelle integritet er i tillegg vedlikeholdt av en relativt ukjent forsvarsmekanisme "cell wall integrity (CWI) maintenance mechanism", hvor celleveggen forsterkes analogt med plantens forsvarsmekanismer. Til tross for at "CWI maintenance" og patogenforsvar fører til overlappende responser, er det begrenset tilgang på kunnskap om deres assosiasjoner. Nyere studier har avdekket at PTI (Pattern-triggered immunity), en lokal forsvarsmekanisme mot vertsløse patogener, inhibierer CWI ved for eksempel nedregulering av hormonsyntetisering. I dette prosjektet ble CWI-induserte responser (med Isoxaben) studert i KO (Knock Out)-mutanter av gener involvert i G3P-metabolisme for å undersøke G3P-signaliseringens forbindelse med CWI i *Arabidopsis thaliana*. Resultater presentert i denne rapporten viser at gener involvert i G3P-metabolisme nedregulerer sentrale responser mot celleveggskade, som for eksempel akumullering av plantehormoner, mens genene trolig ikke er involvert i lignin-syntese, eller vekst-inhibering. Siden G3P spiller en sentral rolle i SAR, og det er vist at SAR og PTI påvirker hverandre, stiller dette spørsmål ved om SAR også nedregulerer "CWI maintenance mechanism", enten direkte gjennom G3P-genaktivitet, eller indirekte gjennom aktivering av PTI.

Table of Contents

List of figures

Supplementary information

Appendix A - Tables

Appendix B - Figures

Appendix C - Glycerol kinase (GK) activity assay

Abbrevations

ACT1 G3P ACETYLTRANSFERASE 1

ACT2 ACTIN 2

ALD1 AGD2-LIKE DEFENSE RESPONSE PROTEIN 1

ANOVA Analysis of variance

Aza Azealic acid

AZI1 AZEALIC ACID INDUCED 1

BAK1 BRI1-ASSOCIATED KINASE1

cDNA Complementary DNA

CERK1 CHITIN ELICTOR RECEPTOR KINASE 1

CESA CELLULOSE SYNTHASE A

Col-0 Colombia-0

CWD Cell wall damage

CWI Cell wall integrity

CWDE Cell wall degrading enzyme

DA Dehydroabietinal acid

DAMP Damage associated molecular pattern

DHAP Dihydroxyacetone phosphate

DIR1 DEFECTIVE IN INDUCED RESISTANCE

DMSO Dimethyl sulfoxide

ETI Effector triggered immunity

flg22 flagellin 22

FLS2 FLAGELLIN SENSITIVE 2

G3P Glycerol-3-phosphate

GDPH Glycerol-3-phosphate dehydrogenase

GK Glycerol kinase

GLI1 GLYCEROL INSENSITIVE 1,

HR Hypersensitive response

HSD Honest significance test

ISC1 ISOCHORISMATE SYNTHASE 1

ISX Isoxaben

JA Jasmoic acid

KO Knock-out

LB Left-Boarder

LRR Leucine-rich repeat

MAMP Microbe-associated molecular pattern

MAPK Mitogen-associated protein kinase

MeSA Methylated Salicylic acid

MQ Milli-Q

MS Murashige and Skoog

MS/MS Tandem mass spectrometry

NAD Nicotinamide adenine dinucleotide

NB-LRR Nucleotide binding-leucine rich repeat

PAMP Pathogen associated molecular pattern

PCR Polymerase chain reaction

Pip Pipecolic acid

PRR Pattern recognition receptor

PR Pathogenesis-related

PTI PAMP-triggered immunity

qRT-PCR Quantitative Reverse-transcriptase polymerase chain reaction

R-protein Resistance protein

RHOHD Respiratory burst oxidase homolog protein D

RLK Receptor-like kinase

RLP Receptor-like protein

ROS Reactive oxygen species

RT Room temperature

RT-PCR Real-time polymerase chain reaction

SA Salicylic acid

SAMT SA METHYLTRANSFERASE

SAR Systemic acquired resistance

T-DNA Transfer DNA

UFLC Ultrafast liquid chromatography

WAK1 WALL-ASSOCIATED KINASE 1

Chapter 1

Introduction

As the global human population is growing at an ever-increasing rate, the food requirements of tomorrow are likely to grow as well. In this context, crop plants are important food sources to human kind, both directly as sources to essential nutrients and indirectly by providing food for other food sources to the omnivore humans. It is estimated that by 2050, the global requirement for human and animal food will be at least double compared to today's demand (Godfray et al., 2010; Ray et al., 2013). Due to nutrient deficiency, pathogen attacks and stress related to climate change, such as drought and elevated temperatures, crop species have to adapt to adverse conditions negatively affecting productivity (Pessarakli, 2016).

It is estimated that large quantities of agricultural crop produce is lost prior to harvest each year (Godfray et al., 2010). In order to increase productivity of crop species, herbicides and pesticides are frequently used, chemicals which have been shown to also have negative side-effects on both the surrounding ecosystem and consumers (Pimentel and Edwards, 1982; Kolpin et al., 1998; Bolognesi and Morasso, 2000). One major problem regarding crop production is pathogen attack, causing severe losses of crops annually (Oerke, 2006). Research into the defense mechanisms of plants against biotic stress may therefore give insight into how to optimize plant's resistance towards pathogens, reduce crop plant loss and the usage of pesticides in the future to ensure food availability to the growing human population, and decrease chemical components used in agriculture.

As a structural barrier towards pathogens, the cell wall is a central component in pathogen defense in plants (Bellincampi et al., 2014; Bacete et al., 2018). Functional integrity of the cell wall is maintained by the dedicated mechanism called the cell wall integrity (CWI) maintenance mechanism (Hamann and Denness, 2011; Hamann, 2015a). Defense responses against pathogen infections in plants also includes reinforcement of the cell wall to prevent further in-

fection (Moura et al., 2010). These cell wall reinforcements can be regulated by plant defense responses such as the Systemic Acquired Resistance (SAR), which is responsible for activating whole-plant resistance towards secondary infections by the same pathogen (Gao et al., 2014). However, there exists limited knowledge of how cell wall integrity maintenance mechanism operates and its connections to plant defense responses (Hamann and Denness, 2011). In this thesis, the relationship between (CWI) maintenance mechanism and a central component in SAR; glycerol-3-phosphate (G3P), will be investigated to possibly increase the knowledge of how defense and CWI are interconnected.

Chapter 2

Background

2.1 The plant cell wall

A characteristic feature which distinguishes plant- and animal cells, is the cell wall, a complex carbohydrate network surrounding the plasma membrane of plant cells (Cosgrove, 2005). The cell wall provides strength and stability to plant cells and is involved in structural support, elongation, differentiation, cell-to-cell communication and protection against biotic and abiotic stress (Keegstra, 2010). Plant cell walls consist of several layers correlating with biological functions of the respective cells; the primary cell wall, middle lamella and secondary cell wall. The primary cell wall is generated directly after cell division and includes a framework of cellulose microfibrils, embedded in a matrix of pectic polysaccharides and structural proteins (Cosgrove, 2005). Cellulose microfibrils, the major structural component in primary cell walls, are synthesized by the cellulose synthases (CESAs), which form a rosette-shaped protein complex located at the plasma membrane (Doblin et al., 2002; McFarlane et al., 2014). Hemicelluloses and pectins are synthesized in the Golgi apparatus, and translocated to the growing cell wall through vesicle transport (Cosgrove, 2005). The middle lamella, with pectin as the main structural component, contributes to attachment of the primary cell walls of neighboring cells and thereby allows cell-cell communication (Iwai et al., 2002). Many cell types in most plants, including *Arabidopsis thaliana*, generate a secondary cell wall between the primary cell wall and plasma membrane during cell differentiation to enhance mechanical strength (Zhong and Ye, 2014). Secondary cell walls are mainly composed of cellulose microfibrils, hemicelluloses and lignin, an aromatic alcohol complex consisting of monolignols such as p-coumaryl, coniferyl and sinapyl alcohols (Davin and Lewis, 2005). In specific tissue types, such as tracheary elements, the highly lignified cell walls provides water-proofing and high mechanical strength, thus allowing long-distance water transport in plants. In addition, as a compound difficult to degrade, lignin is syntesized and deposited to plant cell walls as reinforcement against pathogen

infections, providing enhanced protection (reviewed in (Moura et al., 2010; Wang et al., 2013).

2.2 Pathogen resistance in plants

Plants and pathogens are in a constant battle of survival. In order to win the battle, plants have evolved complex defense signalling mechanisms (Jones and Dangl, 2006). As a general defense against intruding pathogens, plant epidermal cells exhibit thickened outer cell walls, covered by the cuticle; a protective film composed of cutin and waxes (Yeats and Rose, 2013). However, most fungi, including *Magnaporthe oryzae*, *Botrytis cinerea* and *Fusarium graminearum*, can break down and penetrate both the cuticle and plant cell wall through secretion of hydrolyzing and cell wall degrading enzymes (CWDEs), respectively, leading to loss of plant cell wall integrity (Mendgen and Hahn, 2002; Bellincampi et al., 2014). Bacteria on the other hand cannot directly penetrate the plant epidermis similar to fungi but gain access to plant cells through surface openings such as stomata or wounds (Melotto et al., 2008). Once the pathogens have penetrated the plant cell wall, the resulting specific infection effects depend on the particular pathogen type. Necrotrophic pathogens destroy cell wall integrity and gain nutrients from dead plant material, while biotrophs proliferate in living plant cells, and feed on them (Dangl and Jones, 2001). Hemibiotrophs on the other hand, start of their life-cycle as biotrophs, followed by necrotrophy at a later life stage. These different life styles result in various types of cell wall damage and affect cell wall integrity in different ways (Bellincampi et al., 2014).

In contrast to the circulatory immune system found in most animals, plants exhibit an isolated immune system within each plant cell (Nurnberger et al., 2004). Plant resistance towards pathogens includes two levels of defense; resistance at local and distal level (Jones and Dangl, 2006). Local resistance involves perception of non-self compounds or damage to locally infected plant tissue, which triggers defense responses favoring plant proliferation. In addition, local defense response induces the second level of defense (distal); also termed systemic acquired resistance (SAR), a broad-spectrum and long-lasting resistance towards secondary infection at whole-plant level (Durrant and Dong, 2004; Dempsey and Klessig, 2012; Shah and Zeier, 2013) (Figure 2.1).

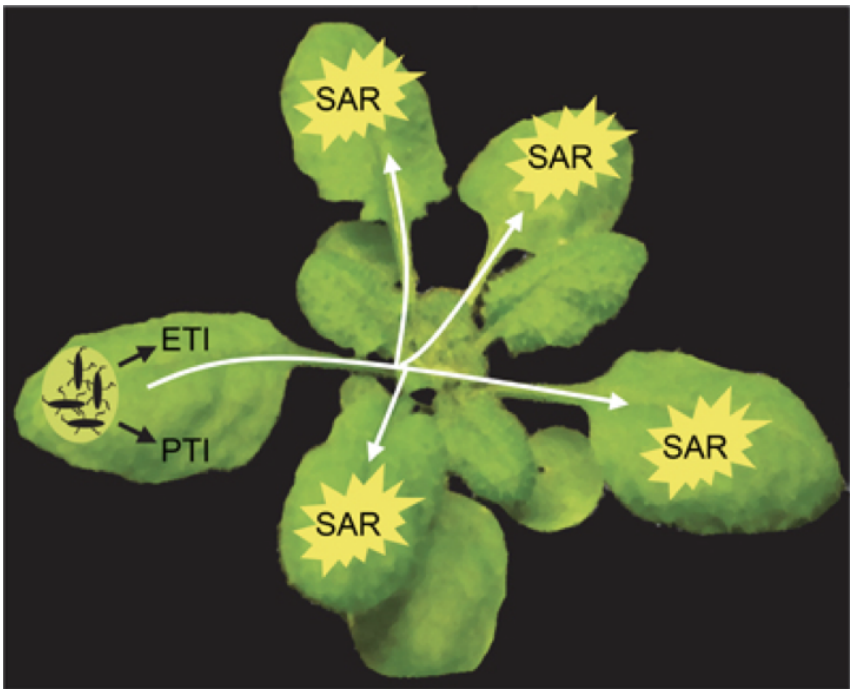

Figure 2.1: Model illustrating the two levels of plant defense. Pathogen infection (light green circle) activates two types of local plant defense; pattern-triggered immunity (PTI) or effector-triggered immunity (ETI), based on host specificity. Local defense responses also induce another level of defense (distal); systemic acquired resistance (SAR), resistance towards secondary infection in tissue initially not affected. Figure adopted from Shah and Zeier (2013).

2.2.1 Local defense responses

Local defense response consists of two types of resistance, depending on host specificity. Basal defense or pattern-triggered immunity (PTI) involves plant resistance towards non-host pathogens (Jones and Dangl, 2006). PTI is initiated upon perception of pathogen-associated molecular patterns (PAMPs) by pattern recognition receptors (PRRs); transmembrane leucine-rich-repeat (LRR)- receptor-like kinases (RLKs) or - receptor-like proteins (RLPs) located at the cell exterior (Dangl and Jones, 2001; Jones and Dangl, 2006; Gust et al., 2017). Common PAMPs include flagellin, a compound present in the flagellum of gram-negative bacteria, and chitin, a common component of fungal cell walls (Jones and Dangl, 2006). Flagellin (or its derivative flg22) and chitin are recognized in *Arabidposis thaliana* by the well-known PRRs; FLAGGELIN-SENSITIVE 2 (FLS2) and CHITIN ELICTOR RECEPTOR KINASE (CERK1), respectively. Moreover, PTI is also induced through PRR-based perception of damage to its own tissue, such as degraded cell wall fragments, compounds known as damage-associated molecular patterns (DAMPs) (Boutrot and Zipfel, 2017). To transfer the danger signal downstream, PPRs often require a co-receptor, such as BRI1-ASSOCIATED KINASE1 (BAK1), which interacts with PAMP- or DAMP- bound PRRs, followed by transphosphorylation and activation

of the receptor complex (Couto and Zipfel, 2016).

PRR activation induces multiple well-known downstream signaling events, leading to transcriptional activation of pathogenesis related (PR)-genes, which initiate several defense responses in plants (van Loon et al., 2006). PRR-based activation of plasma membrane-localized calcium channels cause intracellular Ca^{2+} burst, a common second messenger involved in activation of calcium-dependent protein kinases (CDPKs) (Seybold et al., 2014). CDPKs, in parallel with mitogen-activated protein kinases (MAPKs), phosphorylate and activate several transcription factors of the WRKY family, leading to transcriptional activation of PR genes. In addition, CDPKs activate the nicotineamide adenine dinucleotide phosphate (NADPH) oxidase and RESPIRATORY BURST OXIDASE HOMOLOG (*RBOHD*), causing intracellular accumulation of reactive oxygen species (ROS) (Kadota et al., 2014). The intracellular ROS burst creates a toxic environment for the intruding pathogens, and is also involved in phytohormone production. Common phytohormones, produced upon pathogen attack, includes salicylic acid (SA), jasmonic acid (JA) and ethylene, with the specific type dependent on the specific pathogen (Bari and Jones, 2009). Phytohormones act as second messengers to activate transcription of PR genes. PR proteins are involved in reinforcement of the cell wall through lignin and callose deposition to prevent further degradation and in synthesis of antimicrobial toxins and proteins, creating a hostile environment for intruding pathogens (Jain and Khurana, 2018). In addition, pathogen defense responses are coupled with alternations of cellular metabolism, and other energy-demanding processes such as growth are down-regulated to restrict the resources to an efficient defense (Huot et al., 2014). Phytohormones constitutes a central component of such regulation, whereas biotic stress-related phytohormones, such as SA, repress central responsive genes of the growth-inducing phytohormone, auxin, and vice versa if growth is required (Bari and Jones, 2009).

In order to overcome PTI and promote their own proliferation, host-specific pathogens have evolved a defense-suppressing mechanism, through secretion of effectors, or avirulence proteins, which interact with, inhibit or destroy components required for either pathogen perception or downstream signaling events in PTI (Jones and Dangl, 2006). As a response, plants have co-evolved a second mode of local resistance; effector triggered immunity (ETI). ETI is initiated upon direct (binding) or indirect (recognition of activity) perception of effector proteins by intracellular nucleotide- binding leucine-rich repeat (NB-LRR) proteins, called resistance (R)-proteins (Jones and Dangl, 2006; Wu et al., 2014). Activated R-proteins relay signals to downstream components in a similar manner than PRRs during PTI. However, ETI is a faster, stronger and more persistent defense, which often results in the specialized local programmed cell death; hypersensitive response (HR) and is also involved in activation of SAR (Morel and Dangl, 1997; Dempsey and Klessig, 2012).

2.2.2 Systemic acquired resistance; A defense response towards secondary infection in non-affected tissue

SAR is initiated 4-6 hours after the primary infection occurred by synthesis of several mobile inducers in locally infected plant tissue, which are translocated to distal tissue through vascular tissue where they induce SAR (Durrant and Dong, 2004; Gao et al., 2014). Known inducers of SAR include SA, glycerol-3-phosphate (G3P), pipecolic acid (Pip), azelaic acid (AzA), JA and dehydroabietinal acid (DA) (Dempsey and Klessig, 2012; Kachroo and Robin, 2013; Shah and Zeier, 2013; Gao et al., 2014) (Figure 2.2). Several mobile inducers of SAR are generated in primary infected tissue through activation of the relevant biosynthetic enzymes. SA accumulates in locally infected cells through upregulation of ISOCHORISMATE SYNTHASE 1 (ICS1), a central component in chorismate-derived SA biosynthesis (Wildermuth et al., 2001; Shah and Zeier, 2013). Methyl SA (MeSA) functions as the transposable SA isomer during SAR, and conformation is modified by SA methyltransferases (SAMT/BSMT) in *A. thaliana* (Dempsey and Klessig, 2012; Shah and Zeier, 2013). G3P is synthesized by several enzymes (see chapter 2.2.3) and transported as an unknown derivative (Chanda et al., 2008, 2011; Dempsey and Klessig, 2012). Pip is synthesized from lysine by the AGD2-LIKE DEFENSE RESPONSE PROTEIN1 (ALD1) (Návarová et al., 2012). AzA is generated through oxidation (during the ROS burst) of the C9 double bond of C18 unsaturated fatty acids (Yu et al., 2013). Studies suggests that Aza´s main role in SAR is promotion of G3P synthesis (see chapter 2.2.3) (Yu et al., 2013). However, a small fragment of the Aza pool (approximately 7%) is translocated to distal tissue as an unknown derivative.

Mobile transducers are transported to distal tissues through the vasculature (Shah and Zeier, 2013; Gao et al., 2014). Several mobile inducers depend on interaction with transport proteins to reach distal tissues (Yu et al., 2013; Keshun et al., 2013). G3P and Aza require interaction with the lipid-transfer proteins DEFECTIVE IN INDUCED RESISTANCE 1 (DIR1) and AZELAIC INDUCED 1 (AZI1) and are transported symplastically in the phloem under regulation of plasmodesmata localized proteins (Yu et al., 2013; Lim et al., 2016) (See chapter 2.2.3).

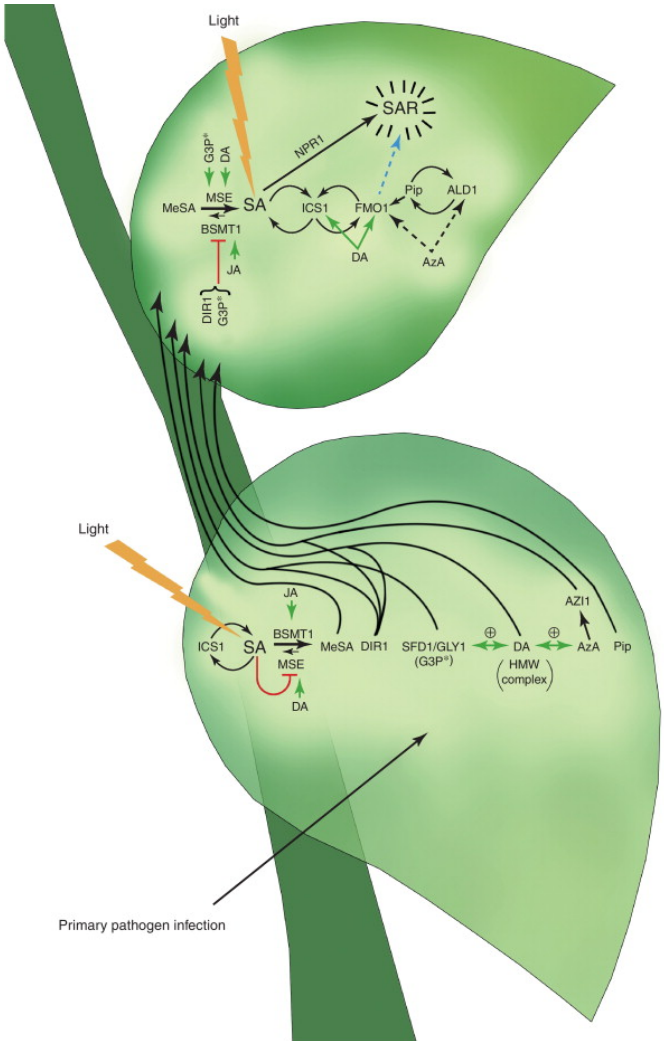

Figure 2.2: Model illustrating SAR. Inhibition is illustrated by red arrows, while transcriptional activation of central SAR-inducing proteins are illustrated by green arrows. In tissue exposed to primary pathogen infection, local defense responses initiate SAR through accumulation of several mobile inducers. SA is synthesized by ICS1, and further converted to its mobile derivative; MeSA, by SA methyl transferases (BSMT), a reaction controlled by JA, DA and light. G3P is synthesized by glycerol kinase (GK) or several G3P dehydrogenases (GDPHs), such as *GLY1*, and translocated as an unknown derivative. In addition, other mobile inducers of SAR, such as Pip, DA and Aza are synthesized. The mobile inducers of SAR is translocated to systemic tissue through the vasculature, which require interaction with transport proteins such as DEFECTIVE IN RESISTANCE 1 (DIR1) and AZEALAIC ACID INDUCED 1 (AZI1). In systemic tissue, MeSA is converted back to SA, a mechanism which is controlled by G3P and DA, DIR1 and JA. In addition, a feedback loop cause transcriptional activation of ISC1, further elevating the cellular SA levels. SA, through the SA-responsive NPR1 initiates SAR, protecting non-affected tissue towards secondary pathogen infections. Figure adopted from Dempsey and Klessig (2012).

SAR-induction is dependent on SA and SA-regulated proteins, including NPR1, NPR3 and NPR4, which are involved in transcriptional regulation of SA responsive genes (Durrant and Dong, 2004; Ding et al., 2018). Therefore, the latter mobile inducers are assumed to be respon-

sible for regulation of SA accumulation in systemic tissue. Cellular SA levels can be elevated in several, different ways in *A. thaliana*. Firstly, the translocated derivative MeSA is converted back to SA by METHYL ESTERASE (MES/SABP2), a reaction involving G3P and DA (Shah and Zeier, 2013) (Figure 2.2). In addition, G3P down-regulates *AtBSMT1* to prevent convertion of SA to MeSA. Secondly, SA accumulation is promoted through a loop involving ALD1, Pip, Flavin-containing monooxygenase 1 (FMO1), Aza and DA, leading to increased expression of the SA synthesizing enzyme; ICS1 (Shah and Zeier, 2013).

SA changes intracellular redox potential and binds the regulatory protein, NPR1, which trigger its conversion from an inactive cytosolic oligomer to an active nuclear monomer (Durrant and Dong, 2004; Mou et al., 2003; Ding et al., 2018). NRP1 monomers interact with TGA transcription factors in nucleus (Shah and Zeier, 2013). In addition, SA inhibits the repressing activity of NPR3/4 on TGA transcription factors, which, in parallel with NPR1 activates the TGAs, leading to transcriptional reprogramming and activation of PR-genes (Shah and Zeier, 2013; Ding et al., 2018). A characteristic feature of SAR is priming, creating the memory of previous attacks and thereby ensures less energy-demanding and more efficient defense responses towards later infections by the same pathogens (Conrath, 2011). Priming involves chromatin modifications leading to enhanced expression of defense related transcription factors. This is exemplified by increased expression of several transcription factors of the WRKY family, such as WRKY6, WRKY29 and WRKY53 in *A. thaliana*, all involved in defense caused by an initial *Pseudomonas syringae* (Jaskiewicz et al., 2011). This reinforces resistance at whole-plant level, and thereby contribute to enhanced local defense (PTI and ETI) towards secondary infection, illustrating connections between the two levels of defense (Fu and Dong, 2013).

2.2.3 Glycerol-3-phosphate (G3P) - A central component in SAR

In this thesis, G3P is the main focus. G3P is a phosphorylated sugar derivative and serves as a precursor in several cellular processes, including glycerolipid biosynthesis and glycolysis (Gee et al., 1988; Wei et al., 2001). Studies have shown that increased cellular levels of G3P is correlated with increased resistance towards the hemobiotroph *Colletotrichum higginsianum* and SAR initiation in *A. thaliana* (Chanda et al., 2008, 2011). In parallel, G3P reduction is related to impaired SAR and increased susceptibility to *C. higginsianum*, reinforcing the importance of G3P´s role in SAR. G3P production or - translocation during SAR are associated with several different precursors and genes (Figure 2.3). Glycerol kinase (GK), encoded by *GLYCEROL INSENSITIVE 1* (*GLI1*), synthesizes G3P from glycerol through phosphorylation, using ATP as phosphate source (Chanda et al., 2008). In parallel, nicotinamide adenine dinucleotide (NAD)-dependent G3P dehydrogenase isoforms (GPDHs) can synthesize G3P through reduction of dihydroxyacetone phosphate (DHAP), an intermediate of glycolysis and the Calvin cycle (Wei

et al., 2001). GPDH isoforms are located in various cellular compartments, including plastids and cytosol. Previous work have shown that knock out (KO)-mutants of *GLI1* and *GPDH* isoforms such as *GDPHC1*, *GDPHC2*, *GLY1* and *GDPHP1*, were more susceptible to several pathogens, supporting their involvement in SAR (Chanda et al., 2008, 2011). Interestingly, Venugopal et al. (2009) showed that *gly1* mutants were more susceptible to *C. higginsianium* compared to *GLI1*, suggesting that GPDHs contribute more to the G3P pool during SAR. In addition, the *ACT1* encoded acyl-acyl carrier protein (ACP) G3P acyltransferase (GPAT), localized in plastids, utilizes the G3P pool in the plant through acetylation of the G3P backbone with oleic acid (18:1) during the prokaryotic pathway of glycerolipid biosynthesis (Kunst et al., 1988). Chanda et al. (2008) have shown that KO-mutants of *ACT1* caused enhanced resistance towards *C. higginsianum*, suggesting *ACT1* act as a negative regulator of SAR in *A. thaliana*.

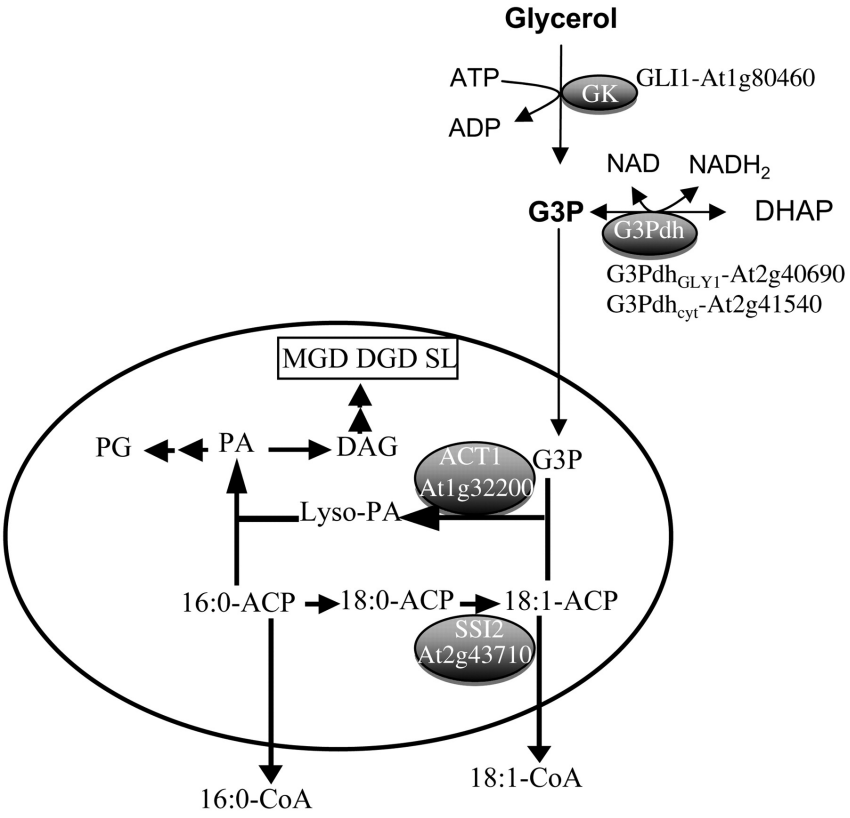

Figure 2.3: Glycerol 3 phosphate (G3P) metabolism in SAR. During initiation of systemic aquired resistance (SAR), several G3P synthesizing enzymes contribute to cellular G3P accumulation. G3P is synthesized through phosphorylation of glycerol, a reaction catalyzed by Glycerol kinase (GK) using ATP as a phosphate source. In addition, G3P is synthesized by several NAD-dependent GPDH isoforms which synthesize G3P through reduction of dihydroxyacetone phosphate (DHAP), a precursor involved in several other metabolic pathways in plants. The intracellular G3P pool is utilized by G3P acetyltransferase, encoded by *ACT1*, in plastids. G3P acetyltransferases acetylate the G3P backbone with oelic acid (18:1) during the prokaryotic pathway of glycerolipid biosynthesis in plastids (illustrated by the circle). Figure adopted from Chanda et al. (2008).

G3P synthesis is also dependent on Aza, another mobile inducer of SAR (Gao et al., 2014). It was previously shown that pathogen perception causes release of C18 fatty acids from membranes, which are involved in Aza production through oxidation at C9. Aza accumulation leads to activation of G3P-synthesizing proteins, including GK and GPDH isoforms, which generate G3P in local infected tissue (Gao et al., 2014) (Figure 2.4).

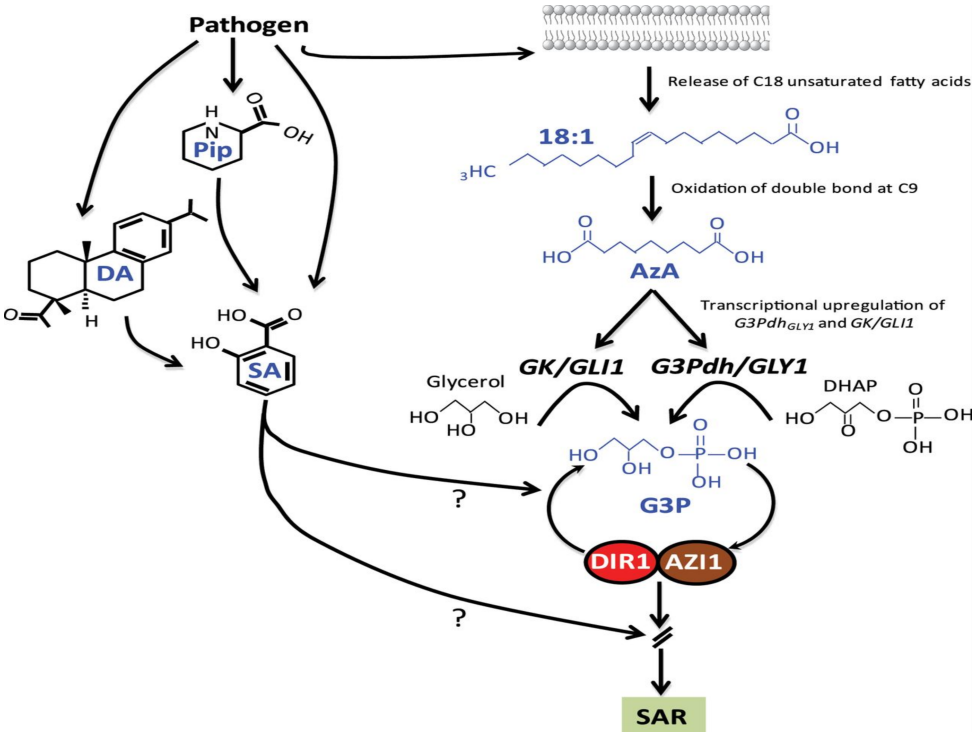

.

Figure 2.4: Model illustrating synthesis and translocation of central mobile inducers of SAR. Pathogen perception leads to synthesis of several mobile signaling metabolites involved in SAR. C18 fatty acids released from membranes are oxidized at C9, creating azelaic acid (Aza). Aza accumulation cause transcriptional activation of G3P-synthesizing genes, including *GLI1* (Glycerol kinase; GK) and several Glycerol-3-phosphate dehydrogenase (*GPDH*) isoforms, causing G3P accumulation. G3P is translocated to systemic plant compartments through the vasculature in association with AZI1 and DIR1. There is observed an interdependence between G3P and its translocators. G3P induce SAR in systemic tissue in collaboration with several other mobile metabolites. Figure adopted from Gao et al. (2014).

In order to translocate G3P to systemic tissue and induce SAR, lipid transfer proteins (LTP)-like DIR1 and AZI1 are required, and form therefore a part of the mechanism regulating SAR (Keshun et al., 2013; Gao et al., 2014) (Figure 2.4). AZI1 and DIR1 facilitate the movement of SAR signals from the synthesis to target sites in vascular tissue via plasmodesmata for symplasmic movement, or across the plasma membrane to the apoplast for apoplastic movement (Cecchini et al., 2015). Symplasmic movement are further regulated by plasmodesmata (PD) localized proteins 1 and 5 (PDLP1 and PDLP5), controlling permeability of the PD (Lim et al., 2016). Previous studies have shown that *A.thaliana* plants defective in *AZI1* and *DIR1* are more

susceptible to pathogens such as *C. higginsianum*, suggesting their association in SAR (Jung et al., 2009; Chanda et al., 2011). In addition, AZI1 and DIR1 require G3P for transcriptional stability, and G3P synthesis is dependent on AZI1 and DIR1, illustrating inter-dependency (Gao et al., 2014).

2.3 The cell wall integrity maintenance mechanism in plants

Plant cell wall integrity can be impaired during cell morphogenesis and enlongation, and upon abiotic and biotic stress (Hamann, 2015a). The plant cell wall integrity (CWI) maintenance mechanism maintains the cell wall's functional integrity and is triggered by perception of cell wall damage (CWD), with the perception mechanism and downstream responses exhibiting similarities to yeast (Hamann and Denness, 2011). In yeast, the CWI maintenance mechanism induces upregulation of biotic stress- related phytohormones such as SA and JA, which cause alternations in cell wall composition (lignin-deposition) and intracellular metabolism in response to CWD, resulting in growth inhibition (Hamann, 2015b). Limited knowledge is available regarding plant's CWI maintenance. However, similar to yeast, CWD seems to be perceived by three groups of plasma membrane-localized sensors involved in mechano-, osmo- and CWD-perception in plants (Hamann, 2015a; Bacete et al., 2018) (Figure 2.5. These groups of sensors have been shown to serve a function in both plant development and response to cell wall stress and pathogen infections (Hamann, 2015a).

Osmotic perception is recognized by sensors such as ARABIDOPSIS HISTIDINE KINASES (AHK1-3, AHK4/CRE1) which are involved in perception of hyperosmotic stress (Hamann, 2015a). Osmotic sensors recognize changes in turgor pressure, an important element in cell wall stress signalling and previous work suggests their involvement in CWD response (Wormit et al., 2012; Hamann, 2015a,b).

To date, two main groups of mechano-sensitive proteins have been discovered in *A. thaliana*; stretch-activated ion channels, and RLKs (Engelsdorf and Hamann, 2014; Hamann, 2015a). Stretch-activated Ca^{2+}-channels sense changes in the plasma membrane relative to the cell wall, which cause intracellular Ca^{2+} burst upon activation, a common second messenger in stress responses. Well known calcium channels includes *MID-COMPLEMENTING ACTIVITY 1/2* and *2* (*MCA1/2*) (Yamanaka et al., 2010; Hamann and Denness, 2011). RLKs have been shown sense CWD through perception of multiple CWD damage signals, such as cellulose inhibition and release of cell wall fragments or peptides (Engelsdorf and Hamann, 2014; Hamann, 2015a). Several known CWD-sensing RLKs are in the *Catharanthus roseus* Receptor-Like Ki-

nase 1-Like (CrRLK1L) family, which are assumed to be involved in CWI maintenance during growth and development (Engelsdorf and Hamann, 2014). Known CrRLK1Ls involved in CWI maintenance mechanism includes e.g. THESUS1 (THE1) and FERONIA (FER). Previously, it have been shown that mutants deficient in THE1 were impaired in perception CWD-signals and activation of CWD responses caused by inhibition of cellulose biosynthesis (CESAs), suggesting its role in CWI maintenance mechanism (Bacete et al., 2018). Until recently, the mode of CWD-perception by THE1 have been unknown. However, (Engelsdorf et al., 2017) have shown that THE1-based perception of CWD might be turgor sensitive. FER are assumed to be involved in mechano-perception and binds signaling peptides such as RAPID ALKALINIZATION FACTORS 1 (RALF1). (Bacete et al., 2018).

Interestingly, the CWI maintenance mechanism might also be linked to defense responses towards pathogens, since it senses CWD. (Bellincampi et al., 2014). Previous work have shown that FER interacts with BAK1 during growth regulation, a co-receptor of the RLK family also shown to be required for PRR-based immune signalling (Engelsdorf et al., 2017). Moreover, during infection, pathogens release cell wall degrading enzymes, causing a loss of function of the cell wall of its plant host and release of cell wall fragments (DAMPs) such as the prectin degradation residue; olicosaccharides (OGs) (Bellincampi et al., 2014; Bacete et al., 2018). OGs are percepted by several WALL-ASSOCIATED KINASEs (WAKs), RLKs which are linked defense against necrotrophic pathogens and likely as a modulator CWI maintenance during growth, as OGs are shown to suppress auxin-induced growth and development (Brutus et al., 2010; Bellincampi et al., 2014; Engelsdorf and Hamann, 2014).

Detection of CWD by CWI-sensors leads to initiation of abiotic and biotic stress responses. These include production of phytohormones like JA and SA, as well as ROS and possibly Calcium release, which serve as signal molecules to activate downstream responses including production of lignin and changes in gene expression to reinforce the cell wall (Moura et al., 2010; Hamann et al., 2009; Hamann and Denness, 2011). CWD have also been shown to cause to growth inhibition to prevent cell growth or -division substituted with damaged cell walls Gigli-Bisceglia et al. (2018). Moreover, as a major sink to fixed carbon, damage to the cell wall are assumed to be involved in regulation of intracellular metabolism such as photosynthesis, through down-regulation of central genes or precursors based on limited demand of new cellulose material (Wormit et al., 2012).

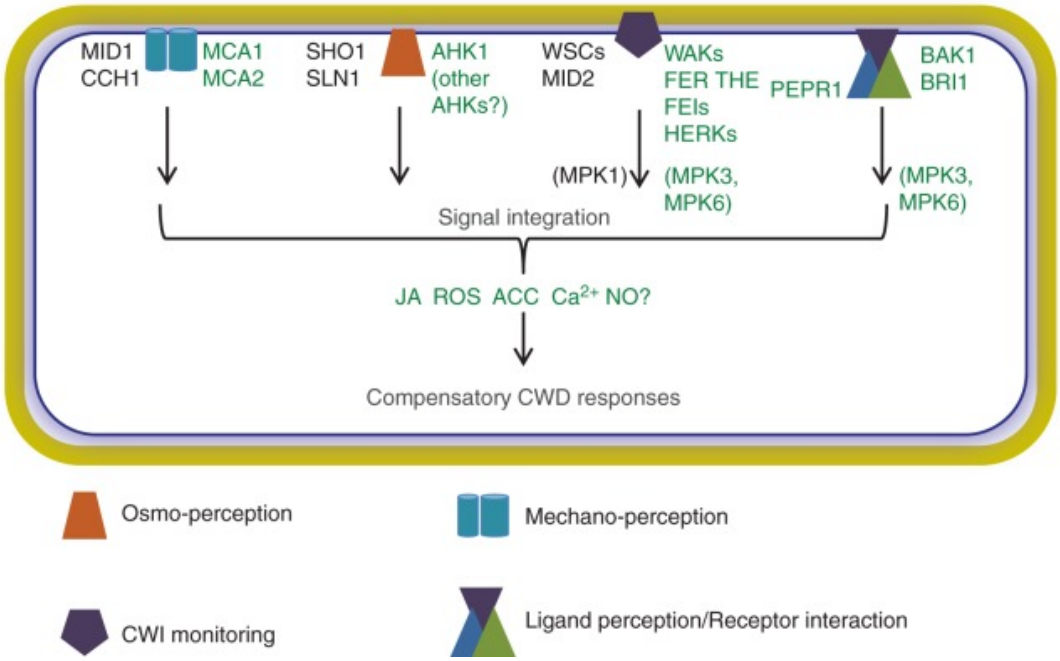

.

Figure 2.5: Model illustrating the cell wall integrity (CWI) maintenace mechanism in plants. CWI is monitored by several classes of sensors located at the plasma membrane, recognizing CWD through DAMPs, changes in tugor or alternations in the plasma membrane relative to the cell wall.One major class of sensors consists of RLKs, including FER, THE1 and WAK1. Detection of CWD cause several downstream signalling events through second messengers such as CA^{2+} and ROS, followed by accumulation of stress-related phytohormones such as JA and SA, leading to CWD responses. Late responses to cell wall damage includes reinforcement of the cell wall through synthesis and deposition of lignin. Figure adopted from Engelsdorf and Hamann (2014).

The CWI maintenance mechanism and its associated signalling pathways are often investigated by inducing CWD in a controlled manner, followed by observation of the stress responses induced (Hamann et al., 2009). CWD can be initiated in several ways. Treatment with isoxaben (ISX), a herbicide, leads to inhibition of cellulose synthesis during generation of the primary cell wall and affects the location of the cellulose synthesizing CESA complex (Desprez et al., 2002). A phenotypic response to ISX-induced CWD in *A.thaliana* is bloating of epidermal cells in the root elongation zone in seedlings, which is likely due to the plant cell‘s decreased ability to contain the turgor pressure (Hamann, 2015b). The importance of turgor pressure is illustrated by sorbitol treatments which can induce hyperosmotic conditions and suppress both the bloating of cells and other ISX-induced responses, such as hormone accumulation and lignification, reinforcing the notion that the observed phenotypic effects are due to CWD induced by high turgor levels prevalent in plant cells (Hamann et al., 2009). Another source of CWD can be enzymatic wall degradation when phytopathogen fungi penetrate plant cell walls during infection (Mendgen and Hahn, 2002). ISX-based and pathogen-based CWD have different modes

of action. ISX cause turgor dependent CWD by preventing availability of by cellulose material to growing cells, while enzymatic degradation leads to breakdown of the existing cell wall (Engelsdorf et al., 2017). Interestingly, plants impaired in cellulose biosynthesis by mutations in cellulose synthase genes, are more resistant to pathogens, possibly due to enhanced JA levels or increased lignin production (Ellis and Turner, 2001). These observations highlight the intimate involvement of cell walls in pathogen responses.

2.4 Hypothesis and aims of thesis

G3P has been shown to be an important signaling molecule regulating systemic plant immunity (Chanda et al., 2008, 2011). CWI surveillance has been implicated both in pathogen defense and stress signaling, and might thus contribute to establishment of SAR, e.g. by inducing accumulation of SA and JA. In addition, it is known that SAR-induced responses in distal tissue involves strengthening of the cell wall by lignin, a characteristic feature of the cell wall integrity maintenance mechanism. Therefore, the aim of this thesis is to investigate if G3P metabolism is modified in response to CWD and if G3P contributes to regulation of CWI maintenance in *A. thaliana*.

Specifically, the following questions have been addressed in this thesis to improve our understanding of the possible connections between the CWI maintenance mechanism and systemic plant defense.

1. Are the activities of G3P generating enzymes (GK, GPDH isoforms) changed upon CWD?
2. Which specific enzymes involved in G3P metabolism or translocation are important in the context of cell wall damage signaling?

The first question was supposed to be addressed by performing enzyme activity assays of GK and GDPH isoforms in ISX treated *A. thaliana* Col-0 seedlings to investigate effects of CWD on G3P synthesis. The second question was addressed by studying the impact of enzymes involved in G3P metabolism on CWD signalling. This investigation was examined using knock out (KO)-alleles for selected candidate genes. Here, mock and ISX-treated KO-mutants in the *A. thaliana* Colombia-0 (Col-0) background, impaired in G3P-biosynthesis: *gdphc1-2*, *gdphc2*, *gdphp1*, *gli1-3*, -translocation: *azi1-2*, *dir1*, and -utilization: *act1-1*, *act1-2* and *fad-gdph* were analyzed. Investigation of how and if these mutants were associated with CWI maintenance was performed by quantification of phytohormone levels (JA/SA), lignin production, cell-cycle marker gene expression, and root length. In addition, sorbitol treatment was combined with ISX exposure to observe how hyperosmotic conditions affected the responses.

Time limitations restricted the scope of this project. Therefore, only the 2nd question was examined experimentally, and will be presented in this thesis. For the 1 st question, a procedure to perform the enzyme activity assay of GK was established, but not fully tested, and is presented in Appendix C.

Chapter 3

Materials and Methods

All chemicals were obtained from Sigma Aldrich (St.Louis, MO, USA) unless stated otherwise.

3.1 Plant material and treatment

25-35 g of seeds from *A. thaliana* ecotype Col-0 and each G3P-metabolism mutant were sterilized in 1 ml 70% ethanol for 10 minutes, followed by treatment with 50% Bleach (Klorin; Lilleborg, Oslo, Norway) for 5-10 minutes, and three rounds of washing with 1 ml sterile Milli-Q (MQ) water. The sterilized seeds were transferred to flasks containing 125 ml autoclaved $\frac{1}{2}$ strength Murashige and Skoog (MS) medium (0.22% MS salts, 0.1% MES, 1% sucrose. pH 5.7) in sterile environment and grown in flasks in long-day conditions (16 hours light at 22°C/8 hours dark at 18°C) at 150 µmol m^{-2} s^{-1} photon flux density on a Conical Flask Shaker with a speed of 130 rotations per minute. After 6 days, the seedlings from each flask were divided in four and transferred to new flasks containing 125 ml of fresh $\frac{1}{2}$ strength MS medium with 600 nM ISX (diluted in Dimethyl sulfoxide (DMSO)), 600 nM ISX (diluted in DMSO)/300 mM Sorbitol, DMSO /300 mM Sorbitol or mock conditions (DMSO) under sterile conditions, and grown as described above.

Approximately 15 seedlings were collected before treatment start and stored in 70% ethanol for root length assay. Plant material was collected at 7, 9 and 24 hours after treatment start to be used for hormone analysis, analysis of cell cycle marker gene expression, lignin staining and root length assay, respectively. Plant material to be used in the time course experiment of phytohormone accumulation was collected at 0, 4, 7, 10 and 24 hours after ISX treatment. Plant material collected for phytohormone analysis were flash-frozen on liquid nitrogen, freeze dried for 24 hours and stored in -20°C. Plant material collected for analysis of cell cycle marker gene expression was flash-frozen in liquid nitrogen and stored in -80°C. Plant material collected for lignin quantification and root length assay were stored in 70% ethanol at room temperature.

3.2 Genotyping of T-DNA insertion mutants

In this thesis, KO-mutant lines of the genes involved in G3P-biosynthesis: *GLI1* (SALK_067205), *GPDHC1* (SALK_020444), *GPDHC2* (SALK_033040), *GPDHP1* (SALK_062006), G3P-utilization: *ACT1* (SALK_069657; CS200), *FAD-GPDH* (SALK_080169) or G3P-translocation: *DIR1* (SAIL_583_F07) and *AZI1* (SALK_085727) were investigated. G3P-metabolism mutant lines were in *A. thalina* Col-0 background and were obtained from the Nottingham Arabidopsis Stock Centre (SALK_020444, SALK_067205, SALK_033040, SALK_062006, SALK_069657, SALK_080169, CS200, SALK_080169) and the Kachroo laboratory, University of Kentucky, USA (SAIL_583_F07).

Several different strategies exist to create KOs, including Transfer DNA (T-DNA) insertion, introduction of transposable elements and by using chemical mutagens (Krysan et al., 1999). In the T-DNA insertion approach, foreign DNA is introduced randomly into the plant genome by infecting plants with *Agrobacterium tumefaciens*, followed by extended screening processes identifying the locations of T-DNA insertions (Bechtold and Pelletier, 1998; Clough and Bent, 1998). Use of the T-DNA insertion strategy has several advantages. The T-DNA itself serves as a marker for identification of the insertion site, and as opposed to introduction of transposable elements, the T-DNA insertion will not transpose throughout the genome, resulting in a stable alternation (Krysan et al., 1999).

Mutant lines generated by T-DNA insertion included *gli1-3*, *gpdhc1-2*, *gpdhc2*, *gpdhp1*, *act1*, *fad-gpdh* and *azi1-2*. Initially, genotyping of T-DNA lines was performed on 7-10 day-old seedlings grown in soil under long-day conditions as described previously. The screening procedure was repeated on 6-day old seedlings grown in $\frac{1}{2}$ strength MS medie (1% sucrose) under conditions as described before, for further confirmation. Screening of homozygous T-DNA insertion mutants was carried out by a polymerase chain reaction (PCR) using two primer pairs for each mutant line. One primer pair included a left-border (LB) primer corresponding to the inserted T-DNA, and a reverse (rev) primer, specific for the gene of interest, to screen for T-DNA presence in the gene of interest. The other primer pair was used to screen for presence of an intact wild type gene and included a forward (for) and rev primer, corresponding to the wild-type gene of interest.

3.2.1 DNA extraction

DNA extractions were performed as described in Edwards et al. (1991), and included two steps; lysis of plant material and isolation of nucleic acids. Plant material was flash-frozen in liquid nitrogen, and ground to fine powder using a Tissue Lyzer (Qiagen) for 1 min at 20 Hz. 400 µl extraction buffer (200 mM Tris-HCl (pH 7.5), 250 mM NaCl, 25 mM EDTA and 0.5% SDS)

was used for nucleic acid extraction. The extracts were vortexed briefly and centrifuged at 13 000 rpm at room temperature (RT) for 3 minutes to precipitate larger cellular components. 300 µl of the supernatant were added to 300 µl Isopropanol, mixed and incubated for 2 minutes, followed by centrifugation at 13 000 rpm at RT for 5 minutes. The supernatant was discarded, and the pellets were dried upside down on clean paper for 30-60 minutes to remove residual isopropanol. Finally, the pellets were re-suspended in 30 µl sterile MQ water. The re-suspended samples were vortexed, incubated at 40°C for 2 minutes, vortexed again, and incubated at 40°C for 1 minute. DNA-content (ng/µl) and -purity were measured using a Nanodrop-100 spectrophotometer (Thermo Fischer). The samples were stored at -20°C.

3.2.2 Polymerase chain reaction

Polymerase chain reaction (PCR) is a DNA amplification method and includes a repeated, temperature-based cycle of three steps; DNA double strand denaturation, annealing of primers and synthesis/elongation of new DNA strands (Mullis et al., 1986). In the first step, the DNA strands are separated by a temperature increase to approximately 94 °C which breaks up hydrogen bonds holding the two strands of the DNA double helix together. When the DNA strands are separated, the temperature is decreased to approximately 50-65°C which initiates the second step of PCR; annealing of primers. In this step, primers specific for the DNA sequence of interest attach to its complementary sequence on the DNA strands, providing binding sites for DNA polymerase. During the last step of the PCR, the temperature is increased to optimum temperature for the polymerase, and new DNA strands are synthesized using dNTPs. A commonly used polymerase is isolated from the thermophilic bacteria *Thermus aquaticus*, with an optimum temperature of 72°C (Saiki et al., 1988).

PCR used for genotyping of T-DNA insertion mutant lines was performed using a master mix containing 10 mM dNTP mix (VWR), 1 U Taq DNA polymerase (VWR) a 10X key buffer (15 mM $MgCl_2$; VWR), 10 M forward primer and 10 M reverse primer. An overview of primer pairs used in this project is presented in Supplemental table A.1. 19 µl master mix was aliquoted to PCR tubes, and 1 µl DNA template were added. DNA-template from wild type *A. thaliana* of Col-0 ecotype was used as a positive control, while a blank control (BC) lacking DNA template was applied as a negative control. The PCR reaction was carried out in a G-STORM G1 Thermal Cycler (Gene Technologies) or a T100 Thermal Cycler (BIO RAD). Initially, the samples were denaturated at 95°C for 5 minutes to activate the DNA polymerase, followed by 35 cycles of denturation at 94°C for 45 seconds, annealing and elongation at 72°C for 1 minute. The annealing temperature varied across the G3P-metabolism mutants due to primer length and the GC-pair frequency of the primers. Annealing was carried out for 30 seconds, while a tempera-

ture of 54°C was used for *azi1-2* and *gli1-3*; it was 56°C for *gdphc2*, *gdphp1*, *act1-2*; and 60°C for *gdphc1-2*.

3.2.3 Agarose gel-electrophoresis

Gel-electrophoresis is used to separate DNA sequences based on size (Southern et al., 1975). The set-up used in this project consisted of an agarose gel allowing DNA strands to travel in, located in a Tris/Borate/EDTA (TBE) buffer, coupled to an electrode. Tris ensures solubility of DNA, and EDTA binds divalent ions and thereby inhibits metal-dependent nucleases (Brody and Kern, 2004). DNA, which is negatively charged due to its phosphodiester bonds in the backbone, will travel in the agarose gel towards the positive pole, or anode. Longer DNA fragments will travel a shorter distance due to friction between the DNA strand and the network of the agarose gel, while smaller DNA fragments will travel further (Brody and Kern, 2004). The size of a DNA fragment can be determined by adding a ladder with known size markers to the gel. DNA itself is invisible in the gel and needs to be stained in order to be observed. In these experiments, GelRed™ Nucleic Acid Gel Stain (Biotium) was added to the agarose gel to visualize DNA fragments under UV light.

4 µl 6X DNA gel Loading Dye (Thermo Fisher) was added to each PCR product and vortexed briefly. 10 µl of PCR product was loaded into pockets of an 0,8% agarose gel (0,8% agarose, diluted in boiling TBE buffer and 6X DNA stain). 3 µl of 1kB plus DNA ladder (Thermo Fisher) was used to determine DNA-sequence size of the PCR-products. The gel-electrophoresis was run in TBE buffer in a Wide mini sub GT electrophoresis Cell (BIO RAD), coupled with PowerPac™ Basic Power Supply (BIO RAD) at 90 V for approximately 30 minutes. The result was imaged under UV-light using Gel Doc 2000 (BIO RAD).

3.3 Semiquantitative RT-PCR and real-time qPCR analysis

3.3.1 RNA extraction

RNA was extracted from 6 day-old seedlings grown and treated as described before. The seedlings were flash-frozen in liquid nitrogen, and ground to fine powder in a tissue lyser (Qiagen) at 20 Hz for 1 minute. Total RNA was extracted using Spectrum™ Plant Total RNA Kit (Sigma-Aldrich) according to manufacturer's protocol (sigmaaldrich.com). Step 4a (In protocol: 4a Bind RNA to Column) and only one elution step was performed. RNA content (ng/µl) and purity were measured using a Nanodrop-100 spectrophotometer (Thermo fischer) to provide sufficient and equal RNA amounts for further analysis. The samples were stored at -80°C

prior to RT-PCR experiments.

3.3.2 cDNA synthesis using reverse-transcriptase (RT)-PCR

In order to analyze expression of the genes of interest by qPCR, RNA was converted to its complementary DNA (cDNA) by a modified version of PCR, called reverse transcriptase PCR (RT-PCR). RT-PCR resembles traditional PCR in execution, but contrary to traditional PCR using polymerase as DNA synthesizing enzyme to amplify DNA sequences of interest, RT-PCR uses reverse transcriptase, an enzyme synthesizing double-stranded cDNA from single stranded RNA templates (Rio, 2014). Prior to RT-PCR, DNA-digestion was performed using RQI RNase-Free DNase (Promega), according to manufacturers protocol (www.promega.com) to reduce unspecific DNA, which could cause problems. A standarized volume of total RNA (ng/µl) was calculated in advance to ensure a universal amount of 2 ng/µl in each sample.

RT-PCR was performed with the ImProm-II™ Reverse Transcription System (Promega) according to the manufacturers protocol (promega.com), with minor modifications in the master mix and RT-PCR program (N. Gigli-Bisceglia, personal communication). The reaction was performed in a master mix containing dNTP mix (Thermo Fisher), Oligo$(dT)_{15}$ primers, Random primers, $MgCl_2$, ImProm-II™ Reverse Transcriptase and ImProm-II™ 5X Reaction Buffer providing optimum conditions for the reverse transcriptase enzyme (Supplemental table A.2). 15 µl solution from a master mix were aliquoted onto a 96 well PCR plate. 5 µl total RNA (incl. DNase mix) was added, giving a total volume of 20 µl per reaction. The RT-PCR reaction was carried out using a T100™ Thermal Cycler (BIO RAD). The reaction program consisted of annealing at 25°C for 10 minutes, elongation at 42°C for 1 hour and inactivation of reverse transcriptase at 72°C for 15 minutes. The remaining 5 µl of total RNA (incl. DNase) were saved for use as a real-time quantitative PCR (qPCR) control (-RT control). Samples and -RT controls were stored in -80°C prior to qPCR.

3.3.3 Quantitative reverse transcriptase PCR (qRT-PCR

Expression levels of genes of interest were quantified by a real-time quantitative PCR (q-PCR), which monitor DNA amplification in real-time (Bustin, 2000). In this project, PCR-products were detected and quantified using a fluorescence emitting marker molecule. SYBR-green emits fluorescence when attached to double stranded DNA, with the fluorescence intensity being directly correlated to DNA amount present in the sample, and thereby the expression levels of the genes of interest (Morrison et al., 1998).

The qPCR was performed using a LightCycler® 480 SYBR Green I Master (Roche), and a master mix containing a forward/reverse primer mix according to gene of interest or reference gene (Supplementary table A.3) and LightCycler® 480 SYBR Green I Master 2x (Roche) (Supplemental table A.4). Genes investigated in this project were *CYCB1;1* and *CYCD3;1*, central controllers of cell-cycle progression. *ACTIN 2* (*ACT2*), a housekeeping gene with expression levels unaffected by ISX-treatment, was applied as reference gene for normalization (N. Gigli-Bisceglia, personal communication). Two negative controls were used; a -RT control to detect contamination by undesirable DNA and a no template control (sterile MQ-water) to detect presence of unwanted primer-dimers. 15 µl master mix solution were aliquoted into a 96 well PCR plate. 5 µl cDNA (diluted 1:10), -RT control or sterile MQ-water was added, giving a total volume of 20 µl per reaction. The qPCR reaction was performed using a LightCycler® 96 System (Roche). Initially, samples were denaturated at 95°C for 5 min to activate the DNA polymerase. The reaction included 45 cycles of denaturation at 95°C for 10 seconds, annealing at 57°C for 10 seconds and elongation at 72°C for 15 seconds. Fluorescence was measured after each cycle of the reaction. The resulting melting- and amplification curve were analyzed to ensure SYBR Green- and primer-pair precision.

Expression levels of *CYCB1;1* and *CYCD3;1* were calculated relative to the reference gene (*ACT2*) as described in (Ferrari et al., 2006). The algorithm used includes the mean PCR amplification efficiency and the ΔCT value, obtained from LinReg software (Ruijter et al., 2009). The amplification effiency indicates the efficiency of the qPCR reaction. The CT value represents the cycle in which the fluorescence reaches above background levels, while the ΔCT value were calculated as follows:

$$\Delta CT = CT(gene\ of\ interest) - CT(reference\ gene) \tag{3.1}$$

Calculation of relative expression levels of genes of interest and statistical analysis (two-sided Student´s t-test) were calculated using Microsoft® Excel version 16.13.0, while a one-way ANOVA coupled with a Tukey´s HSD post hoc test was performed using MATLAB (MATLAB and Statistics Toolbox Release 2012b, The MathWorks, Inc., Natick, Massachusetts, United States).

3.4 Root length measurement

Root lengths were measured of 6-day old seedlings grown and treated as described before. 15 randomly selected seedlings with similar cotelydon size, were lined up in a parallel manner on a 0.5% agar plate. The seedlings were photographed together with a ruler used as length standard (Supplemental figure B.1). Absolute root length was calculated using the ImageJ software distribution: Fiji (Schindelin et al., 2012). Transformation from pixels to cm was performed using the "Set Scale" plug-in in the "Analyzer" menu bar allowing inclusions of known distance and unit length (cm). Root length was measured with the "Segmented line" tool in the tool bar. The mean of the primary root length was calculated using Microsoft® Excel version 16.13.0. Statistical analysis was performed using Microsoft® Excel version 16.13.0 (two-sided Student´s t-test) and MATLAB (One-way ANOVA coupled with Tukey´s HSD post hoc test).

3.5 Lignin staining and image analysis

Lignin staining were performed on 6-day old seedlings grown and treated as described before. 10 randomly selected seedlings with similar cotyledon size, were lined up in an antiparallel manner on a slide. Lignin staining was carried out using phloroglucinol (1 g phloroglucinol/ 100 ml 20% HCl), which stains 4-O-linked hydroxy-cinnamyl aldehydes, a central component of lignin (Pomar et al., 2002). The seedlings were photographed with a stereo-microscope (ZEISS Axio Zoom.V16) at 63X magnification, 30 ms exposure time, 60% aperture and 80% LED (light-emitting diode) light intensity. Lignification was quantified using the "Bio Formats" plugin of the ImageJ distribution software: Fiji (Schindelin et al., 2012). The lignin quantification was performed using a macro; a script-based program to detect the red-stained lignin areas from pre-determined settings. A root image of Col-0 from each independent experiment, was used as the template for the macro-programming. The "Adjust Color threshold" plug-in under "Image" in the menu bar was used to set the settings of Threshold-color, whereas the settings "Hue", "Saturation" and "Brightness" of the red color was optimized to measure the highly lignified area of the root, without registration of lower- or non-lignified area (Supplemental figure B.2). The ratio of lignification RoL, was calculated in Microsoft® Excel version 16.13.0 as follows:

$$RoL = \frac{a}{b} \tag{3.2}$$

Where a = lignified area and b = total root area. Statistical analysis was carried out using Microsoft® Excel version 16.13.0 (two-sided Student´s t-test) and MATLAB (One-way ANOVA coupled with Tukey´s HSD post hoc test).

3.6 Jasmonic acid and salicylic acid analysis

JA and SA quantifications was carried out using ultrafast liquid chromatografy/tandem mass spectrometry (UFLC-MS/MS). Prior to the quantification, the hormones was extracted from 6-day old seedlings grown and treated as described before.

3.6.1 Hormone extraction

Hormone extraction was performed according to a modified version of the "Forcat method" (Forcat et al., 2008), as described in Engelsdorf et al. (2017). Three replicates of freeze dried plant material from Col-0 and G3P-metabolism mutants of each treatment were weighed to 10 mg $\pm$ 1 mg in 2 ml Eppendorf tubes. A stainless steel bead was added to each tube, and the samples were ground to fine powder using a Tissue Lyzer (Qiagen) at 25 Hz for 2 minutes. 400 µl extraction buffer (10% MeOH and 1% acetic acid suspended in sterile MQ water) with internal standards (10 ng Jasmonic-d_5 acid, 28 ng Salicylic-d_4 acid, CDN Isotopes Inc.) was used for hormone extraction, and the samples were lysed at 25 Hz for 2 minutes followed by incubation on ice for 30 minutes. The extracts were centrifuged at maximum speed (13 000-13 300 rpm) at 4°C for 10 minutes, and 350 µl of the supernatant was transferred to a 1,5 ml Eppendorf tube. The pellet was re-extracted with 400 µl extraction buffer without internal standards, lysed at 25 Hz for two minutes, incubated directly on ice for 30 minutes and centrifuged at maximum speed at 4°C for 10 minutes. Then, the supernatant from both extraction rounds was pooled and centrifuged at maximum speed at 4°C for 10 minutes two times to remove excess plant material. After the first centrifugation round, 650 µl of the supernatant was transferred to a new 1,5 ml Eppendorf tube, and after the second round, 600 µl of the supernatant was transferred to a new 1,5 ml Eppendorf tube. The samples were stored at -20 °C prior to ultra fast liquid chromatography coupled with tandem mass spectrometry (UFLC-MS/MS) analysis.

3.6.2 UFLC-MS/MS

UFLC (ultrafast liquid chromatography) is used to separate a sample based on the component´s interaction with the mobile and stationary phase (Liu et al., 2012). In this project, the Acetonitrile (ACN) was applied as the mobile phase of the chromatography. Use of ACN allows high sensitivity of the chromatography reaction and since it dissolves poorly in water, retention of the solute analyzed relative to the ACN concentration is easier predicted (Snyder et al., 2011). A hydrophobic C18 coulumn was used as the stationary phase. In a hydrophobic column, the components rate of hydrophobicity determines the interaction with the column, where the least hydrophobic components elute first, while the most hydrophobic components elute last (Snyder

et al., 2011). The separated compunds were moved to a mass spectrometer. Tandem mass spectrometry (MS/MS) involves two steps of mass spectrometry selection (Peng et al., 2003). In the first step (M1), the samples are ionized and mass analyzed. Compounds of known mass-to charge-ratio (m/z) are selected, and further separated and recorded in the second mass spectrometer (M2). The selection is based on a specific precursor-to product ion transition (m/z) of each ionized compond; Multiple reaction monitoring (MRM) (Segarra et al., 2006).

The chromatografic separation reaction was carried out in a UFLC XR (Shimadzu) using a Cortecs C18 column (2.7 mm, 2.1 × 100 mm; Waters). Acetonitrile (ACN) or water (0.1% formic acid each) was used as the solvent gradient. Of a total run time of 7 minutes, ACN was run through the column at a flow rate of 0.4 ml/min. The solvent gradient consisted of i) a concentration gradient of 20% to 95% ACN for 4 minutes, ii) 95% ACN for 1 minute and iii) 95% to 20% ACN for 2 minutes. The MS/MS was performed in an AB SCIEX Triple Quad 5500 (Sciex) system to identify and quantify the detected hormones (JA/SA) and their respective internal standards (D_5-JA/D_4-SA). MRM mass transitions (precursor/product) used were: JA: 209/59 (m/z), D_5-JA: 214/62 (m/z), SA: 137/93 (m/z) and D_4-SA: 141/97 (m/z) (Segarra et al., 2006)

Internal standards with known amounts of JA and SA were used for standardization of phytohormone quantification i.e. to calibrate the potenital loss of the analyzed phytohormones during the extraction (Stokvis et al., 2005). Calculation of JA and SA levels (µg/mgDW) and statistical analysis (two-sided Student´s t-test) were performed using Microsoft® Excel version 16.13.0.

3.7 Statistical analysis

Statistical significance of cell wall damage responses between wild type (Col-0) and G3P-metabolism mutants were performed by confirmatory data analysis through hypothesis testing, in which the mean of data sets are compared (Akaike, 1974). The hypothesis test was performed by stating a null hypothesis (i.e. wild type = G3P-metabolism mutant), an alternative hypothesis (i.e. wild type $\neq$ G3P-metabolism mutant) and defining a confidence interval (95%). Similarly, hypothesis testing was used to analyze the impact of the different treatments on one gene line.

Two different statistical tests were performed, based on the data set used. A two-sided Student´s t-test was performed in Microsoft Excel version 16.13.0 if the statistical comparison included only two groups (Haynes, 2013). If several groups were analyzed, a one-way ANOVA (Analysis of Variance) (Keppel and Wickens, 2004) was performed using MATLAB (Matrix Laboratory) (MATLAB and Statistics Toolbox Release 2012b, The MathWorks, Inc., Natick, Massachusetts, United States).

The p-value of the statistical tests provide a retaining ($p > 0.05$) or rejection ($p < 0.05$) of the null hypothesis according to the confidence interval (Akaike, 1974). The ANOVA analysis only stated if there were variation across the groups, not which groups that differed statistically (Keppel and Wickens, 2004). Therefore, a Tukey´s honest significant difference (HSD) post hoc test (α= 0.05) was performed to determine between which groups the statistical difference appeared.

Chapter 4

Results

4.1 Genotyping of T-DNA insertion mutants

To investigate if genes involved in G3P synthesis: *GPDHC1* (At2g41540), *GPDHC2* (At3g07690), *GPDHP1* (At5g40610), *GLI1* (At1g80460); G3P-utilization: *ACT1* (At1g32200) or G3P-translocation: *AZI1* (At4g12470), were associated with CWD signalling, the responses of seedlings with KO-alleles for these genes to CWD were studied. For simplicity, this collection of mutants will be referred to as G3P-metabolism mutants throughout the thesis. To prevent misconseptions, the *act1* mutants will be referred to as *act1-1* and *act1-2*. *act1-1* was a chemically induced KO-mutant, while *gpdhc1-2*, *gpdhc2*, *gpdhp1*, *gli1-3*, *act1-2* and *azi1-2* were T-DNA insertion mutants. The putative positions of the insertions in the genes of interest are shown in Supplemental Figure B.3. Originally KO-mutants of *GLY1* (At2g40690) and *DIR1* (At5g48485) were also planned to be included in this project. However, since the seeds did not arrive within the timeframe of this project, they were excluded from the analysis. Seedlings of *FAD-GPDH* (At3g10370) mutants had germination problems and did not provide enough plant material required for the analyses planned. Therefore, this mutant was also excluded.

Homozygous T-DNA insertion mutant seed batches of G3P-metabolism genes were obtained by using a PCR-based screening strategy involving two sets of primers. The first primer pair included a left-border primer binding the T-DNA insertion and a reverse primer binding the gene of interest to screen for T-DNA insertion within the gene of interest, while the second primer pair included forward and reverse primer to screen presence of a competent gene of interest (see Supplemental table A.1). A particular mutant line was identified as a homozygous mutant if both the T-DNA insertion was detected within the gene of interest (based on T-DNA and gene specific primer PCR reaction), and absence of a fragment amplified in the PCR reaction including the forward/reverse primer pair (if the wild-type gene of interest is intact).

Predicted sequence sizes (basepair; bp) of PCR products are presented in Supplemental table A.1.B.

PCR-based screening of putatively homozygous mutant lines was initially performed on 7-10 day-old seedlings grown in soil. However, *fad-gpdh* germinated poorly in absence of sufficient sucrose concentration and was therefore grown on $\frac{1}{2}$ strength MS agar plates (1% sucrose) (Quettier et al., 2008). For most mutant lines, the PCR-based screening resulted in readable bands after gel-electrophoresis. However, PCR-reactions for *gpdhc1-2* resulted in weak bands, probably due to low annealing rate of the primers used. Therefore, a gradient-PCR, with multiple annealing temperatures was performed for optimization of the results, and 60°C was chosen as annealing temperature (Supplemental figure B.4). The screening procedure was repeated on seedlings grown in ½ strength MS medium (1% sucrose) to further confirm homozygosity. As shown in figure 4.1, for all candidate genes of interests, homozygous T-DNA lines were isolated and used in this project.

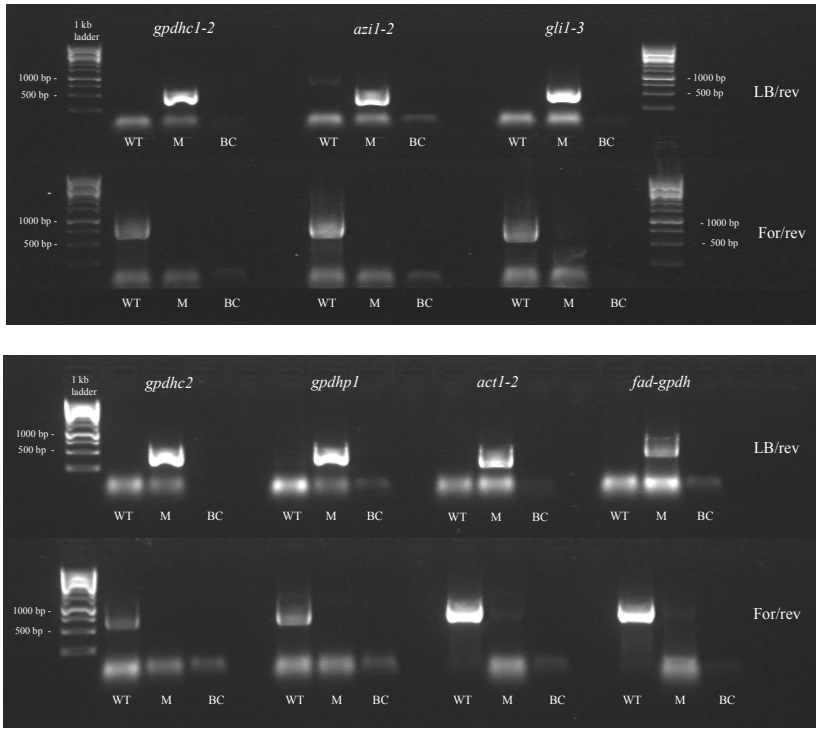

Figure 4.1: Results of PCR-based genotyping of T-DNA insertion lines. PCR was performed using two primer pairs; left boarder (LB) and reverse (rev), binding T-DNA insertion sequence within gene of interest; and forward (for) and reverse (rev) binding wild type fragment of gene of interest. DNA template from *Arabidopsis thaliana* ecotype Col-0 was used as a positive control (WT), M indicates template from the T-DNA lines of interest while a blank control (BC), without DNA template, was used as negative control.

4.2 Analysis of cell wall damage responses in G3P-metabolism mutants

To determine if G3P metabolism genes were associated with cell wall damage response, the impact of KO-mutations in these genes on CWD induced response was analyzed as described in chapter 3. Results for the candidate gene KO lines presented in this chapter are based on three independent experiments with exceptions of *act1-1*, where data from only two experiments was available.

4.2.1 Root growth assays to investigate effects of ISX and hyperosmotic treatments on primary root growth

Genes and precursors associated with G3P-metabolism are also involved in other metabolic processes in plants in addition to SAR, including glycerolipid biosynthesis and Calvin cycle (Kunst et al., 1988; Gee et al., 1988; Wei et al., 2001). To determine if KO-mutants of genes involved in G3P-metablism caused more general unspecific growth defects, a root growth assay was performed. The primary root length of 6 day-old seedlings was quantified using the ImageJ software distribution; Fiji (Schindelin et al., 2012).

The primary root lengths of all G3P-metabolism mutant lines were similar to Col-0, suggesting that none of the KOs in G3P-metabolism genes has a profound effect on root growth in our growth conditions (Figure 4.2.A). Statistical analysis revealed that the primary root of *gli1-3* was longer than *gpdhc1-2*, *gdphc2* and *act1-1*. The primary root of *act1* was longer than *gdphc2*, while the remaining genotypes were not statistically significantly different from others (Supplemental figure B.5).

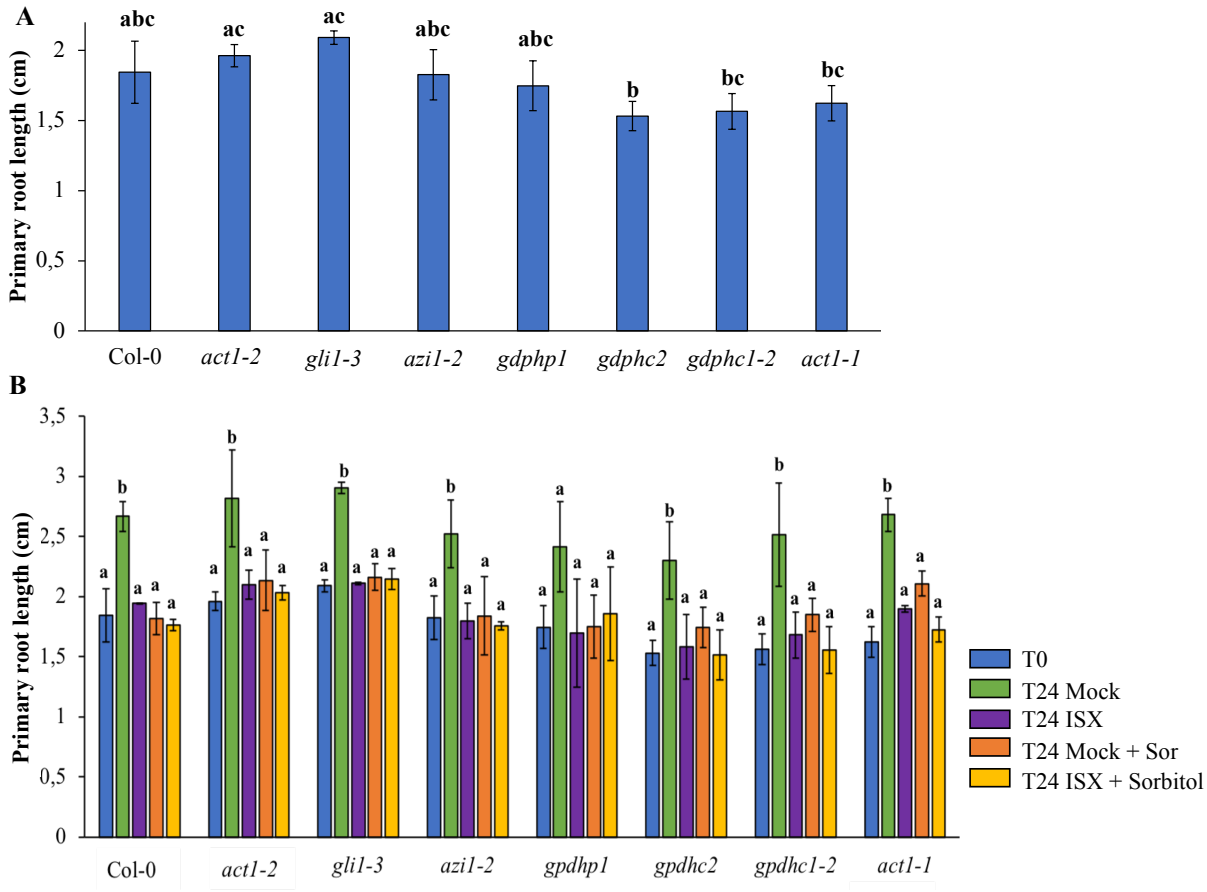

Figure 4.2: Primary root lengths of Col-0 and G3P-metabolism mutants. (**A**.) Root lengths at start of treatment (T0) and (**B**) after 24 hours. Error bars indicate standard deviation based on number of experiments performed (n=2-3). Different letters indicate statistical significant differences between treatments of each gene line, based on a one-way ANOVA with 95% confidence interval coupled with Tukey´s HSD post hoc test (α= 0.05).

Previous work had shown that cell wall damage cause root growth inhibition (Tsang et al., 2011). To investigate if genes involved in G3P-metabolism were associated with growth inhibition upon ISX-induced cell wall damage response and if such a response was suppressed by sorbitol co-treatment, a root growth assay was performed as described previously. Statistical analysis revealed that for Col-0 and all G3P-metabolism mutants except *gdphp1*, ISX-treatments inhibited root growth in all seedlings examined and no significant differences were observed between the Col-0 and most mutants (Figure 4.2.B). Sorbitol treatments inhibited root growth similarly like ISX and co-treated roots did not exhibit differences to ISX alone. On the other hand, no significant difference was observed between any of the treatments in *gdphp1*, suggesting that *GDPHP1* deficiency resulted in reduced sensitivity towards ISX and sorbitol treatment or variation was to high to detect any statistical significance. Since no differences regarding primary root lengths and treatment responses were detectable between the G3P-metabolism mutants and Col-0 across all treatments, these mutants seem neither to have profound effects

on plant growth and metabolism under growth conditions used in this project nor do affect they the response to ISX (cause resistance).

4.2.2 Phytohormone quantification to investigate effects of ISX and hyperosmotic treatments on SA and JA accumulation

Another characteristic response to cell wall damage in *A. thaliana*, is accumulation of the phytohormones salicylic acid SA and jasmonic acid JA, common second messengers in plant stress signaling (Hamann and Denness, 2011). In addition, previous work has detected suppression of ISX-induced accumulation of cellular JA and SA levels by co-treatment of the osmoticum sorbitol (Hamann et al., 2009). To investigate if genes involved in G3P-metabolism were required for the osmo-sensitive, ISX-induced phytohormone accumulation, the same experimental set up was used as before. Phytohormone quantities were measured in mock-, ISX-, Sor- and ISX/Sor-treated Col-0 and G3P-metabolism mutants.

Statistical analysis revealed that ISX-treatments resulted in increased levels of JA and SA compared to mock treatments in both in Col-0 and G3P-metabolism mutants (Figure 4.3). This confirmed previous reports and suggested that G3P-metabolism mutants are not required for ISX-induced phythormone production.

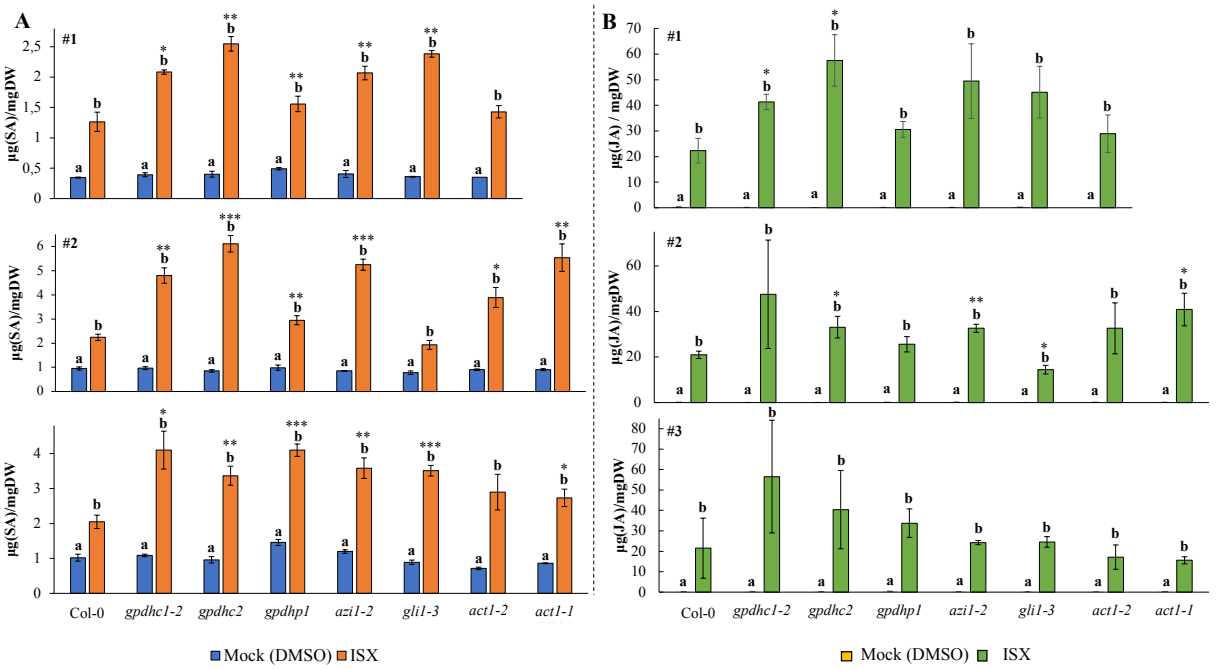

Figure 4.3: SA and JA levels in seedlings treated with ISX or mock (DMSO). 6 days old wild-type (Col-0) and G3P metabolism mutants were mock or ISX-treated for 7h and SA **(A)** or JA **(B)** amounts were quantified. Data shown is derived from three independent experiments (#1- #3) with error bars based on standard deviation (n=3 biological replicates). Different letters indicate statistical significant differences between treatments of each genotype, based on a two-sided Student´s t-test with 95% confidence interval. Asterisks indicates statistical significant difference between phytohormone levels in Col-0 and G3P-metabolism mutants, based on a two-sided Student´s t-test with 95% confidence interval (*: $p < 0.05$, **: $p < 0.01$, ***: $p < 0.001$)

However, it is important to note that all ISX-treated G3P-metabolism mutants except *act1-2*, seemed to exhibit higher SA levels than Col-0 (Figure 4.3.A), suggesting that genes involved in G3P-biosynthesis, -translocation and -utilization negatively regulate SA production in response to CWD. Nevertheless, some variability in SA levels in Col-0 seedlings between the three experiments was observed. Col-0 SA levels were similar in experiments 2 and 3, but reduced in experiment 1. This suggests that biological or environmental factors may influence ISX-induced SA production. ISX-induced JA levels were not as stable as SA levels between different experiments for certain mutants, (SA levels of *gli1-3* seedlings was detected of a range between 14.45 $\pm$ 1.90 and 45.15 $\pm$ 12.39), even though the wild type levels were very reproducible with mean JA levels of 20.97 $\pm$ 1.61 to 22.29 $\pm$ 5.58 µg/mgDW suggesting quite reproducible experimental methods. JA levels in *gdphc2* were higher compared to Col-0 (Figure 4.3.B), implying that *GDPHC2* act as a negative regulator of JA synthesis in response to cell wall damage.

Consistent with previous results, sorbitol-treatment resulted in enhanced biosynthesis of JA in Col-0 and G3P-metabolism mutants compared to mock treatment, suggesting that hyperosmotic stress cause cell wall damage (Hamann et al., 2009) (Figure 4.4.B). However, the sorbitol-effects observed here were much lower compared to ISX-induced CWD, suggesting that ISX cause a more pronounce cell wall damage (Figure 4.4). There were observed variability between sorbitol-induced JA levels in Col-0 seedlings, with experiment 2 exhibiting almost a two-fold increase compared to experiment 1 and 3, suggesting that biological or environmental factors may influence sorbitol-induced JA production. However, most of the G3P-metabolism mutants seemed to exhibit stable JA levels in both treatments, with the exception of mock treated *gpdhp1* experiment 3. *gpdhc1-2*, *gpdhc2*, *gli1-3*, *azi1-2* and *act1* seedlings exhibited a general trend of lower JA levels compared to Col-0 (at laest in experiment 1 and 3), suggesting that these genes might be required in JA synthesis in response to cell wall damage induced by hyperosmotic conditions.

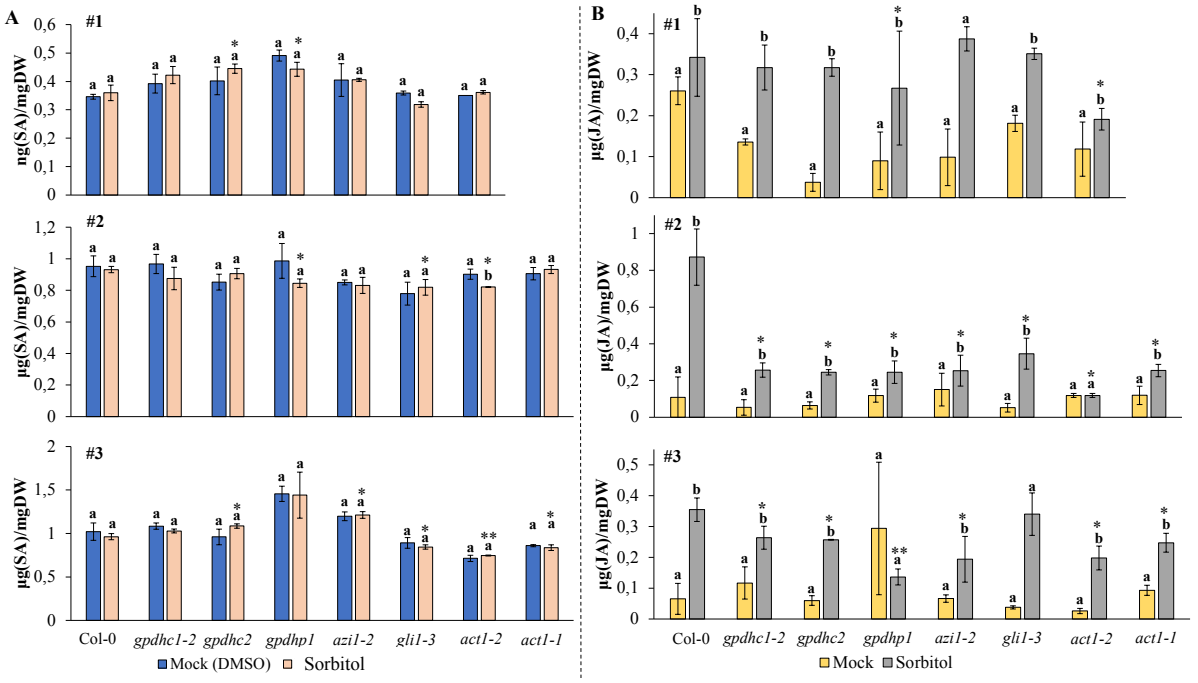

Figure 4.4: SA and JA levels in seedlings treated with Sorbitol or mock (DMSO). 6 days old wild-type (Col-0) and G3P metabolism mutants were sorbitol or DMSO-treated for 7h and SA (**A**) or JA (**B**) amounts were quantified. Data shown is derived from three independent experiments (#1-#3) with error bars based on standard deviation (n=3 biological replicates). Different letters indicate statistical significant differences between treatments of each genotype, based on a two-sided Student´s t-test with 95% confidence interval. Asteriks indicates statistical significant difference between phytohormone levels in Col-0 and G3P-metabolism mutants, based on a two-sided Student´s t-test with 95% confidence interval (*: $p < 0.05$, **: $p < 0.01$, ***: $p < 0.001$)

SA levels in sorbitol-treated Col-0 and G3P-metabolism mutant seedlings were similar to mock treatment (Figure 4.4.A), suggesting that sorbitol-induced CWD did not result in accumulated SA levels. Here as well, there were observed variability between the three independent experiments (SA levels in *gdphp1* seedlings ranged from 0.85 ± 0.033 and 1.26 ± 0.09), while SA levels in Col-0 seedlings were stable, suggesting a reproducible experimental method. However, *gpdhc2* and *azi1-2* seedlings exhibited higher SA levels compared to Col-0, while SA levels in *gli1-3* were lower compared to Col-0 upon sorbitol treatment. Since observations of any variation between SA levels in sorbitol and mock treated seedlings in Col-0 or any of the mutants, this may suggest that these the differences were not based on the sorbitol treatment, or that *GDPHC2*, *AZ11* may be negatively modulate, while *GLI1-3* might be required for accumulation of SA levels in normal conditions. While increased SA levels was observed for *azi1-2* and *act1-1* in single experiments, this data was not reproducible.

ISX+Sor co-treatment resulted in reduced cellular levels of SA and JA in Col-0 and G3P-metabolism mutants compared to ISX treatment alone (as observed in previous work (Hamann et al. (2009)), suggesting that suppression of JA and SA biosynthesis by hyperosmotic conditions is still working (Figure 4.5). Interestingly, *gpdhc1-2*, *gdphp1* exhibited higher cellular JA and SA levels compared to Col-0, suggesting that *GDPHC1* and *GDPHP1* might be required for sorbitol-based suppression of ISX-induced CWD response. However, it is important to bear in mind that the SA levels in these mutants are higher than in Col-0 after ISX-treatment, which might distort the statistical analysis.

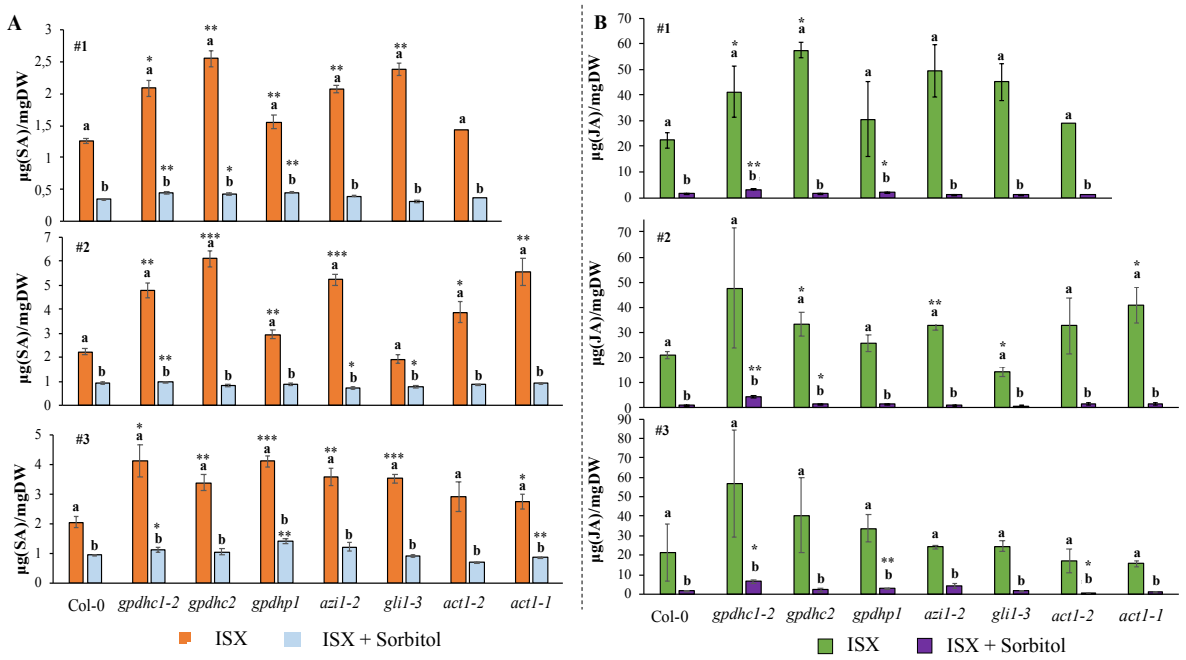

Figure 4.5: SA and JA levels in seedlings treated with ISX or ISX/Sor. 6 days old wild-type (Col-0) and G3P metabolism mutants were ISX- or ISX/Sor-treated for 7h and SA (**A**) or JA (**B**) amounts were quantified. Data shown is derived from three independent experiments (#1-#3) with error bars based on standard deviation (n=3 biological replicates). Different letters indicate statistical significant differences between treatments of each genotype, based on a two-sided Student´s t-test with 95% confidence interval. Asteriks indicates statistical significant difference between phytohormone levels in Col-0 and G3P-metabolism mutants, retrieved with a two-sided Student´s t-test with 95% confidence interval (*: $p < 0.05$, **: $p < 0.01$, ***: $p < 0.001$)

A time-course phytohormone accumulation analysis detected changes in JA and SA levels after 10 hours of ISX treatment

A pilot study performed in the host research group had revealed significantly higher and lower cellular levels of JA in ISX-treated *gli1-3* and *act1*, respectively, compared to Col-0 (Engelsdorf, personal communication). However, similar effects in *gli1-3* and *act1* seedlings were not observed in this project (figure 4.3) (Section 3.2.3). Therefore a pilot study was performed to evaluate if there might be a temporal aspect. This pilot study consisted of a time course experiment where col-0 and *gli1-3* and *act1* seedlings were treated with ISX and JA/SA levels were measured at five time points (0h, 4h, 7h, 10h, and 24h) after start of treatment. Since *gli1-3* seeds germinated at a low rate, only enough plant material for one biological replica for each time point was available, eliminating the possibility of statistical tests.

JA started to increase between 4 and 7 hours post ISX treatment in Col-0, as observed in previous studies (Hamann and Denness, 2011). Increases in JA levels in *act1-1*, *act1-2* were

comparable to Col-0 at T0 and T4 (Figure 4.6). At T7, cellular JA levels in *act1-1* and *act1-2* were similar and lower than Col-0, respectively. *gli1-3* exhibited a similar JA accumulation trend as the other gene lines at T0 to T7. In Col-0, *act1-1* and *act1-2* seedlings, JA levels increased until 10 hours after start of ISX-treatment, followed by a reduction between 10 and 24 hours. In contrast, *gli1-3* mutants continued to synthesize JA after 10 hours post ISX treatment. JA levels in *gli1-3* seedlings seemed to be enhanced compared to Col-0 from T4 onwards until 24h after start of treatment. However, since the graph is based on single data points for each time point this needs to be repeated.

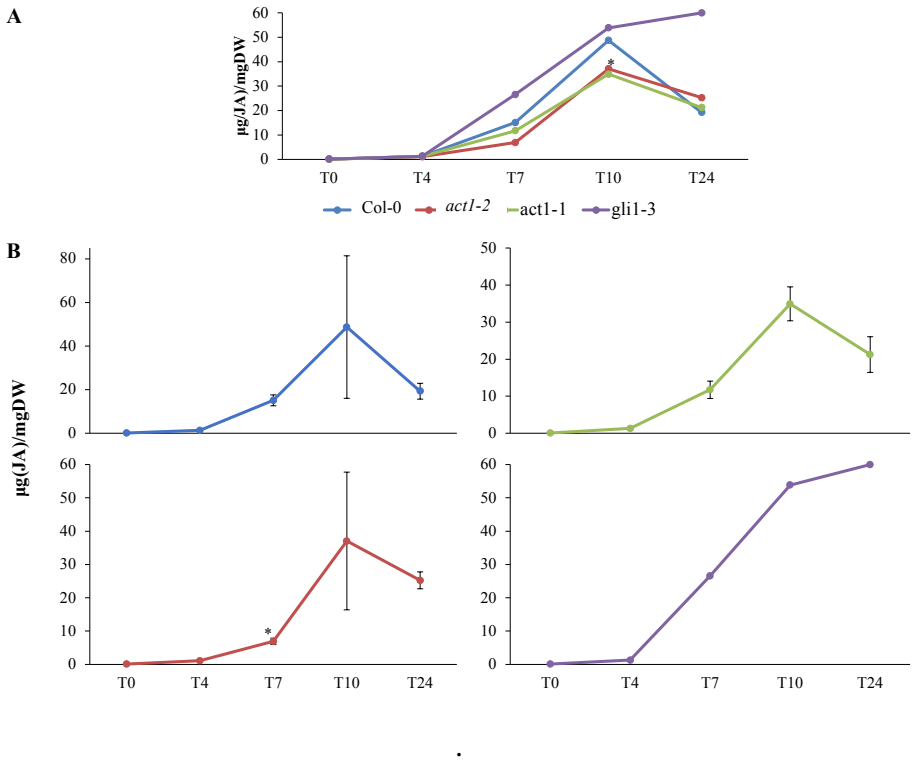

Figure 4.6: JA accumulation time course. 6 days old wild-type (Col-0), *act1-1*, *act1-2* and *gli1-3* were treated with ISX and quantified at five time points; 0 4, 7, 10 and 24 hours post treatment (T4, T7, T10 and T24, respectively). Data shown is derived from one independent experiment (**A**), with error bars based on standard deviation (n=3 biological replicates). For improved visualization of SDs, the single graph of Col-0 and G3P-mutant lines were presented individually (**B**). Asteriks indicates statistical significant difference between phytohormone levels in Col-0 and G3P-metabolism mutants, based on a two-sided Student´s t-test with 95% confidence interval (*: p <0.05, **: p < 0.01, ***: p < 0.001)

Similar to JA, SA levels began to increase between 4 and 7 hours after start of ISX treatment in Col-0 seedlings (Figure 4.7). SA levels in *act1-1* and *act1-2* were similar to Col-0 at all time points examined and showed a similar dynamic like JA. In *gli1-3* SA levels showed a similar trend between T0 and T10 but seemed to increase further until T24.

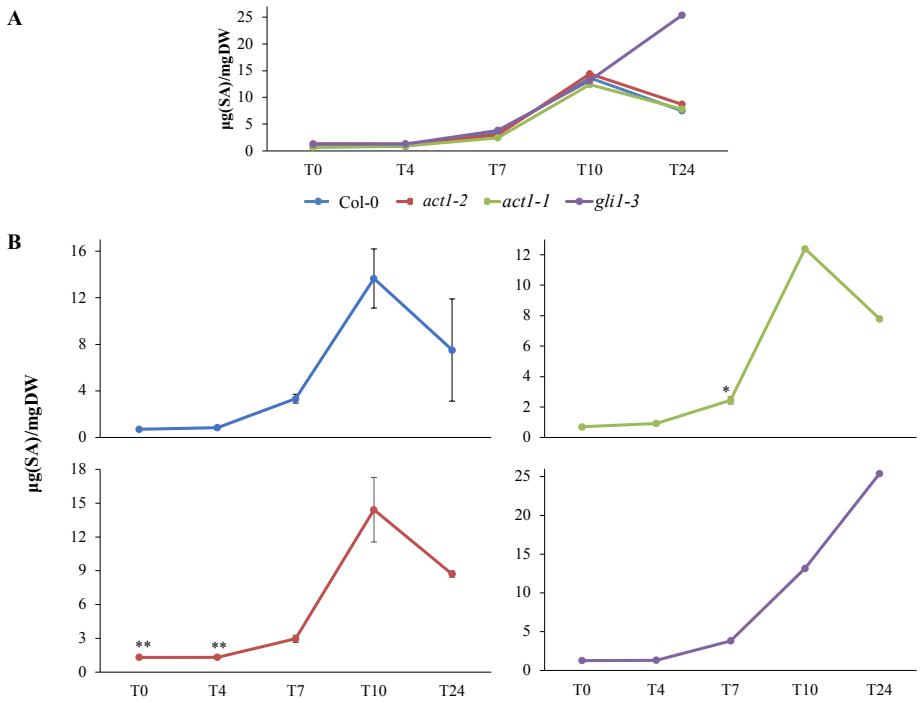

Figure 4.7: SA accumulation time course.6 days old wild-type (Col-0), *act1-1*, *act1-2* and *gli1-3* were treated with ISX and quantified at five time points; 0 4, 7, 10 and 24 hours post treatment (T4, T7, T10 and T24, respectively). Data shown is derived from one independent experiment (**A**), with error bars based on standard deviation (n=3 biological replicates). For improved visualization of SDs, the single graph of Col-0 and G3P-mutant lines were presented individually (**B**). Asteriks indicates statistical significant difference between phytohormone levels in Col-0 and G3P-metabolism mutants, based on a two-sided Student´s t-test with 95% confidence interval (*: p <0.05, **: p < 0.01, ***: p < 0.001)

To summarize, JA and SA levels started to increase after 4 hours of ISX-treatment both in Col-0 and the G3P-metabolism mutants, making T7 a suitable time point for phytohormone measurements. Interestingly, JA and SA pools seemed to be reduced between 10 and 24 hours in Col-0, *act1-1* and *act1-2* seedlings, contrary to *gli1-3*, where they apparently continued to increase. However, since the *gli1-3* data is based on a single sample this result needs to be treated with caution.

4.2.3 Lignification assay to investigate effects of ISX on lignin synthesis and deposition

Previous studies have shown that CWD induced by ISX starts to cause lignin deposition in primary roots of *A. thaliana* seedlings after 6 hours of treatment and the deposition continues to increase (Hamann et al., 2009). To determine if genes involved in G3P-metabolism affected lignin deposition, time course experiments were performed again, examining lignin deposition in Col-0 and G3P metabolism mutants treated with mock or ISX for 24 hours. Lignin deposition

was analyzed both qualitatively (visual inspection) and quantitatively (image analysis). Mock-treated seedlings did not exhibit a detectable deposition in cell walls in the root elongation zone, while ISX treatment caused the characteristic phenotype of highly lignified root elongation zone with bulged cells in both Col-0 and G3P-metabolism mutants (Figure 4.8). However, results from the three experiments performed showed variability in extent of lignification, which is particularly obvious when ISX-treated Col-0 from experiment 2 is compared against the Col-0 controls from experiment 1 and 3.

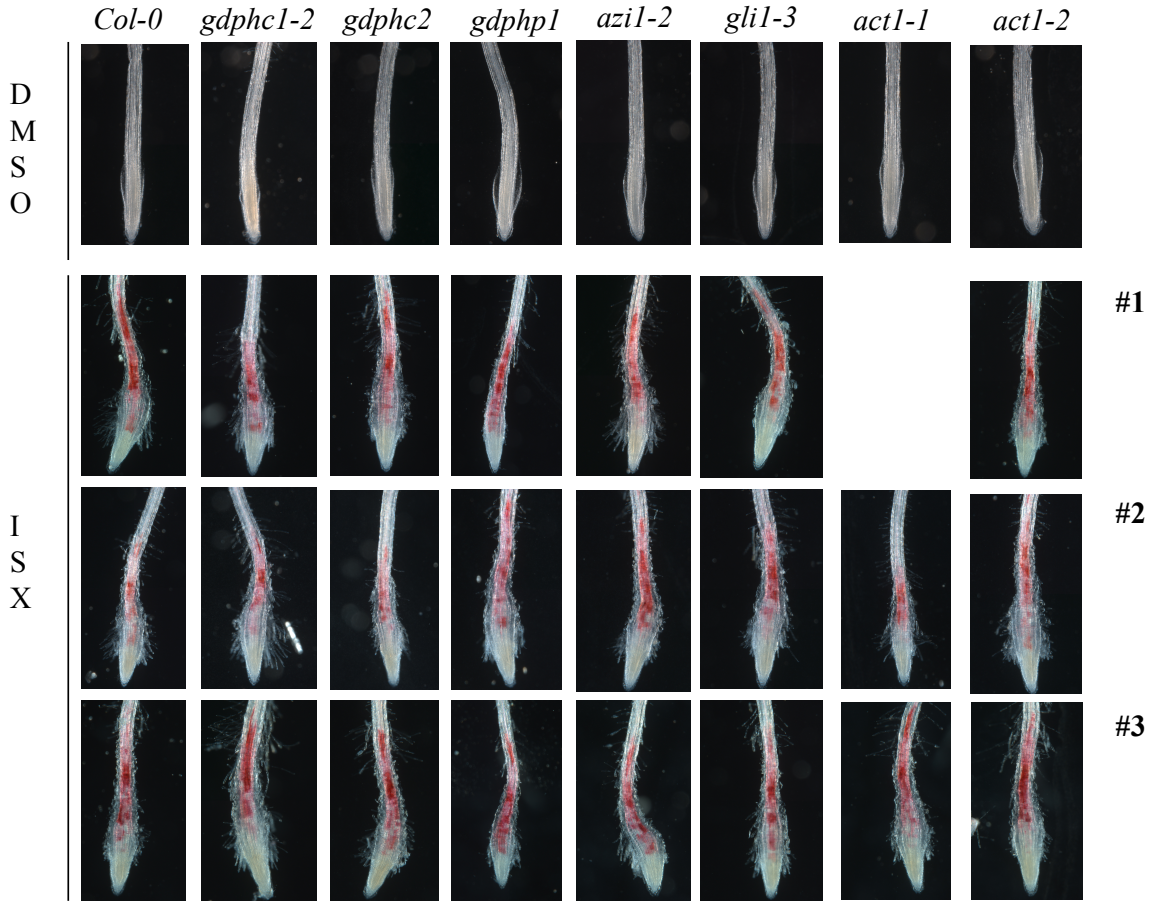

Figure 4.8: Image-based analysis of lignin deposition.6 days old Col-0 and G3P-metabolism mutant seedlings were exposed to ISX or mock conditions (DMSO) for 24 hours. Lignin was detected with phoroglucinol (red stain). # indicates experiment number.

The extent of lignification (stained area vs. total root area) was quantified using a script-based macro in the ImageJ software analogue; Fiji (Schindelin et al., 2012). Due to no observed lignification of primary roots in DMSO-treated Col-0 and G3P-metabolism mutants, these images was not included in the analysis. Figure 4.9, shows the results of the image analysis. The extent of lignification were similar to Col-0 in all G3P-metabolism mutant lines similar to Col-0, suggesting that none of the genes involved in G3P-metabolism is required for ISX-induced lignin deposition in primary seedling roots. While increased lignification was observed for

gpdhc2, *azi1-2* and *gli1-3* in single experiments, this data was not reproducible.

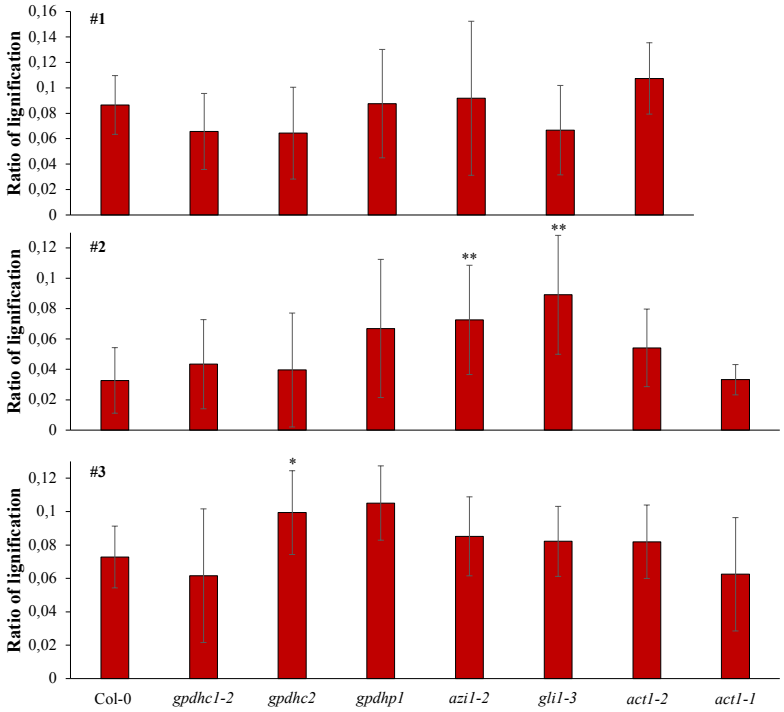

Figure 4.9: Quantitative analysis of lignin depositin. 6 days old Col-0 and G3P-metabolism mutant seedlings exposed ISX or mock conditions for 24 hours. Data is retrieved from three independent experiments (#1-#3). Extent of lignification is presented as means, with error bars based on standard deviations (n= 8-10 seedling roots). Asteriks indicate statistical significant differences regarding extent of lignification, based on a two-sided Student´s t-test with 95% confidence interval. (*: $p < 0.05$, **: $p < 0.01$).

4.2.4 Gene-expression analysis to investigate effects of ISX and hyperosmotic treatments on cell division

ISX inhibits cellulose biosynthesis (Desprez et al., 2002), a central component in cell growth and -division. A recently performed detailed gene expression analysis showed that *CYCD3;1*; regulating the G1-S transition, and *CYCB1;1*; controlling the transition from G2-to-M phase, were negatively affected by ISX-induced cell wall damage, with reduced expression levels after 9 hours treatment Gigli-Bisceglia et al. (2018). Intriguingly, these effects were attenuated by co-treatments with sorbitol.

G3P-metabolism and *FAD-GPDH* have been previously associate with cell-cycle regulations, with as a contributor (Hu et al., 2014). To determine involved in the additional G3P-metabolism may be required for the ISX-induced osmo-sensitive effects on cyclin expression, a gene-expression analysis was performed. Due to time limitations, only two representative mu-

tants (*gdphc1-2* and *gdphp1*) were selected for this investigation, which were chosen based on the phytohormone data, suggesting that they might be required for sorbitol-based suppression of ISX-induced CWD response (Chapter 3.2.2). A time course experiment was performed as described in the material and methods section and changes in *CYCD3;1* and *CYCB1;1* transcript levels were quantified. To assess the quality of the qPCR reactions, melting curves and amplification curves were produced and analyzed (Taylor et al., 2010). As observed in Supplemental figure B.6.A, the melting curves of *CYCB1;1* and *CYCD3;1* expression illustrate similar melting points across all treatments and insertion lines of approximately 81,8°C and 79,5°C, respectively, and no contaminating DNA was detected in the NTC. Likewise, the melting curve of ACT2 expression illustrates a stable melting point at approximately 80,2°C. However, fluorescence was detected in the no template controls (NTCs), indicating primer-dimer formation. Supplemental figure B.7 shows amplification curves indicating fluorescence levels detected at each cycle, data used to quantify expression levels of the genes of interest (Taylor et al., 2010). *CYCB1;1* was detected in cycle 27.53 $\pm$ 0.91, *CYCD3;1* in cycle 26.49 $\pm$ 0.92, while ACT2 in cycle 21.49 $\pm$ 0.78. The double-stranded nucleotide sequences observed in NTC for *ACT2* were detected in cycle 35.82 $\pm$ 2.53, indicating low DNA amounts.

CYCB1;1 and *CYCD3;1* expression are presented relative to *ACT2* in figure 4.10. *CYCB1;1* expression levels in Col-0 were comparable across all treatments, suggesting that *CYCB1;1* expression was not affected upon ISX or hyperosmotic treatment, respectively. *gpdhc1-2* seedlings exhibited *CYCB1;1* expression levels similar to Col-0, but *CYCB1;1* expression were reduced in ISX treated *gdpgc1-2* seedlings, a response which was suppressed by sorbitol co-treatment (Figure 4.10.A; Supplemental figure B.8). Interestingly, *CYCB1;1* expression in *gdphp1* seedlings was universally higher compared to Col-0 across all treatments. Mock (DMSO) treatment of *gdphp1* resulted in more than a 3-fold higher expression of *CYCB1;1* compared to Col-0. In *gdphp1* seedlings, ISX-treatment resulted in reduced *CYCB1;1* expression compared to mock treatment, illustrating ISX-induced reduction of *CYCB1;1*. *CYCB1;1* transcript levels in ISX+Sor treated *gdphp1* were comparable to mock-induced expression levels, suggesting that the ISX-induced changes in *CYCB1;1* expression are still turgor-sensitive.

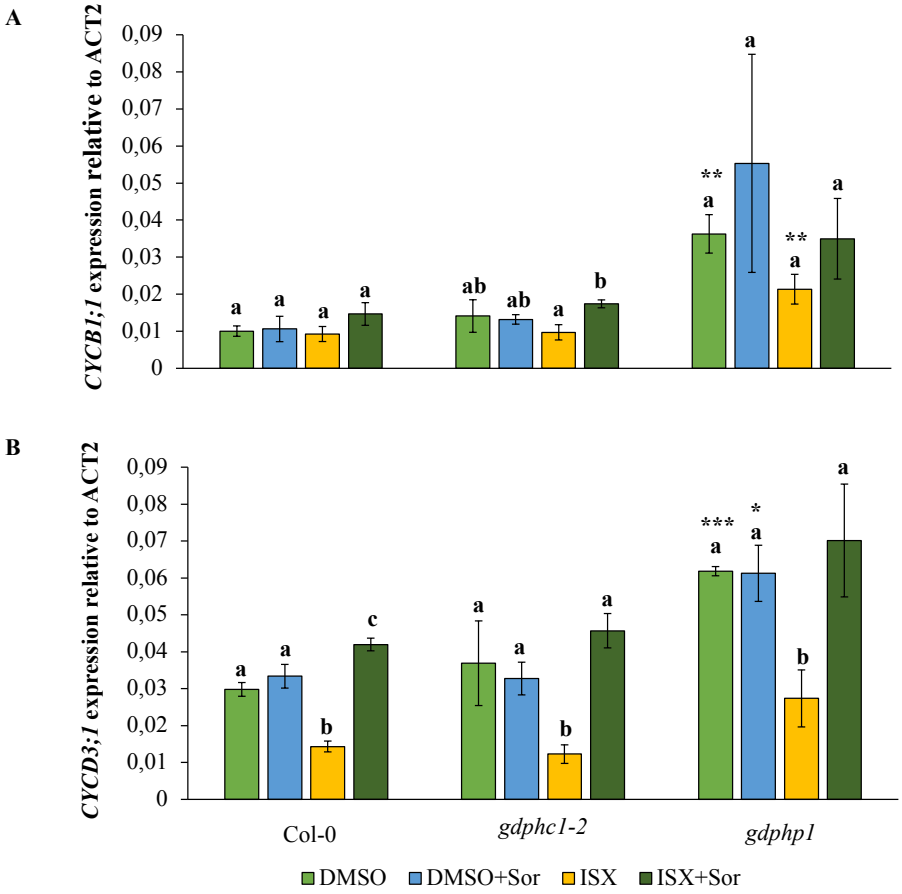

Figure 4.10: *CYCB1;1* and *CYCD3;1* expression relative to *ACT2*. 6 day-old Col-0, *gdphc1-2* and *gdphp1* seedlings were treated as described before for 9 hours. Expression of *CYCB1;1* **(A)** and *CYCD3;1* **(B)** was quantified using qPCR, and normalized to the reference gene ACT2. Error bars are based on standard deviation (n=3 parallel experiments). Different letters indicate statistical significant differences between treatments of each genotype, based on a one-way ANOVA with 95% confidence interval coupled with Tukey´s HSD post hoc test (α= 0.05). Asterisks indicate difference between expression levels in Col-0 and G3P-metabolism mutant lines, based on a two-sided Student´s t-test with 95% confidence interval. (*: $p < 0.05$, **: $p < 0.01$, ***: $p < 0.001$).

Similar to previous results, *CYCD3;1* expression levels were more sensitive to ISX-induced cellulose inhibition and osmoticum than *CYCB1;1* (Gigli-Bisceglia et al., 2018). *CYCD3;1* expression levels in sorbitol-treated Col-0 and *gdphc1-2* seedlings were similar to expression levels in mock-treated seedlings and each other (Figure 4.10.B). This implies that cell cycle progression was not affected by hyperosmotic conditions. However, in mock-treated *gdphp1* seedlings the *CYCD3;1* expression levels were already elevated compared to Col-0. In all three genotypes examined, ISX treatment induced similar reductions in expression levels while in seedlings co-treated with ISX and sorbitol expression levels were similar to mock controls (*gdphc1-2* and *gdphp1*) or even higher (Col-0) (Figure 4.10.B; Supplemental figures B.9, B.10, B.11). These results show that cellulose biosynthesis inhibition possibly negatively affects G1-to-S transition, since *CYCD3;1* is required for this transition. The data also show that *gdphc1-2*

and *gdphp1* do not affect the effects observed, suggesting that these genes are not required for the ISX effects on *CYCD3;1* expression. However, in mock-treated *gdphp1* seedlings, *CYCD3;1* levels were elevated in a similar manner like for *CYCB1;1* observed before, suggesting a role for *GDPHP1* in a process affecting cell cycle gene expression under normal conditions.

Chapter 5

Discussion

In this project, different CWD-induced responses were studied in KO-mutants of genes involved in G3P-metabolism to investigate if G3P-signalling is associated with CWI maintenance in *A. thaliana*. The CWD-induced responses studied were phytohormone accumulation (SA/JA), lignin production, resistance to ISX and changes in cell cycle gene expression. Mutations in the *Arabidopsis* lines resulted from T-DNA insertion or chemichal mutagenesis and homoyzgosity of the T-DNA lines was successfully confirmed by PCR. Results of the phenotypic analysis of the G3P-metabolism mutants suggested that G3P metabolism affects CWD induced responses, however it remains to be determined if the effects observed are direct or indirect.

5.1 G3P-metabolism gene's role in CWD-induced growth inhibition

5.1.1 Impaired G3P metabolism does not affect root growth or Isoxaben resistance

Genes and precursors associated with G3P-metabolism are also involved in other metabolic processes in plants in addition to SAR, including glycerolipid biosynthesis, glycolysis and Calvin cycle (Kunst et al., 1988; Wei et al., 2001). A root growth assay was performed to investigate if mutants deficient in such genes resulted in unspecific growth defects, which could bias analysis of the CWD-response phenotypes. All G3P-metabolism mutants exhibited primary root lengths similar to Col-0, suggesting that loss of gene activity investigated in this project did not result in phenotypic growth defects. These results were consistent with previous work, in which all G3P-metabolism mutants investigated in this project had been morphologically characterized

and were similar to Col-0 controls (Kunst et al., 1988; Xu et al., 2006; Chanda et al., 2008, 2011; Yu et al., 2013; Hu et al., 2014).

ISX inhibits production of cellulose, a major component of new cell walls to new or elongating cells (Desprez et al., 2002). Thus, ISX prevents cells from expanding, dividing and thereby stopping growth (Carpita and Gibeaut, 1993; Desprez et al., 2002). Recently, questions have been asked whether ISX also impairs growth through inhibition of central CESAs in cell wall plate formation (Chen et al., 2018). However, mutations in certain genes, such as *IXR1* and *IXR2* cause resistance to ISX treatment (Scheible et al., 2001; Desprez et al., 2002). These mutations have been characterized and shown to reside in *AtCESA3* and *AtCESA6*, respectively, which encode central proteins in the cellulose synthase complex, giving rise to cellulose deposited in forming and elongating cell walls, and are thereby not affected by ISX-based inhibition of CESA genes (Richmond and Somerville, 2000; Desprez et al., 2002). This suggests that resistance to ISX-treatment can arise, which could indicate involvement in the ISX-based inhibition process.

However, ISX-based growth inhibition was still observed in the primary root length of Col-0 and G3P-metabolism mutants treated with ISX for 24 hours. Sorbitol treatment had very similar effects on growth, indicating that hyperosmotic stress also impairs root growth. Addition of sorbitol to ISX-treatments did not attenuate root growth in Col-0 and G3P-metabolism seedlings as described before, where root length og ISX/Sor cotreated Col-0 seedlings exhibited an intermediate root length of ISX- and sorbitol-treatment (Gigli-Bisceglia et al., 2018). This might be caused by variations in conduction between experimenters in the opposing projects. Further, Col-0 seedlings exhibited similar root lengths between the two projects, but here the standard deviations were higher. Therefore, a larger sample size might be beneficial. These results indicate that loss of G3P-metabolism genes does not affect the growth or response to ISX and sorbitol. This implied that the mutations do not cause growth defects, which may have distorted the planned assays.

5.1.2 Expression analysis of cell-cycle control genes suggested that *gdphp1* seem to be associated with regulation of cell-cycle progression in response to CWD

Gigli-Bisceglia et al. (2018) have recently shown that in *A. thaliana*, ISX-induced cell wall damage reduces expression of *CYCD3;1*; which regulates the G1-S transition, and *CYCB1;1*; which controls the transition from G2-to-M phase in the cell cycle (Ito et al., 2001; Menges

et al., 2006). Based on this knowledge, effects of ISX and sorbitol on gene expression in Col-0 and G3P-metabolism mutants were studied further, by using qRT-PCR to quantify changes in expression of the same two cyclin genes characterized by Gigli-Bisceglia et al.(2018) before.

The quality control measures (incl. melting curve analysis and amplification curve analysis) performed showed that the qRT-PCR based expression analysis was functional. In Col-0, *CYCB1;1* expression levels across all treatments did not differ in seedlings mock-, ISX-, sorbitol- or ISX/sorbitol-treated. These results suggested that ISX- induced cellulose biosynthesis inhibition and hyperosmotic conditions do not affect G2-to-M transition. Recent work had shown a small but significant reduction of CYCB1;1 during ISX-treatment in Col-0 (Gigli-Bisceglia et al., 2018), which was not reproducible in this project. This may be caused by differences in handling / processing of samples performed here and in the previous experiment. Particularly it has to be noted that *CYCB1;1* expression in mock-treated Col-0 controls were two-fold lower in this work compared to Gigli-Bisceglia et al. (2018). *CYCD3;1* expression levels in Col-0 seedlings were reduced upon ISX-treatment and increased upon sorbitol co-treatment compared to mock controls, which confirmed previous results for changes in *CYCD3;1* expression levels in Col-0 (Gigli-Bisceglia et al., 2018). This indicates that ISX-induced CWD affects cell cycle progression in an osmo-sensitive manner, possibly at G1-to-S transition. Such a response was also observed in yeast, in which CWD inhibits G1-to-S transition and thereby cell cycle progression (Kono et al., 2016), suggesting yet a similarity between CWI maintenance in plants and yeast (Gigli-Bisceglia and Hamann, 2018).

Only two of the G3P metabolism mutants was examined regarding cell cycle gene expression levels because they had shown differences with respect to phytohormone levels compared to Col-0. *CYCB1;1* and *CYCD3;1* expression levels in *gdphc1-2* seedlings were similar to Col-0 across all treatments, suggesting no involvement of *GDPHC1* in the effects on cell cycle progression. However, *gdphp1* seedlings exhibited higher expression levels of *CYCB1;1* and *CYCD3;1* compared to Col-0 upon mock (DMSO)-treatment, suggesting that cell cycle activity is elevated in this mutant background. This suggests that *GDPHP1* acts as a negative regulator of G2-to-M and G1-to-S transition, and thereby cell-cycle progression and growth, under normal conditions. *GDPHP1* encodes a NAD-dependent G3P-dehydrogenase located in plastids, which uses DHAP and NADH as substrates (Wei et al., 2001). *GDPHP1* deficiency might thereby cause an intracellular increase in NADH, which was previously observed for another GPDH isoform, *GDPHC1* (Shen et al., 2006) and possibly DHAP. In chloroplasts, NADH and DHAP are a commonly used cofactors (Lambers et al., 2008). Thus, mutants exhibiting compromised *GDPHP1* may accumulate chloroplast-located DHAP and thereby exhibit increase

photosynthetic activity, leading to an enhanced production of carbohydrates, which again could lead to enhanced cell cycle activity (and growth), as shown before (Paul and Pellny, 2003). However, such a growth response was not observed at phenotypic level (root growth assay), since *gdphp1* seedlings exhibited similar root lengths compared to Col-0 at T0 and mock treatments. This might be due to experimental conduction, indicate that the cell-cycle activity is not directly regulating growth or that the expression levels of cyclins much reach a threshold level in order to successfully cause cell-cycle progression (Murray, 2004). In contrast, the other G3P-dehydrogenases investigated here (*GDPHC1*) did not show a similar regulatory role on cell-cycle progression in normal conditions as observed for *GDPHP1*. As a *GDPHC1* located in cytosol, this suggests that compartmental location might impact. As described above, *GDPHC1* deficiency cause NADH accumulation, a central co-factor in glycolysis, and increased levels of cytosolic NADH may contribute to increased activity of glycolysis, if other components are available as well. Shen et al. (2006) proposed a model of a G3P-shuttle between cytosol (*GDHC1* synthesize G3P) and mitochondria (*FAD-GDPH* reduce G3P to produce $FADH_2$), where cellular respiration might be controlled by this G3P-shuttle, and thereby growth (Kim et al., 2006). This not observed in this project. However, there excists at least one additional cytosolic GPDH (GDPHC2), which may cause redundancy.

Moreover, the expression level of *CYCB1;1* was higher in ISX-treated *gdphp1* compared to Col-0, suggesting that *GPDHP1* as a negative regulator of G2-to-M phase transition, and thereby inhibition of cell cycle progression, during cell wall damage response. Similar to Col-0 and *gdphc1-2*, expression levels of *CYCD3;1* were reduced upon ISX treatment in *gpdhp1*, which was suppressed by ISX/Sor co-treatment, showing that *GPDHP1* is not required to mediate the CWD-induced changes in *CYCD3;1* and *CYCB1;1* expression.

To summarize, ISX-induced cellulose biosynthesis inhibition downregulates central cell cycle control genes, and thereby probably inhibits cell cycle progression and plant growth, as observed in the root growth assay. The gene expression analysis detected suppression of ISX-induced downregulation of *CYCD3;1* by sorbitol co-treatment in Col-0, *gdphc1-2* and*gdphp1*. However, such a response was not observed at phenotypic levels (primary root length). This is likely due to the presence of ISX, inhibiting cellulose biosyntheis by CESAs, which prevents expansion of existing and generation of new cell walls during cell division (Desprez et al., 2002). Thus, the hyperosmotic conditions, created by sorbitol, suppress the CWD responses induced by ISX on the gene expression level, but can not prevent the inhibition of CESA, and thereby rescue growth at the phenotypic level.

5.2 G3P-metabolism gene's involvement in CWD responses

5.2.1 Impaired G3P metabolism seem to increase CWD-induced phytohormone accumulation

Another well-known response to cell wall damage in *A.thaliana* is accumulation of stress-induced phytohormones, such as JA and SA (Hamann and Denness, 2011). Cellulose biosynthesis inhibition caused by ISX resulted in accumulation of SA and JA in Col-0, confirming previously published results (Hamann et al., 2009). The G3P-metabolism mutants, with the exception of *act1-2*, exhibited the same baseline levels for SA amounts like Col-0, but exhibited even more pronounced increases than Col-0 upon ISX-treatment. This suggests that alternations in G3P metabolism negatively affect phytohormone accumulation during CWD response. Such a response indicated that either genes involved in G3P-synthesis (*GDPHC1*, *GDPHC2*, *GDPHP1*, *GLI1*) -translocation (*AZI1*) and -utilization (*ACT1*), act as negative regulators of SA accumulation during cell wall damage response, and that modifications of G3P levels, flux through the G3P pathway could amplify the ISX-induced hormone accumulation, or that unimpaired flux through the G3P pathway is required for correct regulation of the signalling response. JA levels in ISX-treated *gdphc2* seedlings were higher compared to Col-0, suggesting that *GDPHC2* might act in a similiar manner as described above on JA biosynthesis during CWD response.

A similar phytohormone-regulating response was recently shown in mutants deficient in *PEPR1* and *PEPR2*; RLKs involved in perception of the endogenous plant elicitor peptide *At*Pep1, which normally enhances defense response during PTI (Engelsdorf et al., 2017). Moreover, if ISX treatments were combined with *At*Pep1, CWD-responses such as phytohormone accumulation were suppressed in an *At*Pep1 concentration-dependent manner. Therefore, Engelsdorf et. al. conclude that PTI represses CWI maintenance mechanisms through *At*Pep1 / PEPR1/2-dependent signaling. Local defenses such as PTI and ETI is known to induce SAR (Dempsey and Klessig, 2012). Further, as a defense response towards secondary infection, SAR enhances local resistance such as PTI, illustrating interconnection between the different levels of resistance (Heil and Ton, 2008; Fu and Dong, 2013). This raises the question if the G3P-metabolism mutants may affect CWD-induced because of their involvement in SAR, which may affect PTI in turn, to prevent energy wastage upon the highly energy-consuming conditions as pathogenic attacks.

Sorbitol treatment caused elevated JA levels in Col-0 and G3P-metabolism mutant seedlings, as described before (Hamann et al., 2009), suggesting that the mild hyperosmotic conditions provided by sorbitol induce cell wall damage responses. However, sorbitol-induced cell wall

damage responses resulted in a approximately 50-fold lower JA levels compared to ISX-treatment. This indicates that ISX-induced cellulose biosynthesis inhibition results in more pronounce cell wall damage, as observed previously (Hamann et al., 2009). *GPDHC1*, *GPDHC2*, *GLI1*, *AZI1* and *ACT1* seedlings were assumed to be required in JA synthesis in response to CWD induced by hyperosmotic conditions. SA levels in Col-0 and G3P-metabolism mutant seedlings treated with sorbitol were similar to mock conditions (DMSO), suggesting that CWD provided by sorbitol-induced hyperosmotic conditions might no affect SA accumulation. However, sorbitol-based accumulation of SA have been observed previously (Hamann et al., 2009). This might be due to differences in experimental handling/processing of the samples between these two projects. A few G3P-metabolism seedlings still exhibited higher SA levels in sorbitol-treatment compared to Col-0. This might suggest that either these the differences were not based on the sorbitol treatment, or that *GDPHC2*, *AZ11* might negatively modulate, while *GLI1-3* might be required for accumulation of SA levels in response to sorbitol-induced hyperosmotic stress.

ISX/sorbitol co-treatment resulted in reduced levels of SA and JA in Col-0 and G3P-metabolism mutants compared to ISX-treatment, indicating that the previously reported suppression of cell wall damage responses by hyperosmotic conditions is reproducible (Hamann et al., 2009). Interestingly, SA and JA levels in ISX/Sorbitol co-treated *gdphc1-2* and *gdphp1* seedlings were higher compared to Col-0. This suggests that either, the suppression was not complete, implying that *GDPHC1* and *GDPHP1* might be required for sorbitol-based suppression of ISX-induced cell wall damage response, or that the elevated phytohormone levels in the mutants (compared to Col-0) lead to less pronounced reduction by sorbitol co-treatments.

The two *ACT1* mutants investigated in this project exhibited different results regarding SA accumulation, which might be due to the differences the mutant alleles have. The *act1-1* mutant is an ethyl methanesulfonate induced mutant with a G to A base change at the 5'intron-exon boarder of exon 6, while the *act1-2* mutant exhibits a T-DNA insertion at exon 10 (Kunst et al., 1988; Xu et al., 2006). This suggests, that the resulting mutants could lead to production of truncated proteins of different sizes, which could lead to different phenotypic effects, as observed in this project. *ACT1* encodes an acyl-acyl carrier protein (ACP) G3P acyltransferase (GPAT), which are involved in the procaryotic pathway of glycerolipid biosynthesis, such as phosphatidylglycerol (PD) (Kunst et al., 1988). Xu et al. (2006) have previously observed a more pronounce effect in *act1-1* seedlings compared to *act1-2* in the context of PG reduction compared to Col-0. This suggests variability in activity of the gene products in the two *ACT1* mutant lines, and might reflect the SA results observed here.

A previous pilot study had suggested that *GLI1* and *ACT1* have opposite effects on JA production during the cell wall damage response, based on measurements performed at a single time point (Engelsdorf, personal communication). Such effects were not observed in the analysis performed here. Since it was also conceivable that the G3P metabolism mutants could change the dynamics of the ISX-induced phytohormone, or that accumulation dynamics were generally different between the various experiments, a time-course experiment was performed to address this. SA and JA levels accumulated between 4 and 10 hours after start of ISX-treatment in Col-0 and the G3P-metabolism mutants investigated in a similar manner, confirming 7 hours as a suitable time point for phytohormone analysis. In Col-0, *act1-1* and *act1-2*, cellular JA and SA pools were diminished between 10 and 24 hours of ISX-treatment, highlighting the often dynamic changes in JA and SA levels and suggesting a possibly specific function for the phytohormones during the early response to CWD (Denness et al., 2011). Indeed, between 7 and 10 hours after treatment JA levels were increased in *gli1-3* and reduced in both *act1* lines compared to Col-0, supporting the initial hypothesis that reduced or increased G3P content in *gli1-3* and *act1* mutants has opposite effects on JA accumulation. At 24 hours after treatment, when levels of JA and SA continued to increase in *gli1-3*, this opposite effect was lost, supporting the notion that hormone accumulation dynamics have to be carefully considered. This suggests that *GLI1* (or G3P) may act as a negative regulator of JA and SA biosynthesis in response to cell wall damage at a later time point. However, since the dataset supporting this conclusion is limited, the experiments have to be repeated before firm conclusions can be drawn.

5.2.2 CWD-induced lignin biosynthesis was not affected by impaired G3P-metabolism

Cell wall reinforcement through synthesis and deposition of lignin has been previously reported (Caño-Delgado et al., 2003; Ellis and Turner, 2001; Denness et al., 2011). In Col-0 and G3P-metabolism mutants, ISX-treatment caused lignification in primary root tips. The extent of lignification was similar in G3P-metabolism mutants and Col-0, suggesting no requirement of G3P metabolism genes in ISX-induced lignin biosynthesis.

Lignin biosynthesis induced by CWD is regulated by ROS and JA in *A.thalina* (Hamann et al., 2009; Denness et al., 2011), in which ROS is required while JA suppresses lignin biosynthesis. Here, it was observed a lower extent of lignification for Col-0 and several of the G3P-metabolism mutant seedlings in experiment 2 compared to experiment 1 and 3. This would be assumed to be correlated with higher JA levels. Interestingly, JA levels were generally lower in

experiment 2 compared to the latter experiments. This suggests potential errors in experimental procedure or that other factors in addition to JA, which was not quantified here (e.g. ROS), impacted the lignin biosynthesis. In this project, most G3P-metabolism mutants exhibited JA levels similar to Col-0, while *gdphc2* seedlings exhibited higher JA levels. Denness et al. (2011) have previously shown that *A. thaliana* seedlings treated with ISX and exogenous MeJA (precursor of JA-Ile, a plant JA-conjugate) exhibited reduced lignin biosynthesis. However, such a response was not observed in *GDPHC2*, even though the seedlings exhibited elevated JA levels. Thus, the JA elevation was apparently not sufficient to suppress lignin biosynthesis.

5.3 Limitations of the current study

In order to critically evaluate the results presented in this project, a number of possible error sources are outlined in this section. Generally, some pronounced standard deviations (SDs) were observed, especially regarding JA levels, primary root length, the ratio of lignification and cyclin gene expression. Plants can exhibit biological variability between individuals, which will impact results and cause high standard deviations in small sample sizes. In this project, three parallel experiments with restricted sample size might therefore not be sufficient to address these problems. Further, a small sample size may lead to higher rates of false positives and negatives in statistical tests (De Winter, 2013). Therefore, a larger sample size and additional independent experiments would provide a significantly more reliable data set, which should address the limitations of the current study. A larger sample size is especially important regarding the time-course experiments where phytohormone levels were measured. This experiment included only one parallel, with three biological replicates of Col-0, *act1-1* and *act1-2*, while *gli1-3* data was obtained from a single biological replicate. This restricted sample size prevented deduction of conclusions, especially regarding *gli1-3* where the limited sample size excluded the possibility to perform statistical tests. Therefore, further studies are needed to observe if the trend is reproducible before any suggestions can be drawn.

The G3P-metabolism mutants investigated in this project, were confirmed to be homozygous using a PCR-based screening. Another well-known method used in genotyping is qRT-PCR, to screen for expression of competent mRNA of the gene of interest (Xu et al., 2006). qRT-PCR was not applied in this project to reduce time spent on screening, since all mutant lines had been characterized by qRT-PCR before to confirm loss of gene expression.

Other factors affecting results in this project is different of variations in experimental handling. Seedlings chosen for the root length- and lignification assays were supposed to be randomly selected based on similar cotyledon size to exclude seedlings with late germination phenotypes. However, selection by the experimentator might have been affected by unconscious bias, which could impact the retrieved results. In addition, some of the seedling cultures only allowed for small sample sizes due to limited plant material for the root growth- and lignification assay. Therefore, an enlarged sample size and a more standardized method for selection of the analyzed seedlings might lead to biologically more informative results.

Plant material used for lignification assays was treated with ISX for 24 hours, opposed to the previously standardized time point of 12 hours (Hamann et al., 2009). Previous work have shown already high ratio of lignification at this time point (Hamann et al., 2009). This expanded treatment period might cause saturation of lignin synthesis, which might obscure the results. Another error factor regarding lignification data includes the macro script used for image analysis, through unspecified detection or negligence of lignified root areas. To further investigate the impact of G3P-metabolism genes on lignin synthesis and deposition, it would be beneficial to repeat the lignification assay to obtain a larger sample size, and determine the lignification ratio after 12 hours of ISX treatment. Further, lignin content and composition can also be quantified through biochemical analysis, but is a more challenging method in the terms of the large sample size (Gall et al., 2017).

Inaccurate weighing of the freeze-dried plant material used in phytohormone analysis due to problems with the scales might lead to misleading cellular levels of phytohormones. However, the same weight was used for the entire sample group across all parallel experiments, possibly causing similar deficiencies in all samples. JA and SA, as stress-related hormones, are quickly synthesized and degraded to provide fast responses in plants (Bari and Jones, 2009). Thus, small variations of the $\frac{1}{2}$ MS medie during growth, ISX and sorbitol concentration during treatment and plant material harvest time may cause deviations between experiments, which was observed especially for JA in this project. In addition, as an easily degraded metabolite, minor differences in extraction buffers or incubation time during hormone-extraction might impact final JA concentration (Pandey, 2017). Such experimental varieties can impact the statistical analysis and invalidate interesting results. Therefore, further repetition of the experiments, can provide further insight of G3P-metabolism gene´s impact on various cell wall damage responses. As a note, in experiment parallel one, two samples of DMSO+Sorbitol treated *act1-2*, and DMSO-treated *Col-0* were pooled. Therefore, these data only included two biological replicates, which might impact the results.

Another error factor that might impact results retrieved in this project is contamination of the PCR-samples used in genotyping, hormone samples and cDNA/qPCR. Contamination can occur through a working with contaminated lab equipment such as pipets, storage units (Eppendorf tubes, measuring cylinders ect.), lab benches, chemicals and machines or inaccurate pipeting by forgetting to change pipet tips between handle of samples. This can lead to unwanted substances in the samples (foreign DNA or chemicals, material from other samples), which can negatively affects the results. However, with the exception of the phytohormone accumulation time course experiment, all experiments performed in this project were repeated three times and genotypes were confirmed independently between the experiments, thereby, results presented in this project are most likely reliable.

Chapter 6

Concluding remarks and future work

In this project, mutants impaired in G3P-metabolism were investigated in a CWD dependent manner to examine a potential association between G3P-metabolism (or its respective genes) and CWD responses. It was shown that impaired G3P-metabolism genes does not seem to be associated with lignin synthesis or growth inhibition (at phenotypic level) in response to ISX-induced CWD. However, the selection of genes or the resulting impaired G3P-metabolism were suggested to act as negative regulators of additional cell wall damage responses. All G3P-metabolism genes investigated here are likely repressors of SA biosynthesis during CWD response. Moreover, GPDHs are suggested to be involved in other cell wall damage responses as well, where *GDPHC2* and *GDPHP1* seem to negatively regulate JA biosynthesis, and cell-cycle inhibition, respectively. As recently described, PTI suppresses CWI maintenance mechanism through repression of CWD responses such as phytohormone accumulation. This raises the questions if a similar inhibitory effect of SAR on CWI maintenance mechanism through G3P metabolism or if the G3P-metabolism genes may affect CWD-induced responses by gene activity or G3P-flux modifications because of their involvement in SAR, which may affect PTI in turn.

Future work

Data collected during this project provided new insights into a potential association of G3P metabolism and the cell wall integrity maintenance mechanism. However, only a small piece of the puzzle has been explored. In order to gain further knowledge, several other aspects need to be investigated. KOs for *DIR1*, *GLY1* and *FAD-GPDH* were not included in this analysis, therefore the analysis is currently incomplete. So the immediate next step would be to investigate their role in cell wall damage responses (with similar experimental set up as described here) to examine if a similar negative regulatory effect on CWD responses is observed for these mutants as well.

As mentioned before, the time course experiment of phytohormone accumulation was performed only once (even if 3 biological replicates were used for most time points), thus providing limited data. Therefore, repetition of the experiment, including an increase of the sample size, will be necessary to confirm the results generated so far. In addition, only a subset of the genes of interest was investigated. Therefore, *gdphc1-2*, *gdphc2*, *gdphp1*, *azi1-2*, *fad-gdhp*, *dir1* and *gly1* should be included in the follow up experiments. This will resolve the function of G3P-metabolism in ISX-induced JA and SA production and the dynamics of the process.

Even though data from this thesis provided extended knowledge of the potential role of genes involved in G3P-metabolism in cell wall integrity maintenance, little is known of how the activity of G3P-synthesizing enzymes or G3P-pools are affected by cell wall damage. Therefore, the second part of this thesis, which has not been be studied so far, should be actually undertaken in the future. These experiments should include development and application of G3P and glycerol quantification assay to investigate intracellular G3P and glycerol pools, and an enzyme activity assay of G3Psynthesizing enzymes including glycerol kinase (*GLI1*) and G3P dehydrogenases (GDPH isoforms). In this thesis, a glycerol kinase activity assay was already established, but not fully tested (Appendix C). Moreover, a G3P and glycerol quantification assay would be beneficial to investigate how intracellular G3P and glycerol pools are affected by CWD. These assays should then be performed with material generated in the same manner as for the phytohormone measurements. This, combinded with G3P-metabolism gene´s associations with CWD response retrieved in this project, can provide further insight in connections between G3P-metabolism and the CWI maintenance mechanism.

Lastly, to investigate associations between SAR and CWI maintenance mechanism, a similar set-up as described in Engelsdorf et al. (2017) can be performed. This involves examination of Col-0 seedlings treated with ISX vs. co-treatment with ISX/driselase (mix of cell wall degrading enzymes) and a concentration gradient of a PAMP/DAMP known to induce SAR, followed by observation of CWD-responses such as phytohormone accumulation in Col-0 seedlings, with plant material generated in a similar manner as described here.

Bibliography

Akaike, H. (1974). A new look at the statistical model identification. *IEEE transactions on automatic control*, 19(6):716–723.

Bacete, L., Mélida, H., Miedes, E., and Molina, A. (2018). Plant cell wall-mediated immunity: cell wall changes trigger disease resistance responses. *The Plant Journal*, 93(4):614–636.

Bari, R. and Jones, J. D. (2009). Role of plant hormones in plant defence responses. *Plant molecular biology*, 69(4):473–488.

Bechtold, N. and Pelletier, G. (1998). In planta agrobacteriummediated transformation of adult arabidopsis thaliana plants by vacuum infiltration. In *Arabidopsis protocols*, pages 259–266. Springer.

Bellincampi, D., Cervone, F., and Lionetti, V. (2014). Plant cell wall dynamics and wall-related susceptibility in plant–pathogen interactions. *Frontiers in Plant Science*, 5:228.

Bolognesi, C. and Morasso, G. (2000). Genotoxicity of pesticides: potential risk for consumers. *Trends in Food Science & Technology*, 11(4-5):182–187.

Boutrot, F. and Zipfel, C. (2017). Function, discovery, and exploitation of plant pattern recognition receptors for broad-spectrum disease resistance. *Annual review of Phytopathology*, 55:257–286.

Brody, J. R. and Kern, S. E. (2004). History and principles of conductive media for standard dna electrophoresis. *Analytical biochemistry*, 333(1):1–13.

Brutus, A., Sicilia, F., Macone, A., Cervone, F., and De Lorenzo, G. (2010). A domain swap approach reveals a role of the plant wall-associated kinase 1 (wak1) as a receptor of oligogalacturonides. *Proceedings of the National Academy of Sciences*, 107(20):9452–9457.

Bustin, S. A. (2000). Absolute quantification of mrna using real-time reverse transcription polymerase chain reaction assays. *Journal of molecular endocrinology*, 25(2):169–193.

Caño-Delgado, A., Penfield, S., Smith, C., Catley, M., and Bevan, M. (2003). Reduced cellulose synthesis invokes lignification and defense responses in arabidopsis thaliana. *The Plant Journal*, 34(3):351–362.

Carpita, N. C. and Gibeaut, D. M. (1993). Structural models of primary cell walls in flowering plants: consistency of molecular structure with the physical properties of the walls during growth. *The Plant Journal*, 3(1):1–30.

Cecchini, N. M., Steffes, K., Schläppi, M. R., Gifford, A. N., and Greenberg, J. T. (2015). Arabidopsis azi1 family proteins mediate signal mobilization for systemic defence priming. *Nature communications*, 6:7658.

Chanda, B., Venugopal, S. C., Kulshrestha, S., Navarre, D. A., Downie, B., Vaillancourt, L., Kachroo, A., and Kachroo, P. (2008). Glycerol-3-phosphate levels are associated with basal resistance to the hemibiotrophic fungus colletotrichum higginsianum in arabidopsis. *Plant Physiology*, 147(4):2017–2029.

Chanda, B., Xia, Y., Mandal, M. K., Yu, K., Sekine, K., Gao, Q.-m., Selote, D., Hu, Y., Stromberg, A., Navarre, D., Kachroo, A., and Kachroo, P. (2011). Glycerol-3-phosphate is a critical mobile inducer of systemic immunity in plants. *Nature Genetics*, 43(5):421–427.

Chen, H.-W., Persson, S., Grebe, M., and McFarlane, H. E. (2018). Cellulose synthesis during cell plate assembly. *Physiologia plantarum*.

Clough, S. J. and Bent, A. F. (1998). Floral dip: a simplified method foragrobacterium-mediated transformation ofarabidopsis thaliana. *The plant journal*, 16(6):735–743.

Conrath, U. (2011). Molecular aspects of defence priming. *Trends in plant science*, 16(10):524–531.

Cosgrove, D. J. (2005). Growth of the plant cell wall. *Nature Reviews Molecular Cell Biology*, 6(11):850–861.

Couto, D. and Zipfel, C. (2016). Regulation of pattern recognition receptor signalling in plants. *Nature Reviews Immunology*, 16(9):537.

Dangl, J. L. and Jones, J. D. G. (2001). Plant pathogens and integrated defence responses to infection. *Nature*, 411:826–833.

Davin, L. B. and Lewis, N. G. (2005). Lignin primary structures and dirigent sites. *Current Opinion in Biotechnology*, 16(4):407–415.

De Winter, J. C. (2013). Using the student's t-test with extremely small sample sizes. *Practical Assessment, Research & Evaluation*, 18(10).

Dempsey, D. A. and Klessig, D. F. (2012). Sos – too many signals for systemic acquired resistance? *Trends in Plant Science*, 17(9):538 – 545.

Denness, L., McKenna, J. F., Segonzac, C., Wormit, A., Madhou, P., Bennett, M., Mansfield, J., Zipfel, C., and Hamann, T. (2011). Cell wall damage-induced lignin biosynthesis is regulated by a reactive oxygen species-and jasmonic acid-dependent process in arabidopsis. *Plant Physiology*, 156(3):1364–1374.

Desprez, T., Vernhettes, S., Fagard, M., Refrégier, G., Desnos, T., Aletti, E., Py, N., Pelletier, S., and Höfte, H. (2002). Resistance against herbicide isoxaben and cellulose deficiency caused by distinct mutations in same cellulose synthase isoform cesa6. *Plant physiology*, 128(2):482–490.

Ding, Y., Sun, T., Ao, K., Peng, Y., Zhang, Y., Li, X., and Zhang, Y. (2018). Opposite roles of salicylic acid receptors npr1 and npr3/npr4 in transcriptional regulation of plant immunity. *Cell*.

Doblin, M. S., Kurek, I., Jacob-Wilk, D., and Delmer, D. P. (2002). Cellulose biosynthesis in plants: from genes to rosettes. *Plant and cell physiology*, 43(12):1407–1420.

Durrant, W. and Dong, X. (2004). systemic acquired resistance. *Annual Review of Phytopathology*, 42(1):185–209.

Edwards, K., Johnstone, C., and Thompson, C. (1991). A simple and rapid method for the preparation of plant genomic dna for pcr analysis. *Nucleic Acids Research*, 19(6):1349.

Ellis, C. and Turner, J. G. (2001). The arabidopsis mutant cev1 has constitutively active jasmonate and ethylene signal pathways and enhanced resistance to pathogens. *The Plant Cell*, 13(5):1025–1033.

Engelsdorf, T., Gigli-Bisceglia, N., Veerabagu, M., McKenna, J. F., Augstein, F., van der Does, D., Zipfel, C., and Hamann, T. (2017). Pattern-triggered immunity and cell wall integrity maintenance jointly modulate plant stress responses. *bioRxiv*, page 130013.

Engelsdorf, T. and Hamann, T. (2014). An update on receptor-like kinase involvement in the maintenance of plant cell wall integrity. *Annals of botany*, 114(6):1339–1347.

Ferrari, S., Galletti, R., Vairo, D., Cervone, F., and De Lorenzo, G. (2006). Antisense expression of the arabidopsis thaliana atpgip1 gene reduces polygalacturonase-inhibiting protein accumulation and enhances susceptibility to botrytis cinerea. *Molecular Plant-Microbe Interactions*, 19(8):931–936.

Forcat, S., Bennett, M. H., Mansfield, J. W., and Grant, M. R. (2008). A rapid and robust method for simultaneously measuring changes in the phytohormones aba, ja and sa in plants following biotic and abiotic stress. *Plant Methods*, 4(1):16.

Fu, Z. Q. and Dong, X. (2013). Systemic acquired resistance: turning local infection into global defense. *Annual review of plant biology*, 64:839–863.

Gall, D. L., Ralph, J., Donohue, T. J., and Noguera, D. R. (2017). Biochemical transformation of lignin for deriving valued commodities from lignocellulose. *Current opinion in biotechnology*, 45:120–126.

Gao, Q.-m., Kachroo, A., and Kachroo, P. (2014). Chemical inducers of systemic immunity in plants. *Journal of Experimental Botany*, 65(7):1849–1855.

Gee, R. W., Byerrum, R. U., Gerber, D. W., and Tolbert, N. (1988). Dihydroxyacetone phosphate reductase in plants. *Plant physiology*, 86(1):98–103.

Gibon, Y., Blaesing, O. E., Hannemann, J., Carillo, P., Höhne, M., Hendriks, J. H., Palacios, N., Cross, J., Selbig, J., and Stitt, M. (2004). A robot-based platform to measure multiple enzyme activities in arabidopsis using a set of cycling assays: comparison of changes of enzyme activities and transcript levels during diurnal cycles and in prolonged darkness. *The Plant Cell*, 16(12):3304–3325.

Gibon, Y., Vigeolas, H., Tiessen, A., Geigenberger, P., and Stitt, M. (2002). Sensitive and high throughput metabolite assays for inorganic pyrophosphate, adpglc, nucleotide phosphates, and glycolytic intermediates based on a novel enzymic cycling system. *The Plant Journal*, 30(2):221–235.

Gigli-Bisceglia, N., Engelsdorf, T., Strnad, M., Vaahtera, L., Jamoune, A., Alipanah, L., Novak, O., Hejatko, J., and Hamann, T. (2018). Cellulose biosynthesis inhibition reduces cell cycle activity in a nitrate reductase-and cytokinin-dependent manner. *bioRxiv*, page 286161.

Gigli-Bisceglia, N. and Hamann, T. (2018). Outside-in control–does plant cell wall integrity regulate cell cycle progression? *Physiologia plantarum*.

Godfray, H. C. J., Beddington, J. R., Crute, I. R., Haddad, L., Lawrence, D., Muir, J. F., Pretty, J., Robinson, S., Thomas, S. M., and Toulmin, C. (2010). Food security: the challenge of feeding 9 billion people. *Science*, 327(5967):812–818.

Gust, A. A., Pruitt, R., and Nürnberger, T. (2017). Sensing danger: Key to activating plant immunity. *Trends in plant science*, 22(9):779–791.

Hamann, T. (2015a). The plant cell wall integrity maintenance mechanism–a case study of a cell wall plasma membrane signaling network. *Phytochemistry*, 112:100–109.

Hamann, T. (2015b). The plant cell wall integrity maintenance mechanism—concepts for organization and mode of action. *Plant and Cell Physiology*, 56(2):215–223.

Hamann, T., Bennett, M., Mansfield, J., and Somerville, C. (2009). Identification of cell-wall stress as a hexose-dependent and osmosensitive regulator of plant responses. *The Plant Journal*, 57(6):1015–1026.

Hamann, T. and Denness, L. (2011). Cell wall integrity maintenance in plants: Lessons to be learned from yeast? *Plant Signaling & Behavior*, 6(11):1706–1709.

Haynes, W. (2013). Student's t-test. In *Encyclopedia of Systems Biology*, pages 2023–2025. Springer.

Heil, M. and Ton, J. (2008). Long-distance signalling in plant defence. *Trends in plant science*, 13(6):264–272.

Hu, J., Zhang, Y., Wang, J., and Zhou, Y. (2014). Glycerol affects root development through regulation of multiple pathways in arabidopsis. *PLOS ONE*, 9(1):1–18.

Huot, B., Yao, J., Montgomery, B. L., and He, S. Y. (2014). Growth–defense tradeoffs in plants: a balancing act to optimize fitness. *Molecular plant*, 7(8):1267–1287.

Ito, M., Araki, S., Matsunaga, S., Itoh, T., Nishihama, R., Machida, Y., Doonan, J. H., and Watanabe, A. (2001). G2/m-phase–specific transcription during the plant cell cycle is mediated by c-myb–like transcription factors. *The Plant Cell*, 13(8):1891–1905.

Iwai, H., Masaoka, N., Ishii, T., and Satoh, S. (2002). A pectin glucuronyltransferase gene is essential for intercellular attachment in the plant meristem. *Proceedings of the National Academy of Sciences*, 99(25):16319–16324.

Jain, D. and Khurana, J. P. (2018). Role of pathogenesis-related (pr) proteins in plant defense mechanism. In *Molecular Aspects of Plant-Pathogen Interaction*, pages 265–281. Springer.

Jaskiewicz, M., Conrath, U., and Peterhänsel, C. (2011). Chromatin modification acts as a memory for systemic acquired resistance in the plant stress response. *EMBO reports*, 12(1):50–55.

Jones, J. D. G. and Dangl, J. L. (2006). The plant immune system. *Nature*, 444:323–329.

Jung, H. W., Tschaplinski, T. J., Wang, L., Glazebrook, J., and Greenberg, J. T. (2009). Priming in systemic plant immunity. *Science*, 324(5923):89–91.

Kachroo, A. and Robin, G. P. (2013). Systemic signaling during plant defense. *Current opinion in plant biology*, 16(4):527–533.

Kadota, Y., Sklenar, J., Derbyshire, P., Stransfeld, L., Asai, S., Ntukakis, V., Jones, J. D., Shirasu, K., Menke, F., Jones, A., and Zipfel, C. (2014). Direct regulation of the nadph oxidase rbohd by the prr-associated kinase bik1 during plant immunity. *Molecular Cell*, 54(1):43–55.

Keegstra, K. (2010). Plant cell walls. *Plant physiology*, 154(2):483–486.

Keppel, G. and Wickens, T. (2004). Simultaneous comparisons and the control of type i errors. *Design and analysis: A researcher's handbook. 4th ed. Upper Saddle River (NJ): Pearson Prentice Hall. p*, pages 111–130.

Keshun, Y., Juliana Moreira, S., Mihir Kumar, M., Caixia, W., Bidisha, C., Andrew N., G., Joanna S., F., Duroy, N., Aardra, K., and Pradeep, K. (2013). A feedback regulatory loop between g3p and lipid transfer proteins dir1 and azi1 mediates azelaic-acid-induced systemic immunity. *Cell Reports*, 3(4):1266 – 1278.

Kim, S.-Y., Sivaguru, M., and Stacey, G. (2006). Extracellular atp in plants. visualization, localization, and analysis of physiological significance in growth and signaling. *Plant physiology*, 142(3):984–992.

Kolpin, D. W., Thurman, E. M., and Linhart, S. (1998). The environmental occurrence of herbicides: the importance of degradates in ground water. *Archives of Environmental Contamination and Toxicology*, 35(3):385–390.

Kono, K., Al-Zain, A., Schroeder, L., Nakanishi, M., and Ikui, A. E. (2016). Plasma membrane/cell wall perturbation activates a novel cell cycle checkpoint during g1 in saccharomyces cerevisiae. *Proceedings of the National Academy of Sciences*, 113(25):6910–6915.

Krysan, P. J., Young, J. C., and Sussman, M. R. (1999). T-dna as an insertional mutagen in arabidopsis. *The Plant Cell*, 11(12):2283–2290.

Kunst, L., Somerville, C., et al. (1988). Altered regulation of lipid biosynthesis in a mutant of arabidopsis deficient in chloroplast glycerol-3-phosphate acyltransferase activity. *Proceedings of the National Academy of Sciences*, 85(12):4143–4147.

Lambers, H., Chapin, F. S., and Pons, T. L. (2008). *Photosynthesis*. Springer.

Lim, G.-H., Shine, M., de Lorenzo, L., Yu, K., Cui, W., Navarre, D., Hunt, A. G., Lee, J.-Y., Kachroo, A., and Kachroo, P. (2016). Plasmodesmata localizing proteins regulate transport and signaling during systemic acquired immunity in plants. *Cell host & microbe*, 19(4):541–549.

Liu, H., Li, X., Xiao, J., and Wang, S. (2012). A convenient method for simultaneous quantification of multiple phytohormones and metabolites: application in study of rice-bacterium interaction. *Plant methods*, 8(1):2.

McFarlane, H. E., Döring, A., and Persson, S. (2014). The cell biology of cellulose synthesis. *Annual Review of Plant Biology*, 65(1):69–94.

Melotto, M., Underwood, W., and He, S. Y. (2008). Role of stomata in plant innate immunity and foliar bacterial diseases. *Annual Review of Phytopathology*, 46(1):101–122. PMID: 18422426.

Mendgen, K. and Hahn, M. (2002). Plant infection and the establishment of fungal biotrophy. *Trends in Plant Science*, 7(8):352 – 356.

Menges, M., Samland, A. K., Planchais, S., and Murray, J. A. (2006). The d-type cyclin cycd3; 1 is limiting for the g1-to-s-phase transition in arabidopsis. *The Plant Cell*, 18(4):893–906.

Morel, J.-B. and Dangl, J. L. (1997). The hypersensitive response and the induction of cell death in plants. *Cell Death And Differentiation*, 4:671–683.

Morrison, T. B., Weis, J. J., and Wittwer, C. T. (1998). Quantification of low-copy transcripts by continuous sybr green i monitoring during amplification. *Biotechniques*, 24(6):954–8.

Mou, Z., Fan, W., and Dong, X. (2003). Inducers of plant systemic acquired resistance regulate npr1 function through redox changes. *Cell*, 113(7):935–944.

Moura, J. C. M. S., Bonine, C. A. V., De Oliveira Fernandes Viana, J., Dornelas, M. C., and Mazzafera, P. (2010). Abiotic and biotic stresses and changes in the lignin content and composition in plants. *Journal of Integrative Plant Biology*, 52(4):360–376.

Mullis, K., Faloona, F., Scharf, S., Saiki, R., Horn, G., and H., E. (1986). Specific enzymatic amplification of dna in vitro: The polymerase chain reaction. *Cold Spring Harbor Symposia of Quantitative Biology*, 51:263–273.

Murray, A. W. (2004). Recycling the cell cycle: cyclins revisited. *Cell*, 116(2):221–234.

Návarová, H., Bernsdorff, F., Döring, A.-C., and Zeier, J. (2012). Pipecolic acid, an endogenous mediator of defense amplification and priming, is a critical regulator of inducible plant immunity. *The Plant Cell*, 24(12):5123–5141.

Nurnberger, T., Brunner, F., Kemmerling, B., and Piater, L. (2004). Innate immunity in plants and animals: striking similarities and obvious differences. *Immunological Reviews*, 198(1):249–266.

Oerke, E.-C. (2006). Crop losses to pests. *The Journal of Agricultural Science*, 144(1):31–43.

Pandey, G. K. (2017). *Mechanism of Plant Hormone Signaling Under Stress, 2 Volume Set*, volume 1. John Wiley & Sons.

Paul, M. J. and Pellny, T. K. (2003). Carbon metabolite feedback regulation of leaf photosynthesis and development. *Journal of experimental botany*, 54(382):539–547.

Peng, J., Elias, J. E., Thoreen, C. C., Licklider, L. J., and Gygi, S. P. (2003). Evaluation of multidimensional chromatography coupled with tandem mass spectrometry (lc/lc- ms/ms) for large-scale protein analysis: the yeast proteome. *Journal of proteome research*, 2(1):43–50.

Pessarakli, M. (2016). *Handbook of plant and crop stress*. CRc press.

Pimentel, D. and Edwards, C. A. (1982). Pesticides and ecosystems. *BioScience*, 32(7):595–600.

Pomar, F., Merino, F., and Barceló, A. R. (2002). O-4-linked coniferyl and sinapyl aldehydes in lignifying cell walls are the main targets of the wiesner (phloroglucinol-hcl) reaction. *Protoplasma*, 220(1-2):0017–0028.

Quettier, A.-L., Shaw, E., and Eastmond, P. J. (2008). Sugar-dependent6 encodes a mitochondrial flavin adenine dinucleotide-dependent glycerol-3-p dehydrogenase, which is required for glycerol catabolism and postgerminative seedling growth in arabidopsis. *Plant physiology*, 148(1):519–528.

Ray, D. K., Mueller, N. D., West, P. C., and Foley, J. A. (2013). Yield trends are insufficient to double global crop production by 2050. *PloS one*, 8(6):e66428.

Richmond, T. A. and Somerville, C. R. (2000). The cellulose synthase superfamily. *Plant physiology*, 124(2):495–498.

Rio, D. C. (2014). Reverse transcription–polymerase chain reaction. *Cold Spring Harbor Protocols*, 2014(11):pdb–prot080887.

Ruijter, J., Ramakers, C., Hoogaars, W., Karlen, Y., Bakker, O., Van den Hoff, M., and Moorman, A. (2009). Amplification efficiency: linking baseline and bias in the analysis of quantitative pcr data. *Nucleic acids research*, 37(6):e45–e45.

Saiki, R. K., Gefald, G. H., Stoffel, S., Higuchi, R., Horn, G. T., Mullis, K. B., and Erlich, H. A. (1988). Primer-directed enzymatic amplification of dna with a thermostable dna polymerase. *Science*, 239(4939).

Scheible, W.-R., Eshed, R., Richmond, T., Delmer, D., and Somerville, C. (2001). Modifications of cellulose synthase confer resistance to isoxaben and thiazolidinone herbicides in arabidopsis ixr1 mutants. *Proceedings of the National Academy of Sciences*, 98(18):10079–10084.

Schindelin, J., Arganda-Carreras, I., Frise, E., Kaynig, V., Longair, M., Pietzsch, T., Preibisch, S., Rueden, C., Saalfeld, S., Schmid, B., Tinevez, J.-Y., White, D., Hartenstein, V., Eliceiri, K., Tomancak, P., and Cardona, A. (2012). Fiji: an open-source platform for biological-image analysis. *Nature Methods*, 9(7):676–682.

Segarra, G., Jáuregui, O., Casanova, E., and Trillas, I. (2006). Simultaneous quantitative lc–esi-ms/ms analyses of salicylic acid and jasmonic acid in crude extracts of cucumis sativus under biotic stress. *Phytochemistry*, 67(4):395–401.

Seybold, H., Trempel, F., Ranf, S., Scheel, D., Romeis, T., and Lee, J. (2014). Ca2+ signalling in plant immune response: from pattern recognition receptors to ca2+ decoding mechanisms. *New Phytologist*, 204(4):782–790.

Shah, J. and Zeier, J. (2013). Long-distance communication and signal amplification in systemic acquired resistance. *Frontiers in Plant Science*, 4:30.

Shen, W., Wei, Y., Dauk, M., Tan, Y., Taylor, D. C., Selvaraj, G., and Zou, J. (2006). Involvement of a glycerol-3-phosphate dehydrogenase in modulating the nadh/nad+ ratio provides evidence of a mitochondrial glycerol-3-phosphate shuttle in arabidopsis. *The Plant Cell*, 18(2):422–441.

Snyder, L. R., Kirkland, J. J., and Dolan, J. W. (2011). *Introduction to modern liquid chromatography*. John Wiley & Sons.

Southern, E. M. et al. (1975). Detection of specific sequences among dna fragments separated by gel electrophoresis. *J mol biol*, 98(3):503–517.

Stokvis, E., Rosing, H., and Beijnen, J. H. (2005). Stable isotopically labeled internal standards in quantitative bioanalysis using liquid chromatography/mass spectrometry: necessity or not? *Rapid Communications in Mass Spectrometry*, 19(3):401–407.

Taylor, S., Wakem, M., Dijkman, G., Alsarraj, M., and Nguyen, M. (2010). A practical approach to rt-qpcr—publishing data that conform to the miqe guidelines. *Methods*, 50(4):S1–S5.

Tsang, D. L., Edmond, C., Harrington, J. L., and Nühse, T. S. (2011). Cell wall integrity controls root elongation via a general 1-aminocyclopropane-1-carboxylic acid-dependent, ethylene-independent pathway. *Plant Physiology*, 156(2):596–604.

van Loon, L. C., Rep, M., and Pieterse, C. M. (2006). Significance of inducible defense-related proteins in infected plants. *Annu. Rev. Phytopathol.*, 44:135–162.

Venugopal, S. C., Chanda, B., Vaillancourt, L., Kachroo, A., and Kachroo, P. (2009). The common metabolite glycerol-3-phosphate is a novel regulator of plant defense signaling. *Plant signaling & behavior*, 4(8):746–749.

Wang, Y., Chantreau, M., Sibout, R., and Hawkins, S. (2013). Plant cell wall lignification and monolignol metabolism. *Frontiers in Plant Science*, 4:220.

Wei, Y., Periappuram, C., Datla, R., Selvaraj, G., and Zou, J. (2001). Molecular and biochemical characterizations of a plastidic glycerol-3-phosphate dehydrogenase from arabidopsis. *Plant physiology and biochemistry*, 39(10):841–848.

Wildermuth, M. C., Dewdney, J., Wu, G., and Ausubel, F. M. (2001). Isochorismate synthase is required to synthesize salicylic acid for plant defence. *Nature*, 414(6863):562.

Wormit, A., Butt, S. M., Chairam, I., McKenna, J. F., Nunes-Nesi, A., Kjaer, L., O'Donnelly, K., Fernie, A. R., Woscholski, R., Barter, M. L., et al. (2012). Osmosensitive changes of carbohydrate metabolism in response to cellulose biosynthesis inhibition. *Plant physiology*, 159(1):105–117.

Wu, L., Chen, H., Cutris, C., and Fu, Z. Q. (2014). Go in for the kill: How plants deploy effector-triggered immunity to combat pathogens. *Virulence*, 5(7):710–721.

Xu, C., Yu, B., Cornish, A. J., Froehlich, J. E., and Benning, C. (2006). Phosphatidylglycerol biosynthesis in chloroplasts of arabidopsis mutants deficient in acyl-acp glycerol-3-phosphate acyltransferase. *The Plant Journal*, 47(2):296–309.

Yamanaka, T., Nakagawa, Y., Mori, K., Nakano, M., Imamura, T., Kataoka, H., Terashima, A., Iida, K., Kojima, I., Katagiri, T., et al. (2010). Mca1 and mca2 that mediate ca2+ uptake have distinct and overlapping roles in arabidopsis. *Plant Physiology*, 152(3):1284–1296.

Yeats, T. H. and Rose, J. K. (2013). The formation and function of plant cuticles. *Plant Physiology*, 163(1):5–20.

Yu, K., Soares, J. M., Mandal, M. K., Wang, C., Chanda, B., Gifford, A. N., Fowler, J. S., Navarre, D., Kachroo, A., and Kachroo, P. (2013). A feedback regulatory loop between g3p and lipid transfer proteins dir1 and azi1 mediates azelaic-acid-induced systemic immunity. *Cell Reports*, 3(4):1266–1278.

Zhong, R. and Ye, Z.-H. (2014). Secondary cell walls: biosynthesis, patterned deposition and transcriptional regulation. *Plant and Cell Physiology*, 56(2):195–214.

Appendix A

Supplemental tables

Table A.1: Primers used in genotyping of T-DNA insertion lines for G3P-metabolism genes and respective fragment sizes in basepairs. Screening of homozygous T-DNA insertion mutants was performed using a PCR-based strategy involving three different primers (sequence 5'-3') for each T-DNA insertion line to be analysed (**A**). The left boarder (LB) primer binds the T-DNA insertion sequence, while the forward (For) and reverse (Rev) primers bind to sequence in the respective gene of interest.The table provides an overview of expected fragment sizes (in base pairs; bp) of the PCR-product (**B**).

A.

Mutant line	LB primer	For primer	Rev primer
gdphc1-2	ATTTTGCCGATTTCGGAAC	GATGTGAAACTACCCCTTCCC	CTGTGGAGCTGCTAAATGGAG
gdphc2	ATTTTGCCGATTTCGGAAC	TGCAGTGAACGAGAACATGAG	ACCTCCTCAACAATTCTTCCC
gdphp1	ATTTTGCCGATTTCGGAAC	ATTACCCATTTCCAAACCGTC	GGTTGATGATTTGGGTTTGTG
gli1-3	ATTTTGCCGATTTCGGAAC	AAGACGCTATCAAGAAAGGGG	CATAGGCTGCTCCTAATGCTG
azi1-2	ATTTTGCCGATTTCGGAAC	ACCCCTAAAAACCGAATCATG	AAGCACATTGGAAACCAGATG
act1	ATTTTGCCGATTTCGGAAC	CGGCTGTCATTTCTCTATTGC	CTTGGCTGTATGCTTCTTTCG
fad-gdph	ATTTTGCCGATTTCGGAAC	AGTAAATCTCTGAGAGGCCGC	TATGTTACCGTGGTTGGGAAG

B

Mutant line	LB/rev product size (bp)	For/rev product size (bp)
gdphc1-2	488-788	1118
gdphc2	462-762	1010
gdphp1	559-859	1093
gli1-3	432-732	1016
azi1-2	508-808	1126
act1	481-781	1095
fad-gdph	542-842	1124

Table A.2: RT-PCR Master mix. Volume and final concentrations of reagents included in the RT-PCR (Reverse-Transcriptase-PCR) master mix, providing a volume of 15 µl per individual reaction. 5 µl total RNA (including DNase mix; 1 µg final concentration) was added per reaction for a total volume of 20 µl.

Reagent	Volume	Final concentration
ImPromII^{TM} 5x Reaction buffer	4 µl	
ImPromII^{TM} Reverse transcriptase	1 µl	
dNTP Mix (10 mM) (Thermo Ficher)	1.25 µl	0.63 mM
$MgCl_2$ (25 mM)	2 µl	2.5 mM
Oligo(dT)15 Primer (500 µg/ml)	0.5 µl	0.5 µM
Random Primers (500 µg/ml)	0.5 µl	0.5 µM
Sterile MQ water	5.75 µl	

Table A.3: Primers used in qPCR to analyze expression levels of cell-cycle control genes. The table presents the forward and reverse primers (sequence: 5'-3') used in a qPCR-based analysis of *CYCB1;1* and *CYCD3;1* relative to *ACT2*.

Gene	Forward primer	Reverse primer
CYCB1;1	TCAGCTCATGGACTGTGCAA	GATCAAAGCCACAGCGAAGC
CYCD3;1	CTTCAGCTCGTTTCTGTCGC	TGTCTCCTCCACTTGAAAGTCT
ACT2	CTTGCACCAAGCAGCATGAA	CCGATCCAGACACTGTACTTCCTT

Table A.4: qPCR Master mix. Volume and final concentration of reagents included in the qPCR (Quantitative Real-time PCR) master mix, providing a volume of 15 µl. 5 µl total cDNA (diluted 1:10; 5 ng/µl final concentration) was aliquoted for a total volume of 20 µl. Primer mixes used are presented in supplemental table A.5

Reagent	Volume	Final concentration
LightCycler® 480 SYBR Green I Master 2X	10 µl	
Forward/Reverse primer mix	2 µl	5 µM
Sterile MQ water	3 µl	

Appendix B

Supplemental figures

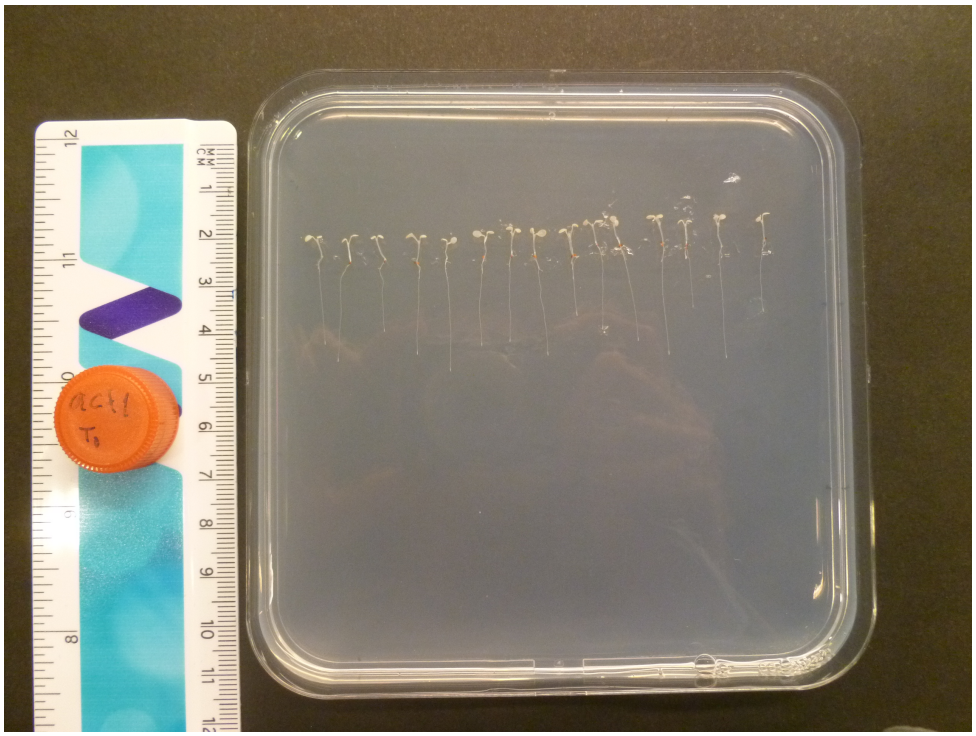

Figure B.1: Picture setup to perform root length measurements. 6 days old wild type (WT) and G3P metabolism mutant seedlings grown and treated as described before were collected prior to treatment start, and after 24 hours of the different treatments. 15 seedlings with approximately equal cotyledons were randomly selected and placed in a square petridish containing 0,5% agarose gel (0,5% agarose and MQ water). The seedlings were photographed next to a ruler, which was used to calibrate the pixel to cm ratio in Fiji for proper root length measurements.

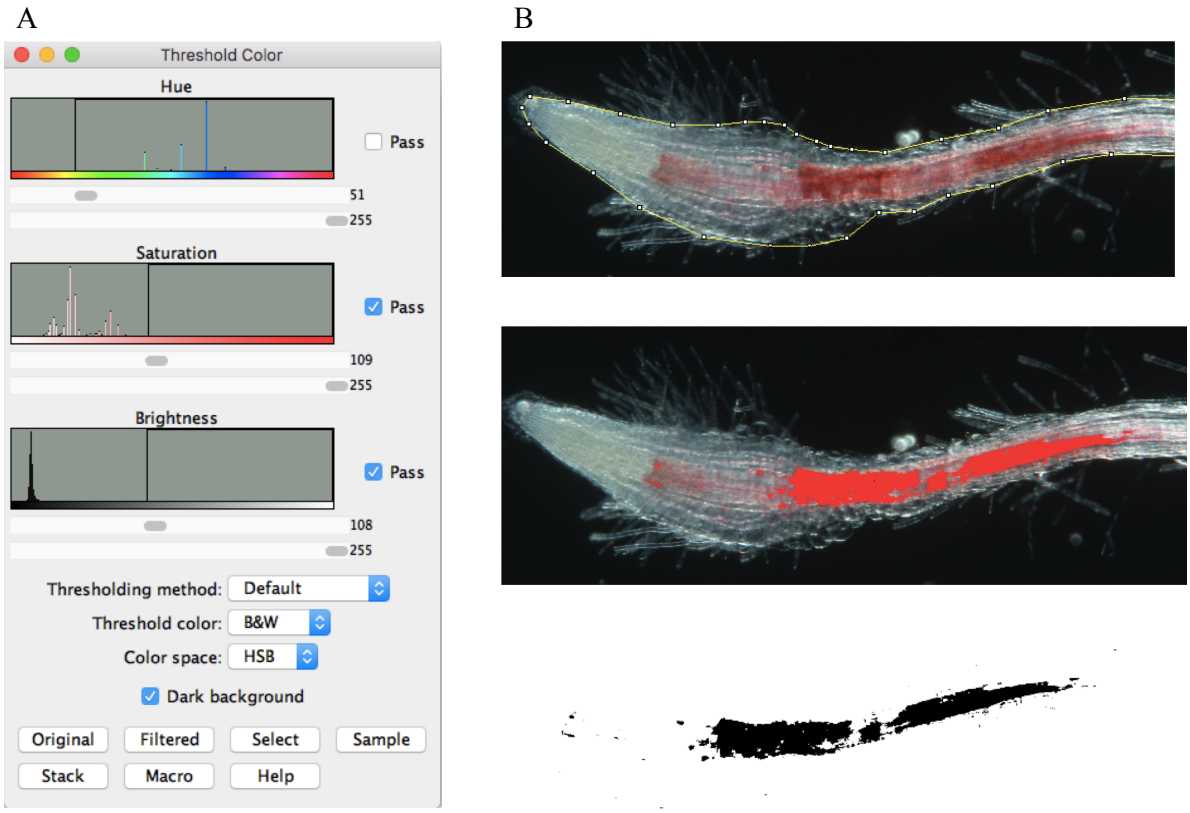

Figure B.2: Macro-script setup in Fiji used for automatized lignin quantification. A script-based macro used for automated lignin quantification, was created in the ImageJ analogue software; Fijo using the ”Adjust to colour thresholds” plugin under ”Image” in the menu bar. **A.** The Dialog box of ”Threshold colour”, in which the three settings ”Hue”, ”Saturation” and ”Brightness” was calibrated to the uploaded image to determine the settings of the macro. **B.**,Illustration of stained root area i.e. the area of lignification detected by the color threshold in the macro set-up. The middle and lower image illustrate the lignified root area (upper picture) that was detected by the macro

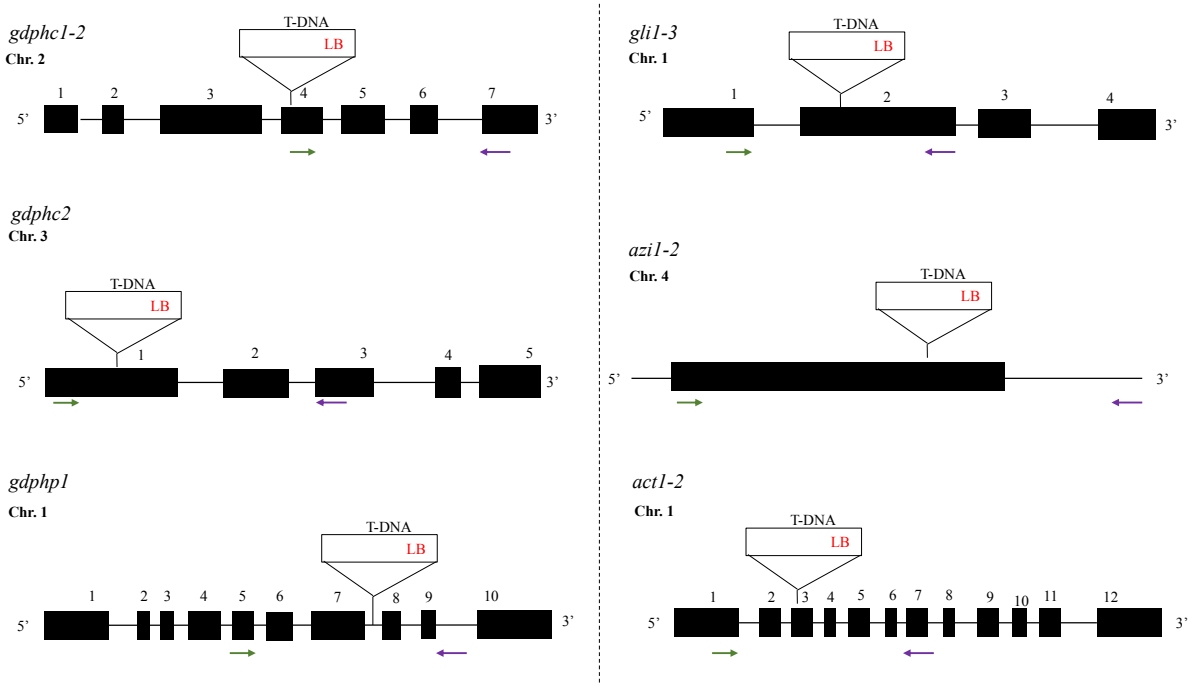

Figure B.3: Putative location of T-DNA insertion in G3P-metabolism mutants. Mutants used in this project were generated using T-DNA insertion carried out by *Agrobacterium*. Each scheme illustrates the appearance of the specific gene of interest, where black boxes illustrates exons, and black lines illustrates introns (information retrieved from primer-BLAST (NCBI)). Chr indicate chromosomal location of the genes of interest. Location of T-DNA insertion are indicated by boxes, whereas LB illustrate the binding cite of the left-boarder primer. Binding sites for additional primers used for genotyping of the genes of interest are illustrated as arrows (green: forward primer, purple: reverse primer).

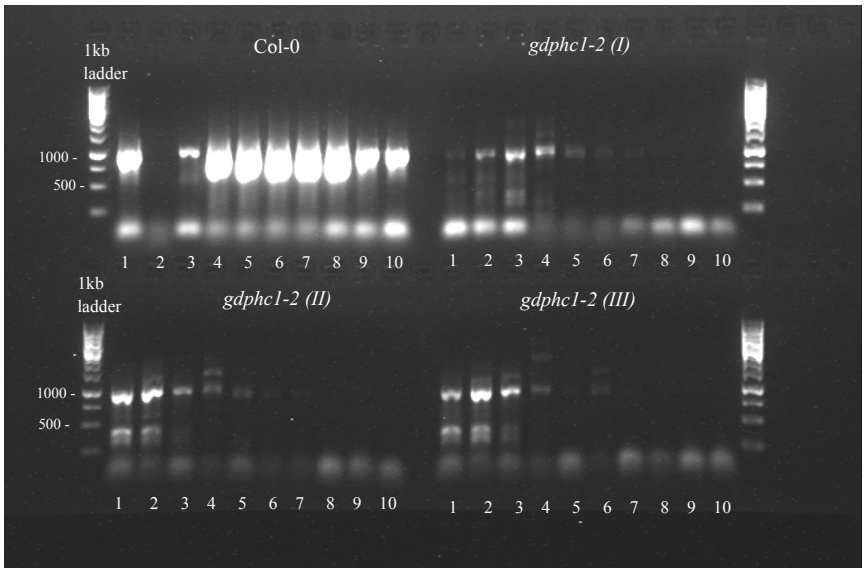

	Temperature
1	50.2
2	50.6
3	51.6
4	53.3
5	55.3
6	57.7
7	60.0
8	62.5
9	65.5
10	66.8

Figure B.4: Gradient PCR for *GDPHC1-2*. DNA was extracted from a rosette leaf of three 7-10 day old *gdphc1-2* seedlings (I-III). A gradient PCR was performed using the gen specific forward/reverse (for/rev) primer pair to determine appropriate annealing temperature to perform the genotyping PCR reactions. Numbers 1-10 correspond to annealing temperatures listed in the table on the right. A 1 kb ladder was included to ensure proper sequence size of the PCR product. DNA-template from Col-0 was used to perform control reactions.

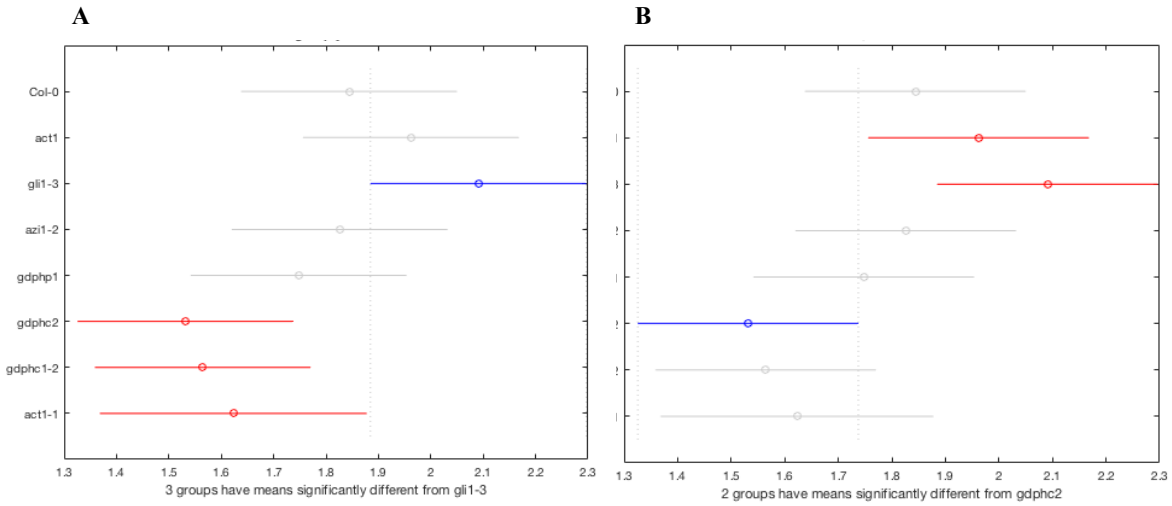

Figure B.5: Statistical analysis of primary root length (cm) for Col-0 and G3P-metabolism mutant seedlings prior to treatment start (T0). A one-way ANOVA ([F(7,15) = 5.37, p = 0.0031] coupled with a Tukey honest significant difference (HSD) post hoc text (s = 0.14) was carried out using MATLAB. The results revealed a statistical significant difference between the primary root length (cm) of *gli1-3* and *gpdhc1-2*, *gdphc2*, *act1-1* (**A**); and between *act1-2* (here:act1) and *gdphc2* (**B**).

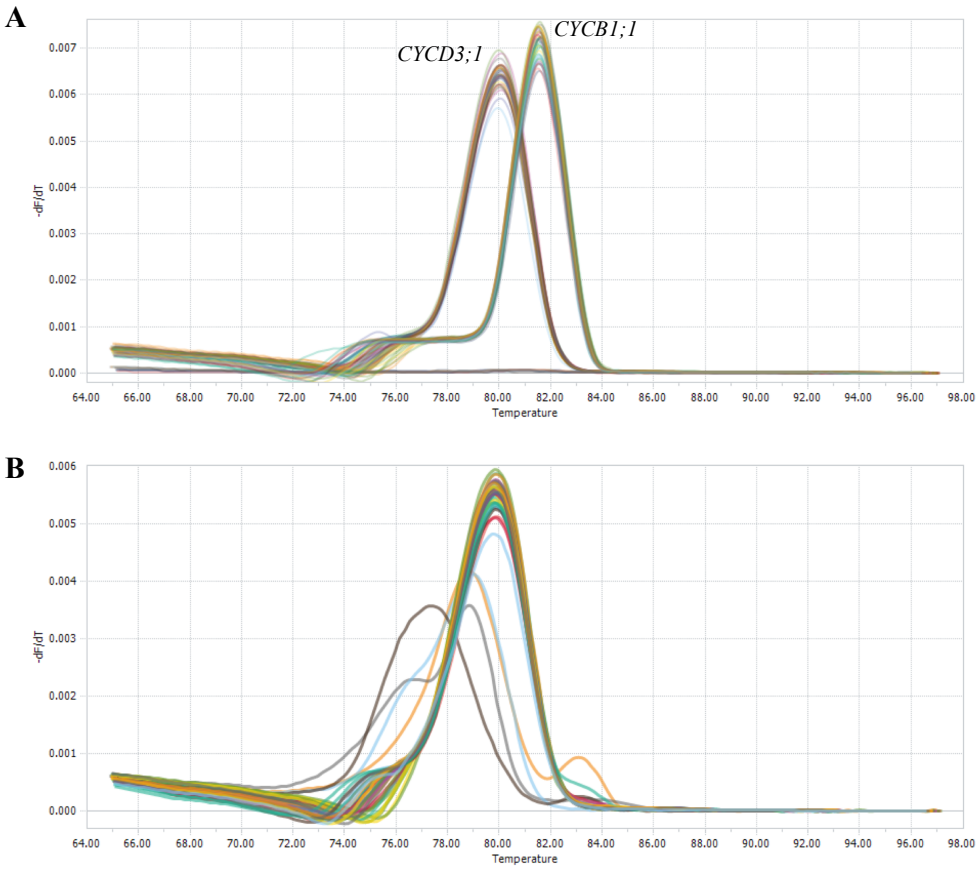

Figure B.6: qPCR melting curves of *CYCB1;1*, *CYCD3;1* and *ACT2*. Melting curves of qPCR reaction retrieved from LightCycler® 96 System. **A**:*CYCB1;1*, *CYCD3;1*, **B**: *ACT2*. The curve illustrates the negative change in detected fluorescence above background across temperatures fluctations applied in the qPCR reaction (-dF/dT).

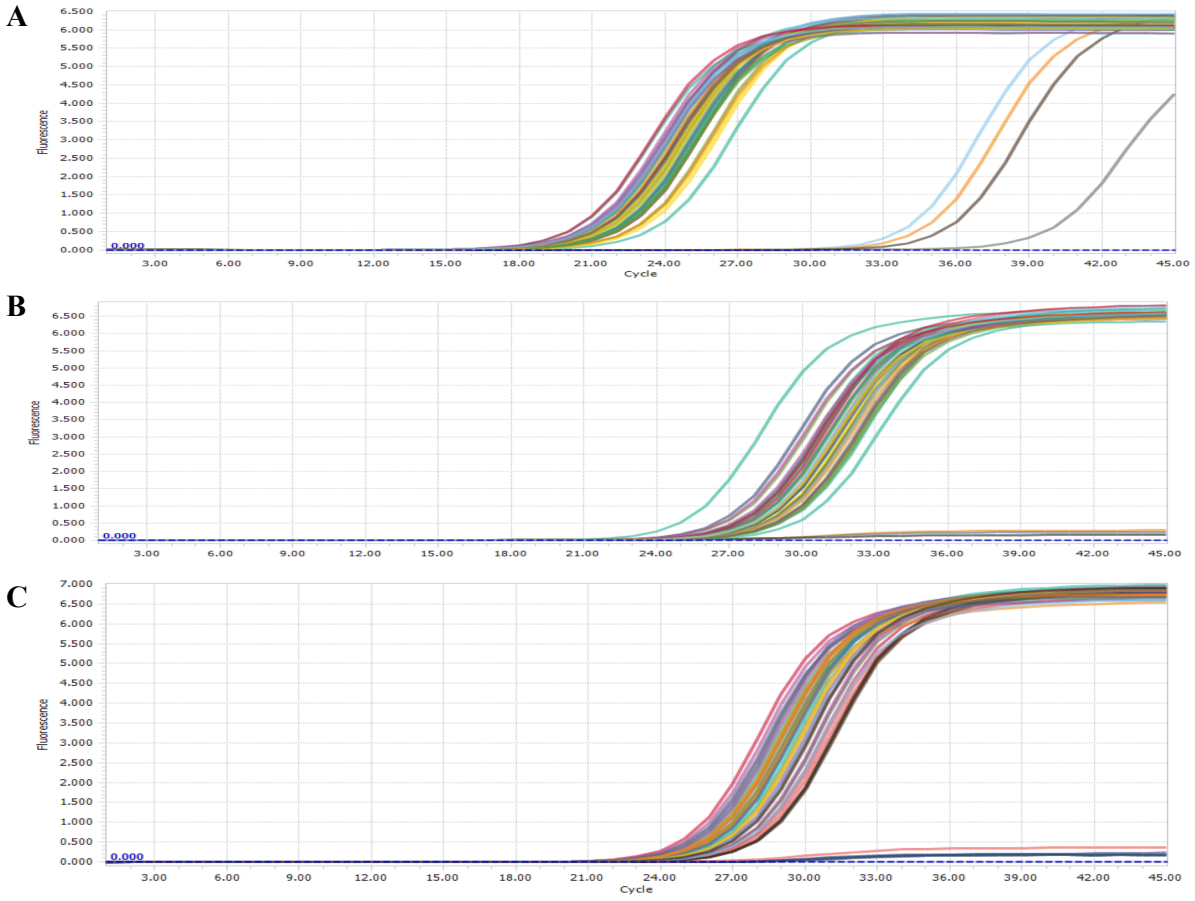

Figure B.7: qPCR amplification curves of *CYCB1;1*, *CYCD3;1* and *ACT2*. Amplification curves of q-PCR reaction from *ACT2* (**A**), *CYCD3;1* (**B**) and *CYCB1;1* (**C**), retrieved from LightCycler® 96 System. The curve illustrates the detected fluorescence above background level after each cycle of the qPCR reaction (of a total of 45 cycles).

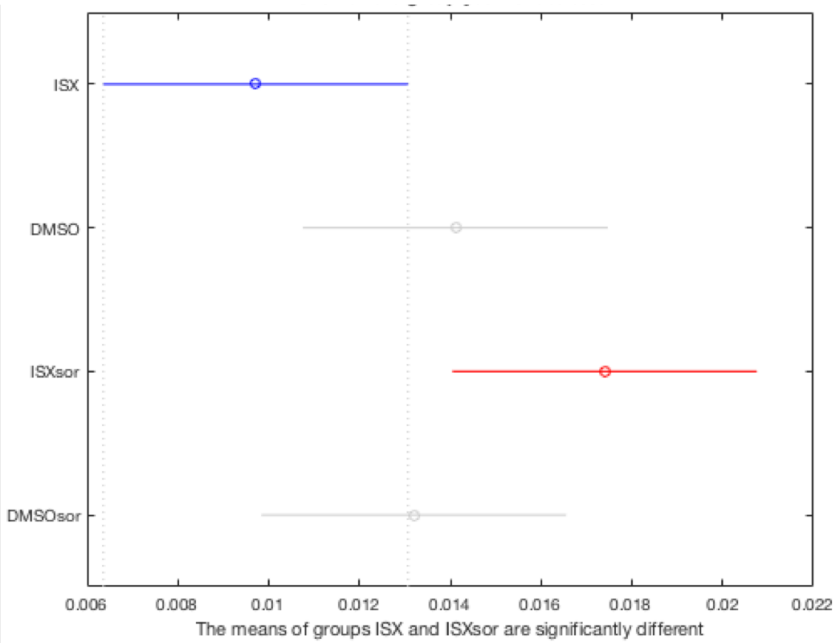

Figure B.8: Statistical analysis of *CYCB1;1* expression levels (represented relative to *ACT2*) in *gdphc1-2* seedlings in response to the treatments performed. A one-way ANOVA ([F(3,8) = 4.85, p = 0.0385] coupled with a Tukey honest significant difference (HSD) post hoc text (s = 0.0026) was performed using MATLAB to compare the expression levels of *CYCB1;1* in *gdphc1-2* seedlings in response to the treatments performed. (ISX, ISX+sorbitol (ISXsor) or mock conditions (DMSO, DMSO+Sorbitol; DMSOsor). The analysis revealed statistical significant difference in *CYCB1;1* expression levels between ISX and ISX+Sor (ISXSor) treated *gdphc1-2* seedlings.

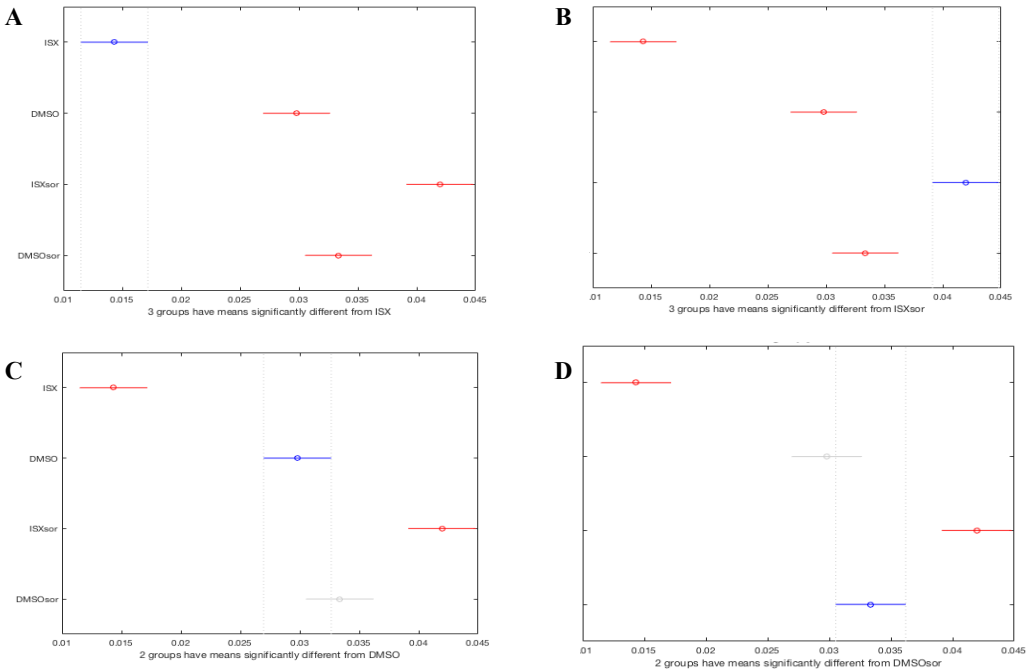

Figure B.9: Statistical analysis of *CYCD3;1* expression levels (represented relative to *ACT2*) in Col-0 seedlings in response to the treatments performed. A one-way ANOVA ([F(3,8) = 84.76, p = 2.1042e-06] coupled with a Tukey honest significant difference (HSD) post hoc text (s = 0.0022) was performed using MATLAB to compare the expression levels of *CYCD31;1* in Col-0 seedlings in response to the treatments performed (ISX, ISX+sorbitol (ISXsor) or mock conditions (DMSO, DMSO+Sorbitol; DMSOsor). The analysis revealed statistical significant difference of *CYCD3;1* expression between ISX-treated Col-0 seedlings and the latter treatments (**A**):, between ISX+Sor treatment and the latter treatment (**B**), while DMSO- (**C**) and DMSO+Sor-treatment (**D**) were different from ISX- and ISX+Sor-treatment, but comparable to each other.

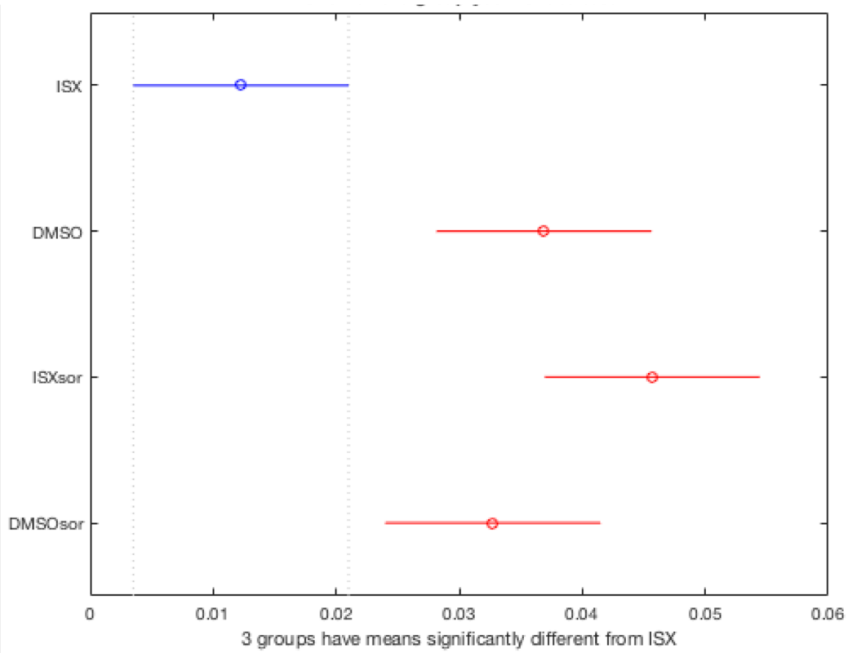

Figure B.10: Statistical analysis of *CYCD3;1* expression (presented relative to *ACT2*) in *gdphc1-2* seedlings in response to the treatments performed. A one-way ANOVA ([F(3,8) = 13.44, p = 0.0017] coupled with a Tukey honest significant difference (HSD) post hoc text (s = 0.0096) was performed using MATLAB to compare the expression levels of *CYCD31;1* in *gdphc1-2* seedlings in response to the treatments performed (ISX, ISX+sorbitol (ISXsor) or mock conditions (DMSO, DMSO+Sorbitol; DMSOsor). The analysis revealed statistical significant difference of *CYC31;1* expression levels in *gdphc1-2* seedlings between ISX-treatment and the other treatments.

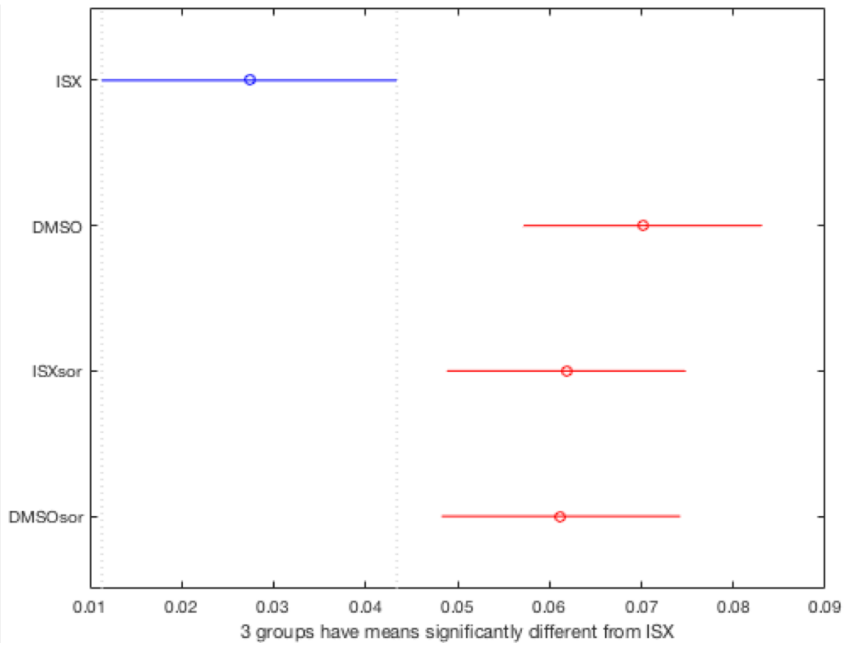

Figure B.11: Statistical analysis of *CYCD3;1* expression (represented relative to *ACT2*) in *gdphp1* seedlings in response to the treatments performed. A one-way ANOVA ([F(3,8) = 8.65, p = 0.0094] coupled with a Tukey honest significant difference (HSD) post hoc text (s = 0.0096) was performed using MATLAB to compare the expression levels of *CYCD31;1* in *gdphp1* seedlings in response to the treatments performed (ISX, ISX+sorbitol (ISXsor) or mock conditions (DMSO, DMSO+Sorbitol; DMSOsor). The analysis revealed a statistical significant difference of *CYCD31;1* expression between ISX-treatment and the other treatments.

Appendix C

Glycerol kinase (GK) activity assay

Originally the plan was to establish an enzyme activity assay for glycerol kinase (GK). This chapter summarizes the the work had been performed. However, due to time limitations and technical problems, this work stream was stopped.

The GK activity assay was modified from procedures originally decribed by Gibon et al. (2002, 2004), and included three steps: protein extraction, a stopped enzyme assay, and a continuous enzyme assay. In the stopped assay, GK was activated by addition of its substrate (glycerol) and ATP, generating G3P. (Supplemental figure C.1.A).

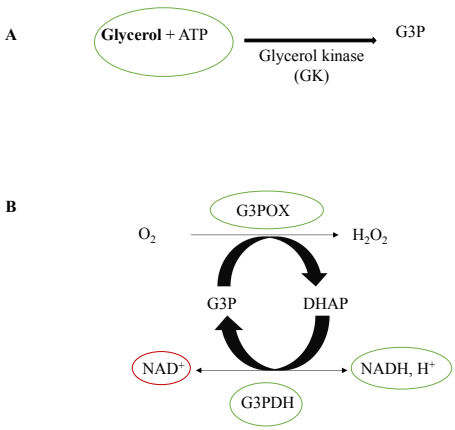

Figure C.1: G3P biosynthesis reactions taking place in the glycerol kinase (GK) activity assay. **A**: Glycerol kinase (GK) generates G3P from glycerol, using ATP as phosphate source. **B**: G3P oxidase (G3POX) oxidizes G3P using O_2, generating hydrogen peroxide (H2O2) and DHAP, a precursor for G3P used by NAD-dependent G3PDH to synthesize G3P from DHAP and NADH, with NAD as a biproduct. NAD is detectable in a spectrophotometer at 340 nm optic density (OD). Green circles illustrate components added in the reaction mixes of the stopped and continous assay used in analysis of GK activity, while red circles indicate quantified product. Figure was modified with permition from (Gibon et al., 2004)

Since G3P is not easily quantified, G3P levels was analyzed in a continuous assay using additional G3P synthesizing enzymes (Supplemental figure C.1.B). GK activity was thereby quantified using G3P oxidase (G3POX) and NAD-dependent G3P degydrogenases (G3PDH). One bi-product of the G3PDH activity; NAD is detectable using a spectrophotometer at 340 nm optic density (OD). Therefore, the NAD levels in the continous assay can be directly correlated with the amount of G3P generated in the stopped assay, which allows quantfication of the GK activity.

A. thaliana ecotype Col-0 seeds were sterilized as described in section (2.1), and grown in 125 ml autoclaved $\frac{1}{2}$ MS medium (1 % sucrose) for six days, followed by treatment with fresh $\frac{1}{2}$ MS medie (1 % sucrose) containing 600 nM ISX (diluted in DMSO) or DMSO (mock) for 24 hours. The seedlings were then harvested, dried down, separated into batches and flash-frozen in liquid nitrogen, ground to fine powder and and weighed to 30 $\pm$ 2 mg per sample. 50 µl/mgFW extraction buffer was used for enzyme extraction from each sample (Supplemental table C.1). The samples were vortexed virgiously and centrifuged at maximum speed to precipitate insoluble plant material. Note that 6-aminoaproic acid, PMSF, Leupeptin and DTT does not store well in the extraction buffer, and must therefore be added shortly before the assays are being performed.

Table C.1: Total protein extraction buffer. Final concentration of reagents included in the protein extraction buffer. The reagents was dissolved in sterile MQ water.

Reagent	**Final concentration**
Glycerol	10 %
Bovine serum albumin (BSA)	0.25 %
Triton X-100	0.1 %
Hepes/KOH (pH 7.5)	50 mM
$MgCl_2$	10 mM
Ethylenediaminetetraacetic acid (EDTA)	1 mM
EGTA	10 mM
Benzamidine	1 mM
6-aminoaproic acid	1 mM
phenylmethylsulfonyl fluoride (PMSF)	1 mM
Leupeptin	10 M
Dithiothreitol (DTT)	1 mM

The stopped assay coupled with a continuous assay was performed in a 96-well plate to measure the GK-activity. A G3P standard (0-0.2 mM G3P with 0.02 intervals) was applied as a control. The stopped assay was performed by adding 40 µreaction mix (minus the ATP) (Supplemental table C.2) to 5 µl enzyme extract or 5 µl the different components in the G3P standard, and the samples were incubated at RT for 5 minutes. Addition of 0.8 mM ATP started the reaction. The reaction was stopped with 20 µl HCl (0.5 M), and incubated at RT for 10 minutes. The time range of the stopped assay remains to be determined.

Table C.2: GK acivity assay reaction mix. Final concentration of reagents included in the reaction mix used in the stopped assay of GK activity measurements. The ingredients was suspended in MQ water. Note that ATP was not added until after incubation for 5 minutes.

Reagent	**Final concentration**
Trisine/KOH (pH 8)	100 mM
$MgCl_2$	8 mM
Glycerol	120 mM
ATP	0.8 mM

Prior to the continuous assay, sodium hydroxide (NaOH) was added to the samples to neutralize the pH. The quantity of NaOH was not completely optimized. 50 µl G3P measurement mix was added to each sample and the samples were heated to a temperature of 30 °C. The continous reaction was started by addition of 1 mM NADH, and absorbance (optimal density; OD) from NAD content wwas measured in a spectrophotometer at 340 nM (30°C incubation temperature) until stable.

Table C.3: G3P measurement mix. Final concentration of reagents added for measurement of GK activity. used in the continuous assay of GK activity measurements. The reagents were dissolved in sterile MQ water. Note that NADH was not added until after incubation for 5 minutes.

Reagent	**Final concentration**
Trisine/KOH (pH 8)	100 mM
$MgCl_2$	1.5 mM %
G3P oxidase (G3POX)	1.8 U/ml
G3P dehydrogenase (GPDH)	0.7 U/ml
NADH (Nicotinamide adenine dinucleotide)	1 mM